Technische Universität München

Lehrstuhl für Energiesysteme

Numerical methods for efficient power generation from municipal solid waste

Dipl. Ing. Univ. Martin Johannes Murer

Vollständiger Abdruck der von der Fakultät für Maschinenwesen der Technischen Universität München zur Erlangung des akademischen Grades eines

Doktor-Ingenieurs

genehmigten Dissertation

Vorsitzender:		Univ.-Prof. Dr.-Ing. Thomas Sattelmayer
Prüfer der Dissertation:	1.	Univ.-Prof. Dr.-Ing. habil. Hartmut Spliethoff
	2.	Univ.-Prof. Dr.-Ing. Helmut Seifert
		Karlsruher Institut für Technologie

Die Dissertation wurde am 19.02.2013 bei der Technischen Universität München eingereicht und durch die Fakultät für Maschinenwesen am 21.01.2014 angenommen.

Preface

This thesis is the result of my time as a researcher at the Institute for Energy Systems at the Technische Universität München. I worked on the project "efficient power generation from municipal solid waste", which is one of 50 projects in the KW21 (power plants for the 21^{st} century) research framework. The project was funded by the Bayerisches Staatsministerium für Bildung und Kultus, Wissenschaft und Kunst (Bavarian State Ministry of Education, Science and the Arts), Bayerisches Staatsministerium für Wirtschaft und Medien, Energie und Technologie (Bavarian Ministry of Economic Affairs and Media, Energy and Technology) as well as by the Company Martin GmbH für Umwelt- und Energietechnik.

First, I would like to thank my supervisor Prof. Dr. Ing. habil. Hartmut Spliethoff for letting me work on this interesting topic, for his very valuable input on technical question and most of all for the space he left me to develop my own ideas.

Same debt of gratitude is owed to Prof. Dr. Ing. Helmut Seifert, who offered to be my co-supervisor and showed a great interest in my results.

Thanks are due to Prof. Thomas Sattelmayer, who was so kind to be the chairman for my thesis defence.

Great thanks goes to Company Martin GmbH and as a representative to Johannes J. E. Martin head of the family owned company for co-funding this project and also by supporting it with company resources and know-how.

I thank my contact person at Martin GmbH Dr. Oliver Gohlke, supporting me and the project in a great manner from the first minute, by being a person who is always open for new ideas.

I am really grateful for a somewhat different way of looking on a broad range of topics, which were shown to me by Dr. Elisa Alonso-Herranz, who is an old friend from the institute for Energy Systems and later co-supervised my project at Martin GmbH.

Further I would like to thank Robert von Raven and Dr. Ralf Koralewska from Martin GmbH R&D department for valuable input and literature suggestions for my work and assistance for preparing my thesis.

My boiler concept would not have been possible without the discussions with Mirjam Troßmann-Göll and Simon Nachreiner from the Martin GmbH boiler department. Thank you!
With Thomas Schäfer I had a really critical discussion about my boiler concept and I am thankful for his comments on my manuscript.
Special thanks goes to company AEB in Asterdam. In person I thank Marcel van Berlo, Chantal de Waal and Saskia Wilpshaar, they supported my research onsite with measuring campaigns for validation of my CFD simulations and process data from the HRC plant for investigating boiler and combustion behaviour.
I would like to thank all the students I had the pleasure to work with in this project. Especially Michael Angerer for providing me a better understanding of detailed NO_x chemistry, and proof reading that part of this thesis. Sandra Dürrschmidt for investigating the effects of the fuel conversion model on combustion simulation but also on NO_x formation. Finally I would like to thank the student which has contributed most to my thesis: Ulrich Martin. Together we developed the fuel conversion model and the coupling to the CFD code. During his time at the Martin GmbH boiler department he proved that my boiler concept could be realised.
I also thank my English speaking friends Matthew McCool Anderson and Garret Fitzgerald which I had the pleasure to meet over the years and who spent quite some time correcting my text. I thank Alex Frank. He did read the NO_x part of my thesis and introduced me to detailed chemistry models, which helped me to better understand the combustion process.
Further I thank my colleagues Daniela Gewald, Matthias Mayerhofer, Markus Fischnaller, Benjamin Kreutzkam for valuable discussion and also for many hours of recreational activities like hiking, camping and cross country skiing.
A thanks goes also to Christian Schuhbauer for discussion on CFD and for keeping my computer hardware running.
I thank my friend Paul Martin Lützkendorf for motivating me to work a little less and do more sports.
Great thanks to the crew of Radioseven for countless hours of "nätets bästa musik", as tension release during my many hours of work on the computer.
Finally I thank my parents Agahte and Helmuth and my sister Johanna! They did support me a lot during the whole time of my thesis and spending time with them at home in the Alps or somewhere else in the nature around the world is still a great source for distraction and regeneration from my work life in Munich.

Munich, February 2013
Martin J. Murer

Zusammenfassung

In einem modernen Abfallwirtschaftssystem trägt neben Recycling und Kompostierung auch Müllverbrennung zu einer nachhaltigen Verwertung von Ressourcen bei. Abfall ist ein Stoff, welcher besonders dort anfällt, wo im gehobenen Maße Energie in Form von Strom und Wärme benötigt wird. Deshalb ist es naheliegend, den bereits vorhandenen Rohstoff effizient und umweltschonend zu nutzen.

Die Europäische Union unterstützt diese Bestrebungen, fordert aber gleichzeitig einen gewissen Effizienzstandard bei der Umwandlung der im Abfall enthaltenen Energie. Dieser Standard ist in der Abfallrahmenrichtlinie festgelegt. Eine weitere Richtlinie regelt die Emissionsgrenzwerte für Abfallverbrennungsanlagen. Diese wurden im Rahmen der 17. BImSchV in Deutschland umgesetzt. Besonders die Grenzwerte für Stickoxidemissionen (NO_x) wurden in den letzten Jahren genauer betrachtet und im Rahmen technischer Entwicklungen und des Umweltschutzes weiter verschärft.

Diese Gesetzeslage definiert die Randbedingungen für diese Arbeit: Effizienzsteigerung und Emissionsminderung ohne die Verfügbarkeit und Wirtschaftlichkeit von Müllverbrennungsanlagen zu reduzieren.

Als erster Schritt wird, in Anlehnung an moderne Kohlekraftwerke, der Wasserdampfkreislauf und die Verbrennungsführung angepasst. Dies macht sich auf der Wasserdampfseite besonders durch leicht erhöhte Frischdampfzustände und eine mehrstufige Speisewasservorwärmung bemerkbar. Zusätzlich wird die Vorwärmung der Verbrennungsluft nicht mehr aus prozesstechnischen Gründen gewählt, sondern als effizienzsteigernde Maßnahme mit Niedertemperaturwärme aus dem Rauchgas betrieben.

Auch bei der Stickoxidminderung in Müllverbrennungsanlagen besteht die Möglichkeit sich am Verbrennungsprozess von Kohlekraftwerken zu orientieren. Abfall ist ähnlich wie Braunkohle ein sehr flüchtiger Brennstoff, somit kann aus einer breiten Palette erprobter feuerungstechnischer Maßnahmen gewählt werden. Für die Müllverbrennung eignet sich hierfür besonders die Luftstufung. Zum besseren Verständnis des Reduktionsprinzips wird die grundlegende NO_x)-Chemie, ausgehend von den Vorläuferspezies Ammoniak (NH_3)) und Wasserstoffcyanid (HCN), genauer untersucht.

Die Verbrennung kann mit Hilfe von numerischer Berechnung (Computational fluid dynamic CFD) optimiert werden. Diese erlaubt Untersuchungen verschiedener Randbedingungen und Einstellungen mit geringerem Aufwand. Die dabei ermittelten Tendenzen decken sich sehr gut mit der betrachteten NO_x-Chemie.

Aus den verschiedenen Berechnungsfällen wird abgeleitet wie ein emissionsarmes Verbrennungssystem ausgelegt werden kann: Die Primärverbrennung auf dem Rostsystem soll unterstöchiometrisch erfolgen. Die Ausbrandluft wird in mehreren Stufen zugegeben, dies verbessert die Durchmischung bei gleichzeitig niedrigen Sauerstoffpartialdrücken. Als erste Ausbrandebene bietet sich die Eindüsung von rezirkuliertem Rauchgas an, um die Gase oberhalb des Brennbetts zu vergleichmäßigen und die Temperatur zu reduzieren.

Als letzter Punkt wird die Auswirkung der geplanten Veränderungen auf die Anlagenverfügbarkeit diskutiert. Eine Reihenfolge für die Umsetzung einzelner Maßnahmen wird präsentiert, um unnötige Risiken bei der Prozessimplementierung zu vermeiden.

Abstract

Waste management plays an important part in a sustainable world. The undesired outputs of society have to be used in such a way that most benefit can be achieved without harming the environment. In the hierarchy of waste management priority options are defined to fulfill this goal. If possible waste should be reduced, reused or recycled (3R). If this is not possible waste can be incinerated. New laws ensure that waste incineration is implemented in such a way to fulfill the sustainable idea. In the European waste framework directive, requirements for energy efficiency for new and existing plants are defined, while the industrial emission directive defines the legal emission limits for this technology. The legal emission limit for nitrogen oxide (NO_x) was the center of attention in the last years and it was aggravated due to technical developments and environmental concern.

These recent law changes are the boundary conditions for this thesis. Increasing energy efficiency and decreasing NO_x emissions without reducing availability and economy of waste incineration plants are its goals.

As a first step, the water steam cycle and the combustion process is adapted from coal power plants. This implies increased live steam parameters and a multiple steps for the feed water preheating in the water steam cycle. Air preheating is not chosen to improve the combustion process, but as a measure to improve energy efficiency. This is achieved by the use of low temperature heat from the flue gas for air preheating.

Also, for the reduction of NO_x emissions in energy from waste plants concepts from coal power plants can be used as an example. Waste has similar high contents of volatile matter as lignite; therefore it is possible to choose from a broad range of proven combustion engineering measures. Staged combustion, using air staging is the most promising concept applicable in a waste incineration plant. For a better understanding of the reduction process the NO_x chemistry is discussed more in detail starting from the precursor species ammonia (NH_3)) and hydrogen cyanide (HCN).

Computational fluid dynamic (CFD) can be used to optimize the combustion process. It allows the effortless investigation of different combustion conditions and settings. The tendencies found during the performed investigations match with the detailed NO_x chemistry found in the literature.

From different simulated furnace and nozzle arrangements a guideline for a combustion system with low emissions was derived. The primary combustion on the grate should be sub stoichiometric. Burnout air should be added in several steps, to improve mixing while keeping the local oxygen partial pressure low. As first stage in the post combustion zone recirculated flue gas should be injected, the jets are used to homogenize the gases above the waste bed and reduce the flue gas temperature.

As a last point the implications of the suggested changes on the plant availability is discussed. An order for the implementation of the individual measures is presented to avoid unnecessary risks, by changing too much of the process in a single step.

Contents

Nomenclature

Greek symbols

Symbol	Description	Unit
α	heat transfer coefficient	$\left[\frac{W}{m^2K}\right]$
η	efficiency	$[-]$
λ	thermal conductivity	$\left[\frac{W}{mK}\right]$
μ	dynamic viscosity	$[Pas]$
ϕ	mass flux	$\left[\frac{kg}{m^2s}\right]$
ρ	density	$\left[\frac{kg}{m^3}\right]$
ρ	emission density	$\left[\frac{mg}{Nm^3}\right]$

Latin symbols

Symbol	Description	Unit
A	Arhenius constant	$[-]$
A	area	$\left[m^2\right]$
b	anergy	$\left[\frac{kJ}{kg}\right]$
c_p	specific heat capacity	$\left[\frac{J}{kgK}\right]$
d	diameter	$[m]$
E	energy	$[MWh]$
e	exergy	$\left[\frac{kJ}{kg}\right]$

E	activation energy	$\left[\frac{J}{mol}\right]$
h	enthalpy	$\left[\frac{kJ}{kg} \quad \frac{kJ}{kmol}\right]$
I	impulse	$\left[\frac{kgm}{s}\right]$
i	iteration index	$[-]$
$\dot{m}$	mass flow rate	$\left[\frac{kg}{s}\right]$
n	iteration index	$[-]$
pf	partition fraction of NO_x intermediate	$[-]$
$\dot{Q}$	heat	$[W]$
q	heat	$\left[\frac{kJ}{kg}\right]$
q'''	volumetric heat source	$\left[\frac{kW_{th}}{m^3}\right]$
R	mean limiting reaction rate	$\left[\frac{kg}{m^3 s}\right]$
R	radius	$[m]$
S	volumetric species source term	$\left[\frac{kg}{m^3 s}\right]$
s	entropy	$\left[\frac{kJ}{kgK}\right]$
t	temperature	$[°C]$
T	temperature	$[K]$
u	velocity in x direction	$\left[\frac{m}{s}\right]$
V	volume	$\left[m^3\right]$
v	velcotiy in y direction	$\left[\frac{m}{s}\right]$
v	velcotiy	$\left[\frac{m}{s}\right]$
w	velocity in z direction	$\left[\frac{m}{s}\right]$
x	mole fraction	$[-]$

Indices

Index	**Description**
0	environment conditions
ad	adiabatic
a	air

aph	air preheating
c	heat sink (cold)
$Carnot$	Carnot
cf	conversion factor / rate
do	downward
dry	dry
ed	educt
f	fossile fuel
for	formation
f	fuel
gc	grate cooling
ghi	gross heat input
h	heat source (hot)
i	imported
i	inner
los	losses
ls	live steam
p	produced
pro	product
ref	refered to specific oxygen concentration
s	stoichiometric
up	upward
w	waste

Abbreviations

Abbreviation	Description
AFR	Air Fuel Ratio
APT	Air Preheating Temperature
BC	Base Case
BIN	Big Improved Nozzles
CFD	Computational Fluid Dynamics
$DCKM$	Detailed Chemical Kinetic Model
ECO	Economizer
EE	Energy Efficiency
EFW	Energy From Waste
ESP	Electrostatic Precipitator
$EVAP$	Evaporator
FRR	Flue Gas Recirculation Rate
$FTIR$	Fourier Transform Infrared Spectroscopy
GP	Gas Phase
GSM	Gas Supply Modified
HRC	Hoog Rendement Centrale (High efficient EFW plant)
IN	Improved Nozzles
max	Maximum
min	Minimum
mwa	Mass Weighted Average
OL	Overload
$RECI$	Recirculated Flue Gas
SC	Switched Combustion
$SC-UP$	Switched Combustion Upward
SH	Superheater
$SH-UP$	Switched (Combustion) Highest Upward
SCR	Selective Catalytic Reduction
$SNCR$	Selective Non Catalytic Reduction
$TAMARA$	Testanlage zur Müllverbrennung, Abgasreinigung, Rückstandsverwertung, Abwasserbehandlung (Test facility for waste incineration, flue gas cleaning, residua treatment and waste water treatment)
TFN	Total Fixed Nitrogen

TGA	Thermo Gravimetrical Analyzer
UBA	Umweltbundesamt
UDF	User Defined Function
UP	Upward
VLN	Very Low NO_x
WB	Waste Bed
WSH	Wall Superheater

1. Motivation, goal and approach

Environmental awareness and sustainable thinking are basic principals in modern society. This includes all aspects in live. A great challenge is to apply these principals also to energy supply and waste management.

Waste incineration along with recycling is a key component in modern sustainable waste management system. The waste hierarchy defined in the European waste framework directive ranks the options for waste treatment. In this hierarchy waste prevention is the most important option followed by reuse and recycle. If recycling of waste is no longer possible the energy of it has to be recovered. Only if energy recovery from waste is not possible due to its low heating value it is allowed to landfill waste. The energy in the waste is traditionally recovered by incineration. However as defined in the European waste framework directive waste incineration is not automatically energy recovery. To promote the sustainable use of the energy in the waste it has to be converted efficiently to electricity and heat. An energy from waste plant (EFW) is considered as a plant with energy recovery by the European legislation if it fulfills an energy efficiency criterion.

During the incineration of waste a great variety of pollutants are formed and released during the combustion process. These emissions can be reduced using flue gas treatment equipment or by optimizing the combustion process. From the wide range of pollutants, nitric oxides (NO_x) are by magnitude the highest emissions with values in the range of 50 mg/Nm^3 to 180 mg/Nm^3. Therefore it can be concluded: at the moment the two main driving factors in the waste incineration sector are:

- Energy efficiency
- NO_x emissions

These two topics are addressed by the research project "Efficient power generation from municipal solid waste", which is one of many projects inside the framework of the "KW21" research initiative. It deals with the improvement of power plant technologies for the 21st century. Challenging is the improvement of the waste incineration process according to these two criteria, while keeping all the other emissions as well as the plant availability at todays levels. For waste incineration the same combustion chemistry and power plant thermodynamics

are applicable as for coal power plants. Regarding the aspects of NO_x emissions and energy efficiency lignite fired power plants can be used as inspiration since they represent an efficient energy conversion of solid fuel into electricity, while complying with the current NO_x emissions limit, by the use of combustion engineering measures only. In 2004 VGB Power Tech published the report "Reference Power Plant North Rhine Westphalia" [1]. This was a study performed by some of the main coal power plant suppliers and operators in Germany to define the current state of the art for coal power plants. The power generating process was investigated and optimized as a whole.

In this thesis a similar approach is attempted on a smaller scale for waste incineration. The goal is to design and optimize an energy from waste plant with focus on:

- Net electric efficiency
- Primary NO_x emissions

This goal is achieved by the use of numerical methods for the optimization of the water steam cycle and computational fluid dynamics (CFD) for the optimization of the combustion process. Numerical methods allow it to account for the inhomogeneous fuel affecting the combustion process, which is one of the main differences to coal power plants. The other main difference is the unit size of a energy from waste plant, which is about one order of magnitude smaller compared to modern coal power plants. This fact has to be considered when designing the power generation process.

To reduce NO_x emissions understanding of NO_x formation and NO_x reduction is necessary. Air and fuel staging is used in other combustion systems like pulverized coal power plants to reduce NO_x emissions. Theory and experimental data of this techniques is presented in Chapter 3.

Numerical methods, such as computational fluid dynamics are considered state of the art in the power plant sector, when combustion and flow are investigated. These methods are used for optimizing the combustion process in EFW plants and are also described in Chapter 3. Only numerical methods make it possible to account for the inhomogeneous composition of the fuel and allow parameter variations without big investments or risk for a real plant.

A special waste conversion model was tailored to model the combustion of waste on a grate. The most important feature of this model is the implementation of inhomogeneous fuel composition and primary air supply, along with the release of NO_x precursor species.

Starting in the 1990's many promising investigations on NO_x emissions where performed in semi industrial scale EFW test facilities. The findings of the test facilities are reproduced using this fuel conversion model and a modeled test furnace at which different combustion settings are applied. This approach along with data measured at two EFW plants was used to validate the computational models.

The water steam cycle is the key component in the generation of electricity from a given heat source. The water steam cycles of energy from waste plants are far less sophisticated compared to coal power plants and offer therefore a huge potential for improvement. This potential must be unlocked without influencing the plant availability. This can be done by transferring proven technologies from other type of power plants as well as implementing emerging EFW technologies, as described in Sections 4.2 and 4.4.

Energy efficiency can be analyzed by a simple first law thermodynamics analysis. However this approach is limited since it gives no direction in which optimization potential is still available. The energy efficiency optimization can be enhanced with a second law of thermodynamics analysis, which allows a more detailed look inside the process. This exergetic analysis is more complex but can be simplified by replacing its formulas with a numerical integral of the Carnot efficiency (heat quality) over the transferred heat. The numerically gained data can be used to generate expressive graphs, which make the results better understandable.

Different measures applied in waste incineration plants like air preheating, grate cooling, flue gas recirculation and different excess air ratios are investigated in Section 4.3. These parameters are not only varied in their normal range of application, but rather pushed to the values known from coal power plants. These optimization measures for the heat supply are finally combined with an optimized water steam cycle to get a high efficient EFW plant.

In Chapter 5 as a last step in the numerical plant optimization, the optimization of the furnace with computational fluid dynamic software is described. The modeling of the furnace allows to find improved nozzle arrangements for the over fire air and recirculated flue gas in order to improve the temperature profile, gas burnout and NO_x formation during the combustion process. The presented methods are finally used to design a waste to energy plant which fulfills the current needs of high energy efficiency, low NO_x emissions and still high availability, respecting the technologies and the knowledge in the field. Along with the steps in the design process details are discussed which are made visible by the application of the numerical methods.

In Chapter 6 additional important points for implementing the improved plant designed during this project are discussed. The guideline in this chapter suggests

an order on how different technologies should be implemented stepwise to gain knowledge and so reduce the risk for implementation.

2. Waste management and legal background for waste incineration

Dealing with waste in a sustainable way implicates the need to clarify the hierarchy of waste management. The waste hierarchy defines the priority in waste prevention and management legislation. The first steps are the so called 3 R's: reduce, reuse and recycle. If none of these three steps are possible, waste can be incinerated for the recovery of energy and resources from the residuals. Only noncombustible waste is allowed for disposal in landfills and underground dumpsites [2]. However energy has to be recovered in an efficient way. The European Commission defines an energy efficiency criteria (EE) in the appendix of the Waste Framework directive as followed [2]:

$$EE = \frac{E_p - (E_f + E_i)}{0.97 \cdot (E_w + E_f)} \tag{2.1}$$

In Equation 2.1 E_p is the annual equivalence energy produced in form of electricity and heat multiplied by there respective weighting factor (2.6 for electricity and 1.1 for heat). E_f is the energy input from other fuels contributing to the production of steam, while E_i is the energy imported by other energy streams, like electricity and auxiliary steam. E_p is the energy released by the combustion of waste and the factor 0.97 is an empirical value accounting for combustion, radiative and convection losses.

Since the end of 2008 new plants have to reach an EE value of 0.65 or higher to qualify for the so called R1 status for recovery. This is easily achieved by the supply of heat to a district heating network, due to the relatively high weighting factor for the supplied heat [3]. For EFW plants with electricity production only, reaching this value is not as easy using state of the art technology.

Other European countries like Austria and Switzerland have defined additional, more strict energy efficiency criteria, while in the Netherlands there is an additional subsidy on the electricity, if it is produced more efficiently than by state of the art technology [3].

The introduction of these criteria shows, that there was a considerable change in the perception of the public and governments. They recognized that landfilling can only be replaced by a combination of recycling and thermal treatment with energy recovery. This is shown by Themelis in the sustainable waste management ladder. Countries with the lowest share of landfill are on the top. These countries have an approximately equal share of recycling, composting and energy from waste [4].

One possibility to further optimize the efficient conversion of waste streams to energy is the use of an energy systems analysis (ESA). Such an analysis was performed by Münster for Denmark for the year 2025. Different technologies like efficient EFW plants ($\eta_{\mathrm{net,el}}$ 26-29 %), gasification, pyrolysis and liquefaction are considered for individual waste streams, with different final products, ranging from electricity and heat to chemical products like hydrogen, methanol or bio diesel. The result of this study showed that even in 2025 the main amount of waste is incinerated in EFW plants with combined heat and power generation [5].

In the study by Münster pyrolysis and gasification are technologies considered to have a big potential in a future waste management system. These technologies offer conversion with higher efficiency and flexibility in the production of either electricity or syngas for further use. However, experience so far showed that the implemented concepts do not achieve the design parameters during continuous operation. This is mainly caused by the inhomogeneous feed stock [6].

Most of the implemented gasification technologies are simply two-step oxidation, without the possibility for syngas production. The processes have a high consumption of auxiliary fuel and energy. Most of the equipment is operated at high temperatures, additionally gas cleaning and processing results in heat losses, which result in a lower fuel conversion efficiency than state of the art EFW technologies [7].

Themelis places anaerobic digestion and aerobic composting in his waste management hierarchy higher than EFW technologies [4]. Gohlke on the other hand presents the biomass paradox, which questions the separate collection and treatment of bio waste completely. The bio waste generated in urban areas is mostly contaminated with other waste and does not have the same quality and quantity as from farms or food processing companies. It should therefore not be composted or digested, but rather be collected and incinerated along with the normal municipal solid waste. At the same time most countries have subsidies on the generation of electricity and heat from different bio fuels, which are produced in huge quantities and high quality [8]. Combined waste incineration of both bio waste and municipal solid waste can help reduce the total processing cost in the waste management system, while keeping emissions low and energy

efficiency high. At the same time a sink is created for dioxins and other toxins otherwise recycled by common bio waste treatment options.

2.1. NO_x emissions

The directive on the incineration of waste by the European Commission has the aim to prevent or reduce the ecological damage imposed by the incineration of waste. The main concern is on the pollution of air, soil, surface and ground water as well as on the resulting risk on human health. In appendix V the emission limits for nitrogen oxides (NO_x) in the European Union are listed [9]. The emissions have the unit milligram per normal cubic meter of flue gas (mg/Nm^3). The flue gas volume flow is converted to normal cubic meters (Nm^3) at 0 °C and 101325 Pa for better comparison. The emissions can be referred to an oxygen (O_2) concentration of 11 vol.% and to dry flue gas. In Germany, referring to 11 vol.% O_2 is only done if the O_2 concentration excceds 11 vol.%. All give NO_x emission values given in this thesis are on a dry flue gas basis and without O_2 reference. The emission limits and how they are calculated is implemented in German law by the 17^{th} "Bundesimmissionsschutzverordnung" [10]. (See Table 2.1)

Table 2.1.: NO_x emission limits according to 17^{th} BImSchV [10], for EFW plants with a gross heat input of more than 50 MW_{th}. These values are valid for plants commissioned after the 1^{st} January 2013.

NO_x as NO_2	Emission limit [mg/Nm^3]
Half hourly average values	400
Daily average values	150
Yearly average values	100

In a study performed for the German Umweltbundesamt (UBA) all German energy from waste plants have been investigated. The yearly average values for different emissions as well as energy efficiency are compared. The study shows that for German plants all emissions except NO_x are far below the legal limits [11]. This fact is also shown for the Amsterdam EFW plant in [12]. The UBA study shows that most plants with selective catalytic reduction (SCR) have a yearly average NO_x emission below 100 mg/Nm^3, while plants using selective non catalytic reduction (SNCR) have higher emissions. So, depending on the NO_x reduction technology there is the possibility to reduce the NO_x emissions from

EFW plants even further. Therefore a change in emission legislation was made in Germany. New plants with a gross heat input of more than 50 MW_{th}, are allowed to emit only 100 mg/Nm^3 as yearly average, starting from 1st January 2013 [13].

2.2. CO_2 emissions

During the combustion of waste, in addition to toxic emissions, CO_2 is also emitted. This is the main source for the anthropogenic greenhouse gas effect. The only way how most of this emission can be avoided is to dump the waste on a state of the art sanitary landfill site with energy recovery. This implies the capture of methane gas (CH_4) and its utilization for power generation. Landfilling is however not an option, since waste contains valuable resources for power generation and metal recovery.

Taking CO_2 emissions as an energy efficiency indicator is not practical, since it results mostly in the suggestion of changing the fuel input [14]. Changing the fuel is not an option in this thesis since it deals with the incineration of a given feedstock: municipal solid waste. The energy efficiency of different plant configurations is assessed more practically by comparing the net electric efficiency. The efficiency of different process steps is rather compared by the performance of an exergy analysis.

The contribution of the German EFW plants to the overall CO_2 emissions is investigated by Wünsch. He compares different ways for improving energy efficiency, the achieved CO_2 reduction potential and their cost. The reduction cost of CO_2 emissions in EFW plants ranges between 38 €/t CO_2 and 64 €/t CO_2. The overall reduction potential of the EFW sector in Germany is in the range of 0.3 % of the total reduction potential. He describes an interesting effect: the negative effect of CO_2 emissions, by improving the burnout of the bottom ash, which results in higher energy efficiency as well as CO_2 emissions [15].

3. Theory

In this chapter the basic knowledge is described, which is needed to fulfill the goals defined in Chapter 1 and respecting the legal boundaries described in Chapter 2. It starts with information on the design of the boiler and post combustion zone. Section 3.2 focuses on how NO_x emissions are formed and how they are reduced. In the last Section of this Chapter computational fluid dynamics (CFD)is presented as a tool which is used to design a boiler according the theory described here. Theory on energy efficiency is presented in Chapter 4. Findings from different authors are discussed during the description of the optimization process, since it is important to have the information at hand to better understand the suggested changes in the incineration process and the water steam cycle.

3.1. Basic post combustion zone and boiler design criteria

For the design of an efficient EFW plant superheater corrosion is one of the main issues. Different methods on how corrosion can be reduced are presented in this section. A second issue is the design of the post combustion zone. The theoretical background and possible nozzle arrangements are also discussed in this section.

3.1.1. Superheater corrosion protection

High availability is one of the most important design criteria of EFW plants as stated by Kamuk in an interview [16]. Corrosion especially on the superheaters is one of the main effects responsible for reduced availability. A measure to keep the corrosion in an acceptable range is the use of moderate live steam parameters of 40 bar and 400 °C, as discussed in Section 4.2.2.3. Additionally other possibilities are investigated to keep the corrosion low even for higher live steam parameters to achieve higher efficiencies along with high availability.

3.1.1.1. Injection of sulfuric acid

An option is to inject sulfuric acid (H_2SO_4) into the flue gas. This changes the chemical equilibrium of corrosive components. Chlorine is bound more in form of HCl, than in more corrosive alkali and alkaline chlorides. These elements are rather bound as non-corrosive sulfates. So far a 1000 h test with a corrosion probe at the inlet of the convective pass and different materials have been performed in the Gothenburg EFW plant. For 16 Mo3 steel, typically used in superheaters a corrosion rate of 1 mm/a was determined at 450 °C without H_2SO_4 injection. The same corrosion rate was achieved at a probe with 525 °C with H_2SO_4 injection. For 450 °C no test with injection has been performed. H_2SO_4 for injection is generated in the wet flue gas treatment by using H_2O_2 in the scrubbers [17].

3.1.1.2. Increased residence time by improved boiler design

Similar changes in chemical equilibriums can be achieved by increasing the residence time of the flue gas in the temperature range from 880 °C to 800 °C. Hunsinger suggests a residence time of at least 4 s in this temperature range, preferably longer [18]. The HRC boilers in Amsterdam (Hoog Rendement Centrale) were designed to increase the residence time in this temperature range. Deposit samples taken from the walls of the vertical passes showed a rather high concentration of sulfates and low concentration of chlorides [19]. This is one of the explanations for the low corrosion in the HRC boilers documented by van Berlo and Simoes [20].

3.1.1.3. Reduced heat flux

Spiegel documented a correlation of corrosion rates with heat flux. Lower heat fluxes reduce the temperature gradient in the deposit on the wall [21]. This has an effect on the local chemistry and reduces corrosion. The heat flux in the radiation passes of the boiler depends only on the temperature difference between flue gas and wall. The effect of high temperature stratification in the flue gas is much more important than the average design flue gas temperature. In the convective part of the boiler the heat flux is influenced by the temperature difference but also by the flow velocity. Reducing the velocity decreases the heat flux into the pipes. Low flow velocities are also one of the design criteria of the HRC concept [12].

3.1.1.4. Nano ceramic coating

Another method to reduce corrosion was developed in another "KW21" research project at the University of Bayreuth. It consists of polysilazane derived ceramic coatings with glass filler particles. It is designed to be applied on membrane walls and superheater pipes. It consists of a 100 µm thick layer of ceramic directly backed onto the metal surface. The coatings can be easily applied and have good surface adhesion. Different modifications have been tested to reduce porosity and increase abrasion resistance. The coating was tested on a chloride containing melt to determine its properties to prevent corrosion [22]. Tests with applying the coating on superheater pipes in an EFW boiler have been performed; however results are not yet available.

3.1.1.5. Supherheaters at high flue gas temperature

An option is the steam boost process from Vølund, which places the superheater in the lower furnace in zones with lower corrosion risk close to the rear wall of the furnace. This is possible since the volatile corrosive elements are released in the early stages of the combustion on the grate [23]. Another option to superheat steam at low risk for corrosion is the use of a wall superheater (WSH) as patented by Rüegg and Ziegler [24]. For the wall superheater the pipes are arranged at high flue gas temperatures in the wall. They are covered with rear ventilated tiles. These are ceramic tiles which have a small gap between the superheater and the tiles. This gap is kept flue gas free by a slight over pressure generated by a low constant air flow introduced into the gap. The superheater pipes are placed over an insulation, which is placed on top of a normal membrane wall. This is a rather expensive construction, however not much experience with superheaters behind rear ventilated tiles is available and therefore the membrane wall is kept to keep the boiler gas tight. With more long-term experience it is possible to remove the evaporator membrane wall and construct the superheater as membrane wall or as tight arranged pipes as it is done in coal power plants [25] and put the tiles in front of it.
The heat transfer from the flue gas to the wall superheater is drastically reduced due to the additional insulation of the tiles. This increases the residence time of the flue gas at high temperatures (See Table 5.2). Therefore the positive effect described in Section 3.1.1.2 is also enhanced, by the use of a wall superheater.

3.1.2. Nozzle arrangement

An next important step in the combustion design is the choice of the nozzle arrangement for injection of recirculated flue gas and air. Optimizing the diam-

eter, quantities and direction of over fire gas nozzles is a typical task performed using CFD simulations [26].

Klasen investigated different nozzle arrangements typically used in EFW plants [27]. The main nozzle arrangements are:

- opposite boxer arrangement: Nozzles are arranged on both sides of the furnace, the jet of the nozzles meets close to the center of the furnace cross section creating an intense mixing zone at this point.
- Stitching arrangement: the nozzles are arranged alternating, so that the jet can cross the furnace cross section with low interaction with other jets. A mixing zone is created on circumference of the jet and between two jets from the opposite wall. A big disadvantage of the stitching arrangement is the increased fouling close to the nozzles. The gas jets accelerate fly ash particles through the hottest zones in the cross section to the opposite wall, where they stick to the wall, since they are partially melted.
- Stitching with big and small nozzles: a more intense mixing can be achieved using nozzles with different injection depths. This can be implemented by using nozzles with different diameters opposite to each other. The big nozzles are arranged in a stitching arrangement, while the small nozzles are used to generate an intense mixing zone not in the middle of the boiler, but rather close to the wall. An additional positive effect of the small nozzles is the counteracting impulse, which breaks the fly ash particles accelerated by the big injections, before they hit the wall.

Mixing is the most important part of the combustion process in EFW plants, since the chemical reactions are not the limiting factor of the combustion.

Doležal simply states this fact as: $mixed = combusted$ [28].

Mixing occurs at different levels: in micro scale it is achieved by diffusion and turbulence, in the macro scale by the fluid flow influence by the arrangement of the injection jets. Shear stress at the outside of the jet results in eddies which are important for the mixing. The shear stress decelerates the jet and broadens it as shown in Figure 3.1. The mass flow rate and impulse of such a jet can be calculated using Equation 3.2 and 3.1 [28]. The deceleration depends on the diameter of the injection nozzle and therefore also the micro scale mixing. For the same mass flow rate nozzles with bigger diameter have less impulse since the injection velocity decreases, the circumference of the injection however increases resulting in bigger part of the furnace with high shear stress.

$$\dot{I} = 2 \cdot \pi \int_0^{\frac{d_0}{2}} \rho \cdot w^2 \cdot R dR \tag{3.1}$$

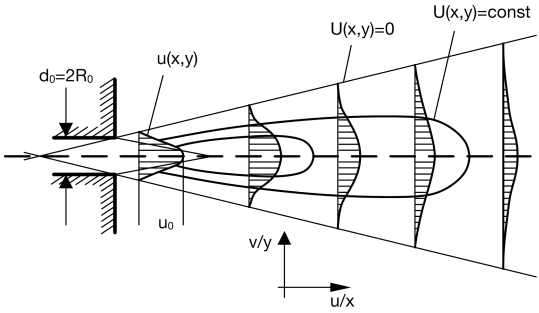

Figure 3.1.: Velocity decrease in an injection jet (adapted from [28])

$$\dot{m} = 2 \cdot \pi \int_0^{\frac{d_0}{2}} \rho \cdot w \cdot R dR \tag{3.2}$$

The impulse ($\dot{I}$) and the mass flow rate ($\dot{m}$) depend on the density (ρ), the velocity in injection direction (w) and the radius of the injection nozzle (d_0) and (R).

3.2. NO_x emissions

In Section 2.1, the demand of lower NO_x emissions from EFW plants due to the change in legislation was discussed. In this section, NO_x formation mechanisms as well as NO_x reduction possibilities, with focus on combustion engineering measures and their implementation are presented.

3.2.1. NO_x formation

Three main formations mechanism for NO_x are known: these are the fuel NO_x mechanism, the thermal NO_x mechanism, and the prompt NO_x mechanism. Depending on the combustion settings, the contribution of the individual mechanism to the total NO_x emissions can vary significantly.

3.2.1.1. Fuel NO_x reaction paths

Every fuel contains a small fraction of nitrogen compounds, which are released during the combustion process. These are converted to N_2, NO, NH_3, or HCN depending on the combustion conditions and the bonding of nitrogen in the fuel. The concentration of N_2 released from the fuel is negligible compared to the concentration of N_2 in the combustion air. NH_3 and HCN are so-called NO_x precursor species, which can react further to NO. All three species relevant for the formation of NO_x emissions are combined by Eberius according to Equation 3.3 to a value called total fixed nitrogen (TFN) [29].

$$x_{TFN} = x_{NO} + x_{NH_3} + x_{HCN} \tag{3.3}$$

In Equation 3.3 the mole fractions of NO, NH_3, and HCN (x_{NO}, x_{NH_3}, and

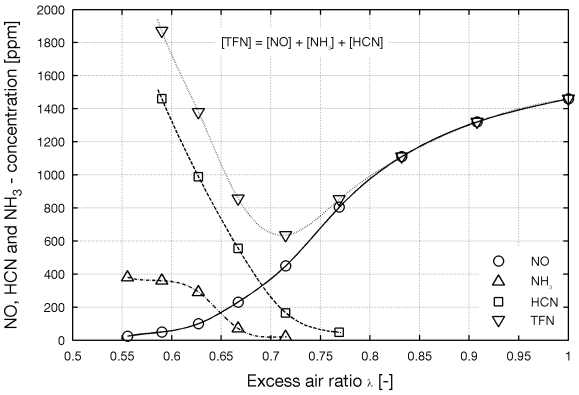

Figure 3.2.: Concentration of NO, NH_3 and HCN and TFN in a methylamine doped propane flame for different excess air ratios (adapted from [30], original diagram from [29])

x_{HCN}) is used to calculate the mole fraction of TFN x_{TFN}. Eberius measures the concentration of NO, NH_3, and HCN in a propane flame doped with methylamine for different excess air ratios and determines the TFN concentrations shown in Figure 3.2. For mixtures with an excess air ratio below 0.7, the concentration of HCN and NH_3 are mainly responsible for high TFN concentrations, while for combustion with a higher excess air ratio, the nitrogen is bound only in NO. A minimum in total fixed nitrogen can be seen for an excess air ratio close to 0.7. The TFN concentration at an excess air ratio of 0.7 is less than half than

for an excess air ratio of 0.6 and lower or 0.9 and higher. The effects causing this minimum can be understood best by looking at the different chemical reactions taking place. These reactions are taken from the detailed chemical kinetic mechanism (DCKM) presented by Miller and Bowman [31]. The reactions are sorted and arranged as presented by Kolb [32]. HCN, as one of the main NO_x precursors, can react with O radicals to NCO and then further to form a NH radical (See Reactions 3.4 and 3.5). NH can also be directly formed from HCN (See Reaction 3.6). As byproduct CO is formed.

$$HCN + O \rightleftharpoons NCO + H \tag{3.4}$$
$$NCO + H \rightleftharpoons NH + CO \tag{3.5}$$
$$HCN + O \rightleftharpoons NH + CO \tag{3.6}$$

An alternative path for the decomposition of HCN is with an OH radical to form CN and H_2O. CN reacts with an additional OH radical to NCO and then follows the path described by Reaction 3.5:

$$HCN + OH \rightleftharpoons CN + H_2O \tag{3.7}$$
$$CN + OH \rightleftharpoons NCO + H \tag{3.8}$$

A third path for the decomposition of HCN also needs an OH radical and forms the intermediate species HOCN or HNCO (See Reactions 3.9 and 3.10). The final species for this pathway is NH_2 along with CO (See Reaction 3.12).

$$HCN + OH \rightleftharpoons HOCN + H \tag{3.9}$$
$$HCN + OH \rightleftharpoons HNCO + H \tag{3.10}$$
$$HOCN \rightleftharpoons HNCO \tag{3.11}$$
$$HNCO + H \rightleftharpoons NH_2 + CO \tag{3.12}$$

All reaction paths are shown in Figure 3.3. The reactions starting from HCN are rather slow due to the strong bonding of the H atom. Therefore these reactions act as a bottleneck during the decomposition of HCN [33]. In a more detailed definition of TFN, the fixed nitrogen of all intermediate species has to be accounted as well (See Equation 3.13).

$$x_{TFN} = \sum x_{Ncontaining\ species\ (excludingN_2)} \cdot n_{Natoms\ per\ species} \tag{3.13}$$

Where the mole fraction of TFN (x_{TFN}) is calculated by summing up the mole fractions of all nitrogen containing species ($x_{Ncontaining\ species\ (excludingN_2)}$) mul-

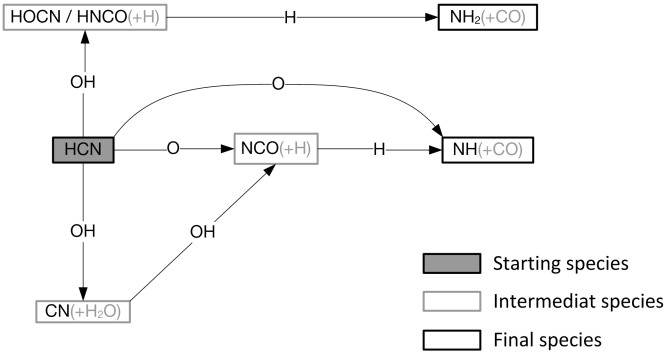

Figure 3.3.: Reaction paths of HCN to NH_i radicals (adapted from [32])

tiplied by their respective number of nitrogen atoms ($n_{Natoms\ per\ species}$). Using this formulation, it can be seen that the total fixed nitrogen does not change along all possible pathways for the HCN decomposition. It has to be pointed out that the presence of O and OH radicals is necessary for the decomposition of HCN. Looking back to Figure 3.2 the effect of the radicals can be seen. For excess air ratios below 0.7, the TFN concentration is mainly dependent on the HCN concentration since there is not enough oxygen available to form the radicals necessary to start the reaction pathways, since the oxygen reacts rather with the main fuel.

As shown above, HCN forms NH and NH_2 radicals. They react further along the same radicals formed during the decomposition of NH_3 (See Reaction 3.14 to 3.18). For these reactions, again the presence of OH radicals is of importance; but the dependence is not so strong since they are also possible with H radicals.

$$NH_3 + OH \rightleftharpoons NH_2 + H_2O \tag{3.14}$$
$$NH_2 + H \rightleftharpoons NH + H_2 \tag{3.15}$$
$$NH_2 + OH \rightleftharpoons NH + H_2O \tag{3.16}$$
$$NH + H \rightleftharpoons N + H_2 \tag{3.17}$$
$$NH + OH \rightleftharpoons N + H_2O \tag{3.18}$$

The NH_2 radical reacts with O radicals to HNO, which can be converted to NO. For all reactions with participation of HNO, the total fixed nitrogen remains

unchanged.

$$NH_2 + O \rightleftharpoons HNO + H \tag{3.19}$$
$$HNO + M \rightleftharpoons NO + H + M \tag{3.20}$$
$$HNO + OH \rightleftharpoons NO + H_2O \tag{3.21}$$
$$HNO + NH_2 \rightleftharpoons NO + NH_3 \tag{3.22}$$

Oxygen for the oxidation of NH radicals in the form of O and OH radicals or O_2 is needed to form NO. This reaction is directly possible or with HNO as intermediate species. For these reaction paths, the total fixed nitrogen is constant.

$$NH + O_2 \rightleftharpoons NO + OH \tag{3.23}$$
$$NH + O \rightleftharpoons NO + H \tag{3.24}$$
$$NH + O_2 \rightleftharpoons HNO + O \tag{3.25}$$
$$NH + OH \rightleftharpoons HNO + H \tag{3.26}$$

Another direction is taken if NH_2 radicals react with NO, a decomposition to N_2 is directly possible. Other paths have NNH as intermediate species. Since N_2 is not included in the TFN concentration, the paths leading to N_2 reduce the TFN concentration.

$$NH_2 + NO \rightleftharpoons N_2 + H_2O \tag{3.27}$$
$$NH_2 + NO \rightleftharpoons NNH + OH \tag{3.28}$$
$$NNH \rightleftharpoons N_2 + H \tag{3.29}$$
$$NNH + NO \rightleftharpoons N_2 + HNO \tag{3.30}$$

NH radicals can also react with NO forming N_2O, which is reduced to N_2. This pathway reduces the TFN concentration, but some of the N_2O remains due to the chemical equilibrium. N_2O is included in the broad range of NO_x emissions.

$$NH + NO \rightleftharpoons N_2O + H \tag{3.31}$$
$$N_2O + H \rightleftharpoons N_2 + OH \tag{3.32}$$

NH_2 radicals can directly react with NH radicals and decompose each other to N_2, without the presence of NO as shown in Equation 3.33 to 3.36.

$$NH_2 + NH \rightleftharpoons N_2H_2 + H \tag{3.33}$$
$$N_2H_2 + M \rightleftharpoons NNH + H + M \tag{3.34}$$
$$N_2H_2 + H \rightleftharpoons NNH + H_2 \tag{3.35}$$
$$NNH \rightleftharpoons N_2 + H \tag{3.36}$$

All reaction paths are shown in Figure 3.4 with NO and N_2 as the final species.

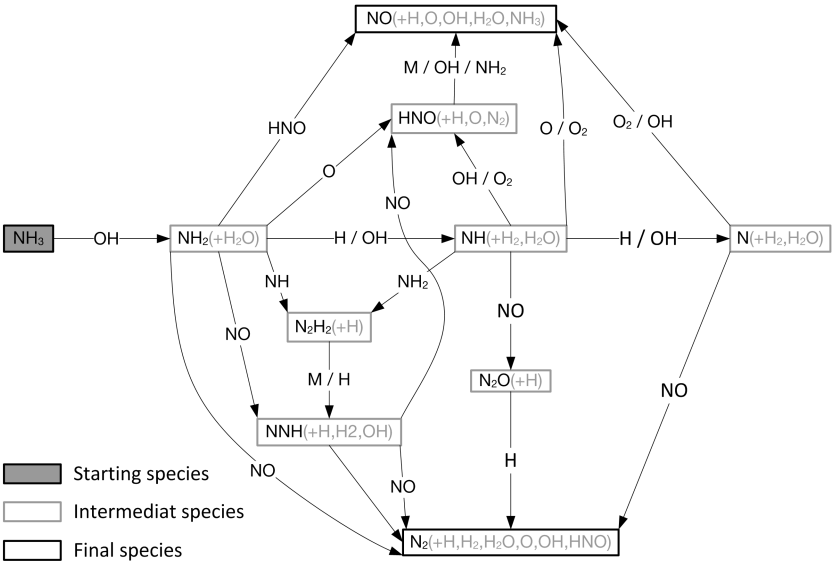

Figure 3.4.: Reaction paths of NH_3 and NH_i radicals to NO and N_2, (adapted and extended from [32])

The reaction paths leading to NO depend on the presence of oxygen, while it is important to point out that nearly all paths toward N_2 require NO as one of the reactants. Theses paths are responsible for decreasing the TFN concentration. For each mole of N_2 formed, two moles of either NO, NH_3 or HCN are needed, which is beneficial for the reduction of the TFN concentration. In Figure 3.2, the NH_3 concentration stays at a level of 380 ppm until the point where the NO concentration starts to rise. Only then the decomposition toward N_2 is

possible. At the TFN minimum in this figure, the oxygen concentration was high enough for the decomposition of HCN, without oxidizing the resulting NH_i radicals. Some NO is however formed, which is needed to reduce NH_i radical concentration. For excess air ratios higher than 0.75, enough oxygen is present so that mainly the oxidation (See Reaction 3.19 to 3.26) of the NH_i radicals takes place.
NO cannot only react with NH_i radicals but also with C, CH_i radicals and HCCO. This mechanism is also known as reburn or NO recycle mechanism, since it forms HCN and CN in the process (See Figure 3.5 and Reactions 3.37 to 3.43). HCN and CN react according the previous discussed reactions, to form new NH_i-radicals. This mechanism also keeps the TFN concentration unchanged. It however allows for a decomposition during the stage as NH_i radicals. As discussed above, the HCN decomposition mechanism is a bottleneck in the NO recycle process due to slow reaction rates.

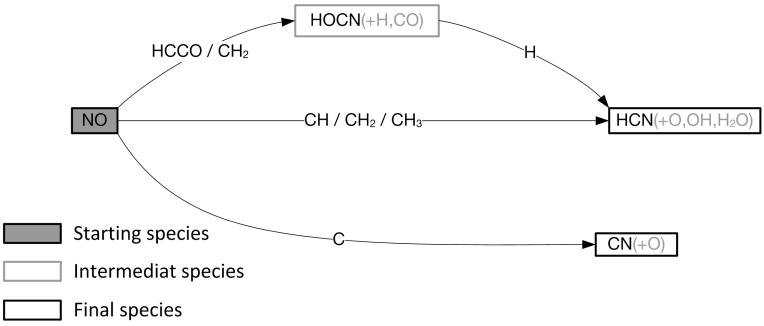

Figure 3.5.: Reaction paths for the NO recycle mechanism (NO to HCN and CN)

$$C + NO \rightleftharpoons CN + O \tag{3.37}$$
$$CH + NO \rightleftharpoons HCN + O \tag{3.38}$$
$$CH_2 + NO \rightleftharpoons HCN + OH \tag{3.39}$$
$$CH_2 + NO \rightleftharpoons HCNO + H \tag{3.40}$$
$$CH_3 + NO \rightleftharpoons HCN + H_2O \tag{3.41}$$
$$NO + HCCO \rightleftharpoons HCNO + CO \tag{3.42}$$
$$HCNO + H \rightleftharpoons HCN + OH \tag{3.43}$$

3.2.1.2. Thermal NO_x reaction paths

Nitrogen is introduced into the combustion process not only by the fuel, but also by the air in the form of N_2. The N_2 molecule is kept together by a stable triple bond and to break this bond much energy is necessary, which is only available for temperatures above 1300 °C. The thermal NO_x mechanism, also called the Zeldovich mechanism, after its discoverer, is only of importance in combustion systems reaching high temperatures in an oxygen rich zone [34]. The mechanism consists of Reactions 3.44 to 3.46. These reactions are partly included in Figure 3.4 and Figure 3.6.

$$O + N_2 \rightleftharpoons NO + N \tag{3.44}$$

$$N + O_2 \rightleftharpoons NO + O \tag{3.45}$$

$$N + OH \rightleftharpoons NO + H \tag{3.46}$$

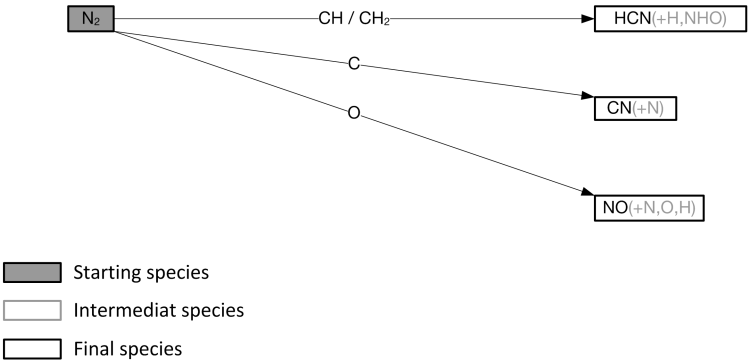

Figure 3.6.: Reaction paths of prompt mechanism (N_2 to HCN and CN) and thermal mechanism (N_2 to NO)

3.2.1.3. Prompt NO_x reaction paths

Nitrogen from the combustion air can also react directly with C or CH_i radicals to form CN and HCN. These products react then along the HCN decomposition paths. This reaction path was first described by Fenimore [35]. The mechanism

requires high temperatures due to the triple N_2 bond and fuel rich zones. For industrial combustion processes it is however rather insignificant compared to the fuel and thermal mechanism [36].

$$CH + N_2 \rightleftharpoons HCN + N \tag{3.47}$$

$$C + N_2 \rightleftharpoons CN + N \tag{3.48}$$

$$CH_2 + N_2 \rightleftharpoons HCN + NH \tag{3.49}$$

All reaction paths of molecular nitrogen N_2 (thermal and prompt) are shown in Figure 3.6. Both the thermal and prompt mechanism result in an increase of the TFN concentration. The combustion process has to be tuned to avoid these reactions, which is simplest done by reducing the temperature in oxygen rich zones.

3.2.1.4. NO_x emissions in grate based EFW plants

Grate based combustion systems for municipal solid waste are operated at low temperatures compared to the combustion of coal, oil or gas, therefore the contribution of thermal and prompt mechanism are low in the overall NO_x formation. Sørum et al. determined that 95 % of all NO_x emissions are in form of NO, the rest are NO_2 and N_2O. Between 80 and 90 % of the emissions can be attributed to the fuel NO_x mechanism. While the thermal NO_x mechanism contributes with a fraction of 5 % to 10 % , only a small fraction is prompt NO_x [37]. Hafner has presented results that these NO_x formation theories are also validated for the incineration of waste, which is supported by data measurements. More than 99.7 % of the total fixed nitrogen measured in different combustion stages is formed out of the three main species NO, NH_3 or HCN [30].

3.2.2. NO_x reduction

The NO_x emissions released during the combustion process are typically higher than the legal limits and therefore it is necessary to reduce the emissions. Spliethoff defines two different categories of reduction technologies [36]:

- methods applied downstream of the furnace, called from now on post combustion measures
- combustion engineering measures

3.2.2.1. Post combustion measures

Post combustion measures, as the name says, are measures which can be applied after the combustion process is already finished. NO_x emissions are reduced

from a given raw concentration below the limits legally effective for the plant. These are options which can easily be implemented as a retrofit installation in the boiler or before the stack of existing combustion facilities.

SNCR: Selective non catalytic reduction A typical method for reducing the NO_x emissions in EFW plants is to inject ammonia (NH_3) or urea (NH_2CONH_2) into the flue gas. This process is called selective non catalytic reduction. Ammonia reduces NO according to the global Reaction 3.50 and urea reacts according to Reaction 3.51 given by Spliethoff [36].

$$4NO + 4NH_3 + O_2 \rightleftharpoons 4N_2 + 6H_2O \tag{3.50}$$

$$2NO + NH_2CONH_2 + 1/2O_2 \rightleftharpoons 2N_2 + 2H_2O + CO_2 \tag{3.51}$$

Detailed intermediate reactions for the SNCR mechanism with ammonia are given by Glarborg in [38]. The injection of the reduction agent has to occur in a narrow temperature window between 850 °C and 1050 °C. With an optimized installation, reduction rates of 85 % can be achieved at the highest point [39]. During the combustion process in EFW plants, the flue gas temperature can change by 150 °C to 200 °C in a few seconds due to the inhomogeneous fuel. Also during load changes the local temperature changes. Therefore several injection levels are necessary and a fast and sophisticated control system based on acoustic pyrometers [40] or infra-red pyrometers [41] is necessary to switch between injection levels and account for temperature strands.

SCR: Selective catalytic reduction An alternative post combustion measure for reducing NO_x emissions is the use of selective catalytic reduction. A catalyst (vanadium pentoxide or, alternatively molybednum, copper or iron oxide) is used to convert NO and NO_2 according to Reactions 3.50 and 3.52 [36] at lower temperatures.

$$2NO_2 + 4NH_3 + O_2 \rightleftharpoons 3N_2 + 6H_2O \tag{3.52}$$

The catalyst can be designed to operate at a temperature between 180 °C and 400 °C and different configurations are possible. As retrofit, a tail end configuration is typical, this implies reheating of the flue gas to operating temperatures. For a new installation, a raw gas catalyst is commonly chosen, since it is more energy efficient [42]. The emission reduction rate is rather high, reaching up to 90 %. This value is however a practical limit due to non-homogeneous emission distribution in the flue gas stream [36]. The pressure drop over a full scale catalyst costs about 0.3 €/t to 0.5 €/t waste in power consumption of the induced

draught fan [43]. This can be arranged in a 2 layer system with an option for a 3rd layer. This is suggested by Chomec for a full SCR catalyst to reduce costs by an optimized catalyst replacement scenario [43]. The pressure drop can be reduced by installing a selective non catalytic reduction (SNCR) system and a smaller catalyst as slip catalyst.

3.2.2.2. Combustion engineering measures

Combustion engineering measures directly influence the combustion process and therefore affect the plant design more severely than post combustion measures. The measures can be divided in two categories [36] (See Figure 3.7):

- fuel staging
- air staging

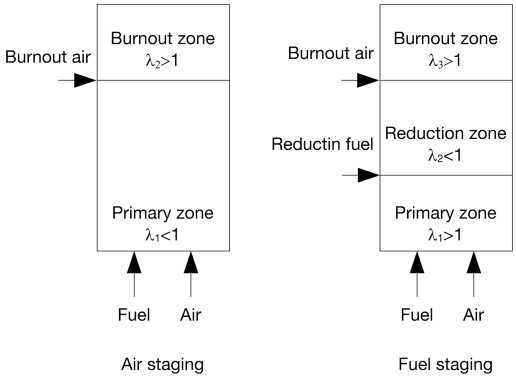

Figure 3.7.: Air and fuel staging in a combustion process (adapted from [36])

Both methods work with a combination of fuel rich and fuel lean zones during the combustion process to reduce the total fixed nitrogen. The different zones favor the respective pathways according to the reaction presented in Figures 3.3, 3.4, and 3.5 and try to avoid the reaction paths from Figure 3.6. For volatile fuels like lignite, the combination of different combustion engineering measures is enough to keep the emissions below the emission limits [36]. Sørum et al. concludes from his experiments that for the incineration of municipal solid waste, an emission reduction of 70 % starting from a NO_x concentration of 350 mg/Nm^3 to 600 mg/Nm^3 is possible [37]. This reduction potential is available due to the volatile nature of the fuel.

Fuel staging As the name suggests, fuel staging involves adding fuel in two steps. In the primary zone, more air is added than needed for complete combustion, resulting in an air rich condition. The NO_x emissions from this zone are rather high and therefore additional fuel is added in a second stage, favoring the NO recycle reactions. New HCN is formed, which is converted to NH_i radicals to reduce some of the NO. This reduces the TFN concentration. As reduction fuel, added in the later stages sometimes a different fuel is used. For coal this can be natural gas or gasified coal. As a last stage of the process air is added. This can be done in one step or in several steps.
Kolb investigated fuel staging for natural gas combustion in a 350 kW_{th} test facility. The primary zone was operated with an excess air ratio of 1.1 to 1.2. In the reduction zone, a temperature of 1300 °C was kept for about 0.5 s and an excess air ratio of 0.84 to 0.92 was tested. The resulting NO_x emissions are in the range of 63 ppm to 168 ppm. The reduction improved if the NH_3 concentration in the reduction fuel was increased [32].
Spliethoff tested fuel staging in a 160 MW_{th} slag-tap furnace with coke-oven gas and tar oil as a reduction fuel. In this large scale test, the homogenous mixing of the reburn fuel into the reduction zone was a critical parameter. The consumption of the reduction fuel could be minimized if the main combustion zone was operated just slightly over stoichiometric. An emission reduction from 1000 mg/Nm^3 to 350 mg/Nm^3could be achieved [44].
Fuel staging for biomass combustion was investigated by Salzmann. Modeling the combustion as a combination of plug flow and mixing reactor using the GRI 2.11 detailed chemical kinetic mechanism, a reduction rate between 82 % and 95 % was determined. From experiments using a similar setup, only a reduction of 72 % could be confirmed [45].
Fuel staging is not used in EFW plants since the emission can be reduced more economically using post combustion measures.

Air staging For air staging, only the air is added in several steps. This is a measure already used in every grate based EFW plant. However, the main aim of this measure is not to reduce NO_x emissions, but rather to guarantee a good burnout of the flue gas. The over fire air is mainly used to mix the gases released from the waste bed and to supply additional oxygen. Also, the residence time between primary zone and burnout zone is rather short.
Maier et al. investigated air staging for pulverized coal combustion. The residence time in the under stoichiometric zone can be influenced by the location at which the burnout air is added. Increasing the residence time in this zone improves the NO_x reduction since there is more time available for the formation of NH_i radicals from HCN and their reaction with NO [46].

Zuberbühler and Baumbach tested air staging for several configurations (A normal, B air staging and E air staging and reduction zone) for a small biomass fired boiler. The tests were performed with fuel doped with nitrogen to investigate the effect for higher TFN concentrations. The results of their investigation are presented in Figure 3.8. NO_x reduction rates for their combustion setup were limited to 40 % [47]. Similar tests and results on the NO_x emissions depending on the nitrogen content of the fuel were performed by Hafner [30].

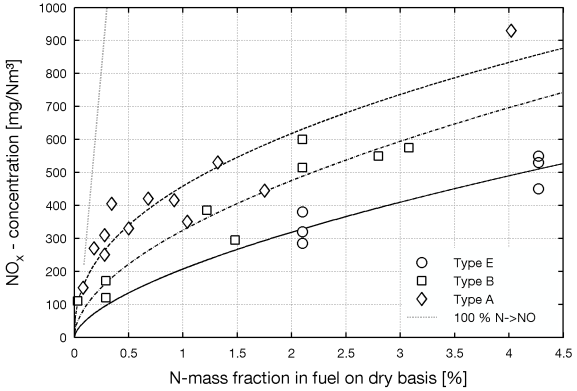

Figure 3.8.: NO_x emissions for different combustion configurations and fuel nitrogen contents,(adapted from [47])

As mentioned above, air staging is already used in EFW plants, however the flue gas is too inhomogeneous in the reduction zone. Some parts of the flue gas are strongly over stoichiometric, while others can have a heating value of up to 5 MJ/Nm^3 [48]. This results in a low NO_x reduction potential by air staging. This can be extremely improved by homogenizing the flue gas before it enters the burnout zone. Husinger presents results of using a jet of water and pressurized air to mix the flue gas in the lower furnace. This improves the reduction of TFN since NO that has already formed can react with NH_i radicals. A reduction of 75 % was achieved in a small scale test facility [48].

Another implementation of air staging in EFW plants is the Very Low NO_x (VLN) technology patented by Martin [49]. Excess flue gas with high oxygen content is sucked from the rear part of the lower furnace to reduce the stoichiometry before the post combustion zone below 1. There the secondary air is supplied so that the flue gas leaves the post combustion zone with an excess air ratio of about 1.1 to 1.2. The secondary air mixes the inhomogeneous flue

gas stream and has the same effect as intended by Hunsinger. The reduction effect is however not so good since air adds oxygen and the NO formation paths dominate. The previously extracted flue gas is reinjected further downstream and has no significant effect on the combustion process. Its main purpose is to reduce inhomogeneity of the flue gas in respect of temperature and species concentration. The stronger under stoichiometric zone results in a NO_x emissions below 300 mg/Nm^3 [50].

Tests on such a VLN boiler with reduced secondary air were documented by Martin. In this case, even after the normal post combustion zone the excess air ratio was below 1. Additional air is injected along with the extracted gas to guarantee good gas burnout. This increases the residence time with reducing conditions and the reduced volume flow rate of secondary air improves the mixing and partially oxidizes the flue gas to improve the reduction of the TFN. A reduction in NO_x emissions of 75 % was achieved [51].

3.2.2.3. Combined staging

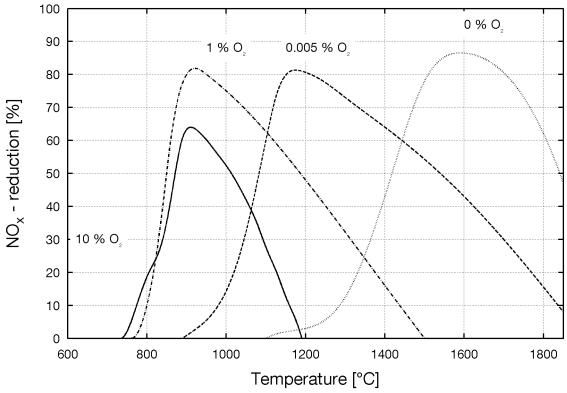

Figure 3.9.: Reduction efficiency and temperature window of ammonia injection for different oxygen contents (adapted from [36] original data from [52])

An additional combustion engineering measure is the so-called combined staging. It is not yet implemented on full scale power plant, however some investigations have been made. Figure 3.9 shows the dependence of NO_x reduction efficiency of ammonia injection from the oxygen concentration in the flue gas. This suggests

that the NO_x emissions can be reduced by injecting ammonia in under stoichiometric zones in the furnace. The temperature window is not as narrow as for higher oxygen contents and the reduction efficiency improves. This works since the concentration of NH_i radicals is increased and so the pathways leading to the reduction of TFN can be used. The combination of fuel staging with ammonia injection was tested by Spliethoff [44].

Zabetta et al. performed a theoretical investigation on combined staging with multi stage burnout air, which resulted in a stepwise reduction of the TFN concentration [53].

The influence of adding NH_3 into the reburn fuel, as well as injecting NH_3 in under stoichiometric zones were investigated by Greul. His results showed no positive effect on the doping of the reburn fuel, since NH_3 oxidized along with the reburn fuel in the burnout stage. Injecting NH_3 in fuel rich zones on the other hand reduced the NO_x concentration from 440 mg/Nm^3 to 250 mg/Nm^3 [54].

3.3. Computational fluid dynamics

The reference document for best available technique for waste incineration suggests the use of physical and computer models to investigate the effect of design features [26]. To describe the processes properly which take place during the combustion of waste complex and computational expensive computer models are necessary, however computer models become more dominant since a doubling in calculation power was postulated by Moore in 1965 in every two years [55]. This trend is still valid and the increase in computational performance allows the use of more sophisticated models. The use of computer models is beneficial since many parameters can be investigated without risk to real plants and with rather low cost. Computational fluid dynamics is used to simulate the flue gas flow along with chemical reactions and heat transfer. ANSYS Fluent 14.0 is used as the CFD software for this work. In this Section, the basics of computational fluid dynamics are presented along with the detailed description of the models used later on to optimize the combustion process. Of most importance are the inlet boundary conditions of the waste bed along with the used NO_x model, which are discussed in detail. The validation of the NO_x model was performed as part of this thesis. The results are however presented in the theory Chapter, since the focus of this thesis lies in using the models to the design an improved plant.

3.3.1. CFD Modelling

Different CFD software packages such as Fluent, CFX, STAR-CCM or OPENFOAM are available to solve fluid dynamic problems numerically. These programs are able to solve balancing equations for mass, species, phases, energy and impulse, as well as characteristic values to describe turbulence on a discrete mesh. Also, transport equations for heat conduction, radiation, diffusion, phase change, and chemical reactions can by analyzed using defined initial conditions and boundary conditions.

Different computational investigations for grate based combustion systems have already been performed for biomass by Dong and waste by Klasen in their PhD thesis [56], [27]. Basic information on numerical investigations can be found in their work.

3.3.1.1. Governing Equations

The governing equations for mass, impulse, energy, species and phases are a combination with specific mathematical models. This results in a complex system of nonlinear, partial differential equations. The complexity of this system cannot be handled analytically and therefore it is solved numerically. The general governing equation is presented below in tensor form (See Equation 3.53):

$$\frac{\partial \rho \Phi}{\partial \tau} = \frac{\partial \rho w_i}{\partial x_i} + \frac{\partial \Gamma_\Phi}{\partial x_i}\frac{\partial \Phi}{\partial x_i} + S_\phi \tag{3.53}$$

The first term in Equation 3.53 is the transient term for the transport equation, the second term represents the diffusion, the third describes the convection and the last term is the source term. The different parameters for the main governing equations are presented in Table 3.1

Table 3.1.: Parameter for the governing equation for mass, impulse, energy and species transport [57]

Governing equation	Transport variable Φ	Exchange coeffcient Γ_Φ	Source S_ϕ
Mass	1	0	0
Impulse	w_i	μ	S_{imp}
Thermal energy	h	μ/Pr	$S_h = S_{rad} + S_{chem}$
Species	y_{comp}	D	S_{comp}

Simplified models are used along with the governing equations to solve specific tasks. Some of these models are presented in Section 3.3.1.2 to 3.3.2.4.

3.3.1.2. Turbulence modeling

Like in most technical applications, the flue gas flow in EFW boiler is turbulent. In comparison to laminar flow, turbulent flow has higher diffusivity, viscosity and thermal conductivity and this is mainly caused by a fluctuation of the velocity. The velocity can be described by a constant part v and a fluctuating part v'. CFD programs offer a wide range of turbulence models. In this work the "realizable k-ϵ" model is used, since it is most commonly used in combustion simulation. For this model two individual transport equations are solved to determine characteristic values for the turbulence. The eddy viscosity μ_t is the relevant value for the turbulence and is determined by the use of Equation 3.54.

$$\mu_t = \rho \cdot C_\mu \cdot \frac{k^2}{\epsilon} \tag{3.54}$$

The "'realizable k-ϵ"' model uses an enhanced formulation for the eddy viscosity (μ_t), where the factor C_μ depends also on the tension and rotation rate of the system as well as the turbulent field itself [57]. Other variables in Equation 3.54 are the density (ρ), the turbulent kinetic energy (k) and the dissipation rate (ϵ).

3.3.1.3. Combustion modeling

The species transport equation is solved to investigate mixing, transport and reaction phenomena. The combustion reactions taking place in the furnace strongly depend on the turbulence of the flow. To model the chemical reactions, a reaction model which couples the reaction rate to the turbulence is necessary. A simple model in this regards is the eddy dissipation model (EDM). This is a simplification of the more complex eddy dissipation concept model. This is acceptable as the combustion processes are mostly limited by mixing. In turbulent reacting flows the mixing of reactants at molecular level occurs only a the lowest turbulent structures. The model assumes no mixing at higher levels as well as infinitely fast irreversible chemical reactions in the lower levels. Therefore it is suggested to be used only in one or two step reactions, to guarantee the quality of the results [57].

The main combustion reaction taking place in gas phase of EFW boiler is the oxidation of CO. Turns lists the Reaction 3.55 to 3.60 for the CO oxidation

process [34].

$$CO + O_2 \rightleftharpoons CO_2 + O \tag{3.55}$$
$$O + H_2O \rightleftharpoons OH + OH \tag{3.56}$$
$$CO + OH \rightleftharpoons CO_2 + H \tag{3.57}$$
$$H + O_2 \rightleftharpoons OH + O \tag{3.58}$$
$$O + H_2 \rightleftharpoons OH + H \tag{3.59}$$
$$OH + H_2 \rightleftharpoons H_2O + H \tag{3.60}$$

A CFD investigation with the detailed chemical kinetic model (DCKM) of Miller and Bowman [31] performed by Angerer showed that more than 99 % of the CO is oxidized by Reaction 3.57 in EFW boilers [58]. Combustion simulation for EFW boilers using DCKM with similar results have been performed by Frank [59].

Using this reaction along with Reaction 3.59 leads to the simplified combustion model using Reactions 3.61 and 3.62 for the burnout of the burnable part of the flue gas released from the waste bed.

$$CO + H_2O \rightleftharpoons CO_2 + H_2 \tag{3.61}$$
$$O_2 + H_2 \rightleftharpoons H_2O \tag{3.62}$$

3.3.1.4. Radition modeling

In comparison to the thermal conductivity and convectional heat transfer, the heat transport by thermal radiation is a function of temperature to the 4 power. Therefore heat transfer by radiation dominates for systems operating at high temperature. This is especially valid in combustion systems. In technical combustion processes, the thermal radiation is emitted from soot and other particles as well as the gases H_2O and CO_2 [60].

Typical CFD models for calculating the radiation interaction in combustion systems are the discrete ordinate (DO) radiation model and the P_1 radiation model. For small geometries like EFW boilers with an optical thick gas the P_1 model can be used.

The P_1 model is a first order approximation of the general spherical harmonics method, which defines the radiation intensity orthogonal to a unity sphere. The resulting simplification can be solved similar to transport equations for impulse. The absorption coefficient is one of the most important coefficients for radiation modeling, since it determines the radiation interaction of the fluid. During the combustion of waste not only gas is released but also fly ash and soot particles. These particles have a significant impact on the absorption coefficient of the

gas. Soot particles are present in very high quantities and therefore cannot be simulated individually, but rather as a continuous phase (Euler-Euler particle simulation).

Soot modeling The used CFD software has a model for the formation and oxidation of soot as well as its radiation interaction readily implemented. The emissions of soot radiation peaks at the infrared spectra [34], therefore it is important to include the impact of soot in the simulation. The soot model adds a term to the absorption coefficient of the gas depending on the soot concentration. The soot concentration depends however on the combustion process on the grate. Hunsinger published soot concentrations along with CO concentration determined above the grate of a small scale waste incineration test facility. CO concentrations of 60 g/Nm^3 and 2.5 g/Nm^3 of soot were measured for a primary excess air ratio of 1.2 [61]. These values have been used by Jell to determine a multiplication factor for the ratio of soot and CO at the waste bed to reach 60 g/Nm^3 CO and 2.5 g/Nm^3 of soot at the same distance from the waste bed [60]. The ratio he determined is 0.038, which was used for some of the simulations. Due to a bug in the used software, only one CFD simulation could be run with a small number of cells. Therefore the soot model was not used on the full boiler geometry investigated in this thesis.

A test was performed by Jell to determine the influence of the soot model on the flue gas temperature. Without soot radiation interaction the flue gas is about 20 °C to 25 °C hotter, especially in the lower furnace [60]. So simulations without the soot model are more conservative regarding the gas temperature in the lower furnace.

A comparison of both radiation models (P1 and DO) for EFW boilers was also performed by Jell and showed a 100 °C higher flue gas temperature for the DO model [60]. This implies less heat is transferred to the walls and the optical thickness of the flue gas is more significant. An investigation on the radiation in coal boilers showed that more heat than generally expected is transferred by radiation from the hotter part of the furnace to colder walls further away [62]. This implies an optical thinner flue gas, which confirms the colder temperatures determined by the P_1 model.

3.3.1.5. Wall heat transfer

Of importance for modeling the temperature profile in the furnace correctly is the representation of the wall and its structure. The wall consists of different layers to protect the metal of the membrane wall from temperature peaks and the flue gas atmosphere and thereby reduces corrosion. This can be tampered concrete

or ceramic tiles. A detailed investigation on the heat transfer for different wall systems for EFW boilers was performed by Grahl and Beckmann [63].

For the CFD simulation, an average thermal conductivity k of the wall is determined depending on the different thermal conductivities k_i and thickness t_i of the layers (See Equation 3.63). This value is applied as boundary condition along with the thickness of the different layers and the evaporation temperature of the water in the membrane walls.

$$k = \frac{\sum_i t_i}{\sum_i \frac{t_i}{k_i}} \tag{3.63}$$

Values from the publication of Grahl and Beckmann have been used to study the effect of different tiles systems (rear filled and rear ventilated) as well as different thicknesses of deposits on the wall [60]. Trends on heat transfer discussed by Grahl and Beckmann have been confirmed by the simulation. It was also shown, that the insulation effect of the first deposit layer has the biggest impact on the overall heat transfer.

The investigation performed by Jell applies the same thickness of deposit on the complete wall. A more realistic approach was tested by Römer in which he simulated the release of fly as particles from the waste bed and determined if the particles stick to the wall by using different viscosity criteria [64]. Using this method, the deposit growth can be simulated. This approach is computationally time intensive and the available models are not yet sophisticated enough to predict realistic growth rates. However these methods can be refined to improve the combustion process in the furnace with simulations not only for burnout and emissions but also for fouling and corrosion.

3.3.2. Waste bed boundary conditions

For a good CFD simulation of an EFW boiler, a realistic representation of the combustion on the grate is necessary. A wide variety of models were developed over the years with focus on different aspects of the combustion process. Models can be rather simple to reduce the computational effort or rather sophisticated to be as close to reality as possible. Some are standalone systems; some can be coupled to a CFD solver, while others are directly integrated into the CFD software. First a general overview of available models is given. However for this work, a new combustion model was developed, since it had to be tailored to the special needs of the NO_x modelling.

3.3.2.1. Overview on modells

Figure 3.10 shows a detailed classification of waste bed models, with a list of available models for the respective classification. All waste bed models focus

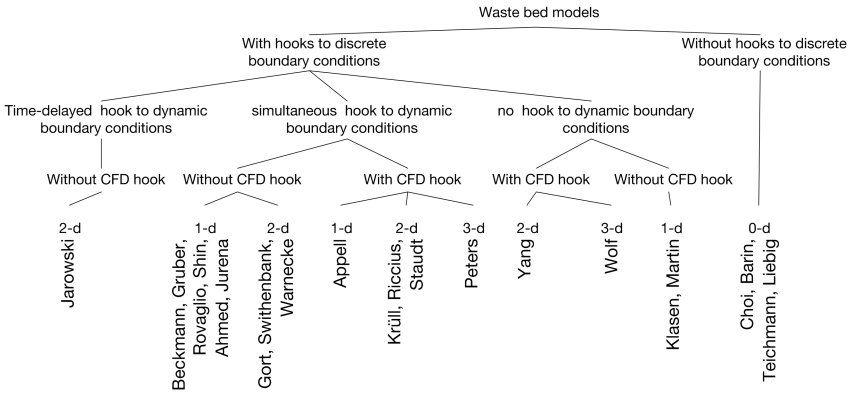

Figure 3.10.: Overview on different waste bed models, classified for different functionalities and dimensional resolution (adapted from [65], with data added from [66] and own literature review)

on the representation of the main combustion processes: drying, pyrolysis, gasification, and char burnout. Some models are presented more in detail here, highlighting special features.

Van Kessel points out the importance in accounting for the stochastically composition of the lower heating values, which depends on the inhomogeneous composition of the waste [67].

Klasen predefines a heat release profile in waste flow direction and adjusts the combustion process accordingly [27].

A modern approach is to model particles on the grate which combust during the movement along the grate. Such a model was presented by Peters [68]. These models are mostly stationary models which have to run for longer time to reach a stable combustion process and the particles are mostly spherical. The viscous interaction of the particles and their exact shape is of importance to simulate their movement on the grate properly [69]. Nakamura and Castaldi developed a model to investigated the residence time and movement of particles with different diameters on a reverse acting grate [70]

A rather well validated model was developed by Warnecke et al. [71]; which is used to predict combustion situations of a real EFW plant online. This model

was improved by coupling it to a CFD simulation of the same boiler and validation by measured data at the plant [72].

Yang et al. presented the "FLIC" model, which is a stationary model that can be coupled to Fluent. One of the main points of this model is to account for the channeling. The formation of channels through the waste bed is an important process for waste combustion [73]. In the channels, as the primary air passes through the waste bed, gasification products are released and transported to the surface.

Kurz et al. developed a fuel bed model for grate based biomass combustion. Instead of discrete particles, he modeled the bed as continuous Eulerian- Eulerian multiphase flow. The advantage is a computational inexpensive model. The model was validated in a small scale furnace and a 60 MW_{th} biomass boiler [74].

A detailed 3 dimensional model was developed by Wolf [65], which also can be coupled to Fluent. This model was validated by an extensive measuring campaign of the waste bed of a revers acting grate [75]. A disadvantage of this model is the high computational effort needed to get data for the inlet condition for a CFD simulation with low resolution. Only a few cells are used in each dimension to model the waste bed.

3.3.2.2. Fuel conversion model

After reviewing some of the available models at the beginning of the project, it was decided to develop a new model specially tailored for the purpose of this research project. The model was developed in cooperation with the company Martin GmbH. Input from different experts in the field were used to produce inlet conditions in a simple way, which however are still realistic [76]. The aim was to have a rather high geometrical resolution of the waste bed surface to be able to model also temperature and CO strands. Release curves for different species from the waste bed are presented by Hunsinger et al. [61], [77].

From their shape, a mathematical model for the release curves was derived (See Figure 3.11), to match the temperature profile presented by Koralewska and Wolf [75]. The model should not emulate the movement of the waste bed. The release curves are defined beforehand and are not influenced by the other combustion parameters. So the release curves have to be changed using observation of the fire and by knowing the primary air distribution and preheating. It is therefore better to speak of a fuel conversion model rather than a waste bed model. The model has a fine discretization in grate length and width, which is in the range of 0.08 m to 0.1 m, which results in several thousand individual sets of boundary conditions at the waste bed inlet of the CFD simulation. It takes only about 60 s to generate one set of boundary conditions.

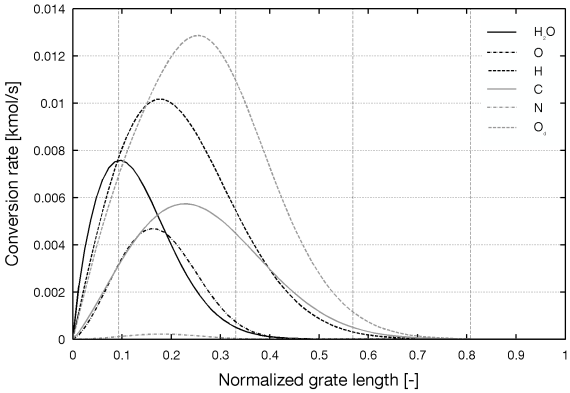

Figure 3.11.: Example of release curves for fuel species and oxygen demand along the grate

Inhomogeneous waste distribution These release curves, however, represent a homogenous combustion over the width of the grate. To account for the inhomogeneous waste distribution a random algorithm was programmed by Martin [76]. Some mass of any species is moved to another location in the main combustion zone. This algorithm is called several times for all species to generate an inhomogeneous combustion. This creates zones which are already on the grate fuel lean, while next to them the oxygen demand for complete combustion is rather high. As an average, this reduces the gas temperature above the waste bed since it is not mixed ideally.

Air supply The formation of channeling is accounted in a similar way. The primary air is distributed on each zone respectively. Inside each zone the air is reallocated randomly by another algorithm. This effect is done with a finer resolution and is overlaid to the inhomogeneous waste distribution. Using this randomization, the generated profiles however represent only a snap shot of a transient combustion situation. This applies as a consequence also, to the CFD simulation generated by these profiles. For research purposes, it is however better to investigate a realistic snap shot, than to have a homogeneous combustion.

CFD coupling The model produces a set of profiles consisting of mass flow, species concentrations and heat release. These are hooked to the CFD simulation using a user defined function (UDF). The hooking function is programmed rather

universally and can also use profiles generated from other waste bed models or from a dynamic input.
The temperature profile of the waste bed is also set as starting value for the boundary condition; it is saved in the profiles only for the first iteration. For the following iterations, the thermal radiation emitted from the waste bed to the boiler and vice versa is accounted. This is done using an energy balance according to Equation 3.64.

$$T_i = T_{ref} + \frac{\dot{Q}_{profile} + \dot{Q}_{radiation,i-1}}{\dot{m} \cdot c_p(T_{i-1})} \tag{3.64}$$

First attempts to couple this rather simple model with a more complex model to account for the movement in the waste bed as well were made by Böcker [78] using the particle movement model of Nakamura and Castaldi [70].

3.3.2.3. Model validation

As a first test of the model, a plausibility validation was performed by Dürrschmidt [66] and all parameters influencing the combustion have been tested in their range. Especially the position of the main species release has been investigated. Also, the difference between homogenous and inhomogeneous waste composition was investigated as well as radiation interaction of the waste bed with the rest of the furnace. Dürrschmidt compared species distribution and temperature profiles in the lower furnace, as well as their influence on heat transfer on different parts of the membrane wall. After the post combustion zone, the temperature and species distribution (especially burnable gas fraction) showed only little differences due to the mixing achieved by the secondary air system. Below the post combustion zone, the spread in temperature was up to 100 °C and also a difference in species distribution was noticed. After these first tests, the model was ready to be applied to real boilers with measured data, some results and works on them are presented below.

Validation with measured data

- HRC block Amsterdam: An extensive measuring campaign combined with a detailed modeling of the combustion of the boiler was performed for the HRC block in Amsterdam. Temperature and species have been measured at different distances form the grate and membrane wall using suction pyrometers with gas analyzers attached to them. An acoustic pyrometer was installed about 15 m above the grate to get a picture of the temperature distribution.

At this level, the SNCR injections are installed. These inject an ammonia / water mixture along with additional dilution water and pressurized air as dispersion medium. This injection has a significant influence on the flow pattern and the temperature distribution in this cross section and must therefore be simulated. This is done by a simplified model developed by Böcker [79]. It uses source terms to inject a gas composition at the respective locations. This avoids the creation of an injection opening at this position, which would result in an increased computational effort, since the nozzle opening would have to be meshed rather fine.

Simulations for 100 % and 110 % load were performed and compared with the measured data. The results are published by Murer et al. in [80] and [81].

- KVA St. Gallen: Dürrschmidt intensively investigated the NO_x model on the St. Gallen EFW boiler with a waste throughput of 4 t/h. After a good understanding of the model, she performed a simulation for conventional and staged combustion which was validated by measured data [82].

  Martin on the other hand used the fuel conversion model and a reduced detail chemical kinetic model to perform simulations for grate based gasification in the same boiler and compared the results with measured data [51].
- SWM Munich: Böcker and Friedrich investigated two EFW boilers with different geometries from SWM in Munich. The main focus of their investigation was to determine the thermal radiation in the lower furnace, especially the incident radiation on the waste bed. The simulation was validated using temperature data from the control system [78], [83].

3.3.2.4. NOx modeling

The Fluent user guide states that the implemented NO_x model should be used to predict trends only and not to get exact values [84]. Dürrschmidt however has shown for the boiler geometry of the EFW plant in St. Gallen that using model parameters from literature a surprisingly good prediction of NO_x emissions in EFW boiler is possible. She applied the model to a conventional and a staged combustion process and compared NO_x emissions, oxygen concentration and temperatures to measured data [82]. Relevant species for NO_x chemistry have concentrations in the range of 0 ppm to 2000 ppm. This is rather low compared to the species involved in the main combustion process. Also, the heat release of the chemical reactions involved in NO_x formation and reduction is negligible. Therefore it is possible to simulate NO_x as a post-processor after a result for the combustion process is obtained. The NO_x contribution of the prompt formation mechanism is low as shown by Sørum et al. [37]. Therefore only the thermal, fuel

and SNCR mechanism are activated in the available NO_x CFD model. These models are presented more in detail in this section, along with sensitivity study for some of the main input parameters influencing the NO_x formation.

Reaction rates The formation and reduction of thermal NO is based on the Reactions 3.44 to 3.46. These reactions are combined in a single equation for the reaction rate according to Equation 3.65. The reaction constants are given in [84] and are presented in Table 3.2.

The reaction rate depends on the concentration of O and OH radicals. Their concentration is not calculated during the simplified combustion simulation. Therefore it has to be determined by an alternative approach. Different approaches are available. In this work, the partial equilibrium approach is selected. This implies the concentration of the radicals depends on the concentration of O_2, H_2O, and temperature which are determined by the main combustion simulation.

$$\begin{aligned}\frac{d[NO]}{dt} =& k_{f,1}[O][N_2] + k_{f,2}[N][O_2] + k_{f,3}[N][OH] \\ & -k_{r,1}[NO][N] - k_{r,2}[NO][O] - k_{r,3}[NO][H]\end{aligned} \tag{3.65}$$

Table 3.2.: Reaction rates for Equation 3.65 implemented in the CFD program [84]

forward reaction rates	backward reaction rates
$k_{f,1} = 1.8 \cdot 10^8 e^{\frac{-38370}{T}}$	$k_{r,1} = 3.8 \cdot 10^7 e^{\frac{-425}{T}}$
$k_{f,2} = 1.8 \cdot 10^4 T e^{\frac{-4680}{T}}$	$k_{r,2} = 3.81 \cdot 10^3 T e^{\frac{-20820}{T}}$
$k_{f,3} = 7.1 \cdot 10^7 e^{\frac{-450}{T}}$	$k_{r,3} = 1.7 \cdot 10^8 e^{\frac{-24560}{T}}$

The formation of NO_x from nitrogen contained in the fuel is extensively discussed in Section 3.2.1.1. Compared to the thermal NO mechanism, many intermediate reactions take place. These reactions are consolidated into 4 global reactions. These are reactions from HCN and NH_3 to NO and reaction of HCN and NH_3 with NO. The NO precursor species are introduced by source terms as described in Equation 3.66 and 3.67.

$$S_{HCN} = \frac{R_{cf} \cdot y_{N,fuel} \cdot pf_{HCN} \cdot MW_{HCN}}{MW_N} \tag{3.66}$$

$$S_{NH_3} = \frac{R_{cf} \cdot y_{N,fuel} \cdot pf_{NH3} \cdot MW_{NH_3}}{MW_N} \tag{3.67}$$

In Equation 3.66 and 3.67 S is the volumetric species source term, R the mean limiting reaction rate, pf the partition fraction of NO_x intermediate and cf the conversion factor / rate.
The reaction rates for these global reactions are calculated by Equation 3.68 for the forward reaction and Equation 3.69 for the reverse reaction. The parameters for these reactions are given by De Soete [85] and are presented in Table 3.3.

$$R_1 = A_1 \cdot x_i \cdot x_{O_2}^a \cdot e^{-\frac{E_1}{R \cdot T}} \tag{3.68}$$

$$R_2 = A_2 \cdot x_i \cdot x_{NO} \cdot e^{-\frac{E_2}{R \cdot T}} \tag{3.69}$$

In Equation 3.68 and 3.69 A is the Arrhenius constant, x the species concentration for HCN, NH_3, NO or O_2, E the activation energy and T the local temperature.

Table 3.3.: Reaction rates for Reaction 3.68 and 3.69 for calculating fuel NO given by De Soete [84] [85]

		HCN	NH_3
A_1	$\left[s^{-1}\right]$	$1.0 \cdot 10^{10}$	$4.0 \cdot 10^6$
A_2	$\left[s^{-1}\right]$	$3.0 \cdot 10^{12}$	$1.8 \cdot 10^8$
E_1	$\left[\frac{J}{mol}\right]$	280451.95	133947.2
E_2	$\left[\frac{J}{mol}\right]$	251151	113017.95

Furthermore, the NO concentration also depends on the SNCR reactions. This is not only the case if ammonia is injected but also if NH_3 is still present at lower temperatures. NO can be reduced according Reaction 3.70 or newly formed by the combustion of NH_3 as shown in Reaction 3.71.

$$NO + NH_3 + \frac{1}{4}O_2 \rightleftharpoons N_2 + \frac{3}{2}H_2O \tag{3.70}$$

$$NH_3 + \frac{5}{4}O_2 \rightleftharpoons NO + \frac{3}{2}H_2O \tag{3.71}$$

Table 3.4.: Reaction rates for Reactions 3.68 and 3.69 given by Fluent theory guide [84] and Schimpf [86]

		Brouwer k_{red}	Brouwer k_{ox}	Schimpf k_{red}	Schimpf k_{ox}
A	$\left[\frac{m^3}{molsK}\right]$	424	0.35	$2.6 \cdot 10^{18}$	$2.05 \cdot 10^{23}$
β	$[-]$	5.3	7.65	0	-4
E	$\left[\frac{kJ}{mol}\right]$	349.9	524.5	334.9	251.2

The reaction rates are calculated using Equations 3.72 and 3.73. Different reaction constants are shown in Table 3.4 and are discussed more in detail in Section 3.3.2.4.

$$R_{NO} = -k_{red} \cdot [NO] \cdot [NH_3] + k_{ox} \cdot [NH_3] \cdot [O_2] \tag{3.72}$$

$$R_{NH_3} = -k_{red} \cdot [NO] \cdot [NH_3] - k_{ox} \cdot [NH_3] \cdot [O_2] \tag{3.73}$$

$$k = A \cdot T^{\beta} e^{-\frac{E}{R \cdot T}} \tag{3.74}$$

Model parameters The used modeling approaches have four input parameters which have to be chosen by the user. These are:

- HCN factor
- N factor
- Partition fraction of HCN
- Partition fraction of NH_3

Are more detailed description follows below.

- HCN factor and N factor:
  HCN factor gives the conversion from the nitrogen bound in the solid fuel into volatile nitrogen compounds in the gases. Since nitrogen is rather volatile this factor is close to 1. The N factor on the other hand gives the conversion ratio of volatile nitrogen to NO_x precursor species. The product of HCN factor and N factor is the conversion factor. This value can be bigger than one if additional NO is formed due to the prompt and thermal mechanism. Values for the conversion factor have been published by Sørum et al. [37] and Seifert and Merz [87].
  Seifert and Merz give not only the conversion factor but also the distribution of species in which the nitrogen is contained [87]. The reported conversion factor ranges from 0.45 to 0.65.

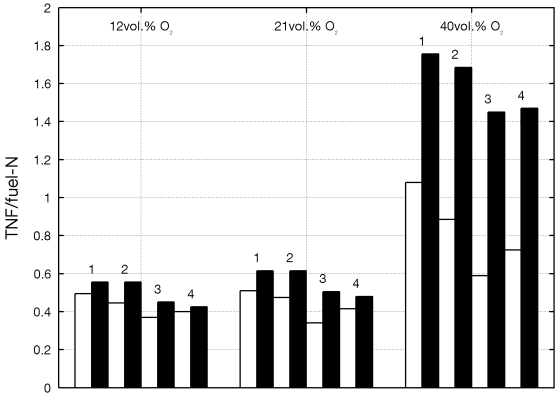

Figure 3.12.: Conversion factors for different waste types and oxygen concentration in the combustion air (adapted from [37])

Sørum et al. on the other hand integrate over time the nitrogen containing species for different waste types. They test different oxygen concentrations for the combustion air. Results are presented in Figure 3.12. As shown in the figure, for normal air (21 vol.%) the conversion factor ranges from 0.38 to 0.52. The experimental data is given by the white bars, while the calculated values are presented by the black bars. With increased oxygen concentration, the conversion factor increases to over 1. This implies the oxidation of almost all fuel nitrogen, along with some additional formation of thermal NO [37]. This is possible since oxygen enrichment of the air increases the combustion temperature and therefore the potential for thermal NO formation. Decreasing the oxygen concentration however results only in a small reduction of NO, which can be explained by the formation of fuel NO. Even though fuel NO formation depends on the availability of oxygen; it is more important how the oxygen is added locally to the system, than the concentration itself.

- Partition fractions:
  Partition fractions give the ratio between the different NO_x precursor species. The sum of the partition fraction for NO, NH_3 and HCN gives 1, therefore only the partition fraction of NH_3 and HCN can be set in the model.

  For the partition fraction two different literature sources are available from KIT in Karlsruhe. Seifert and Merz investigated the release of NO, NH_3

and HCN from different waste samples using a thermo gravimetrical analyzer (TGA) combined with a Fourier transform infrared spectroscopy (FTIR) to analyze the gas composition. As average a composition of 50 % NH_3, 40 % NO, and the rest HCN was determined [87]. Hunsinger on the other hand analyzed the gas above the grate of a test facility scale waste incinerator (TAMARA). The NO concentration was an order of magnitude smaller compared to the NH_3 concentration. HCN was not measured [48].

Using literature values two different sets of factors can be derived. How the distribution of the NO_x precursor species depending on the factors is presented in Figure 3.13.

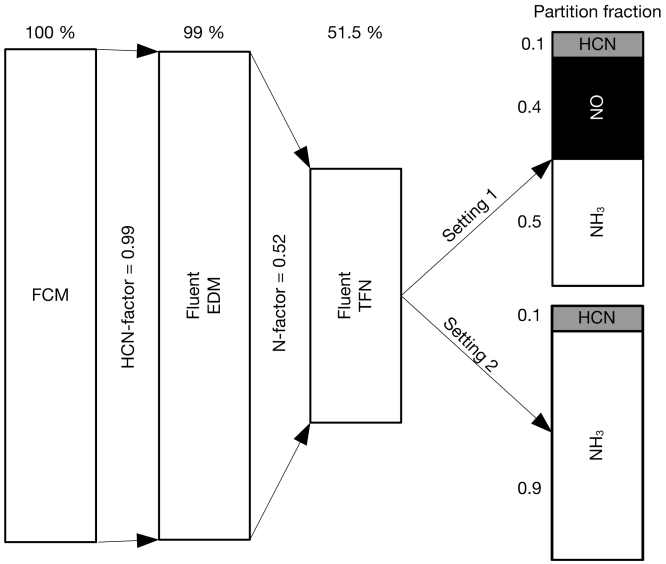

Figure 3.13.: Settings used for the calculations, setting 1 is used for both approaches, setting 2 only for the waste bed approach

The influence of the individual parameters on the NO_x emission is investigated in the next section.

Model validation Vogl investigated the NO_x formation in an EFW furnace. As second stage, he used the available SNCR model which uses reaction constants

from Brouwer. These reaction constants were determined for flue gas from coal combustion with 4 vol.% oxygen [88]. However, the SNCR performance in the EFW boiler was far from the 85 % documented by literature [39]. A simple plug flow model was used to compare the SNCR reduction efficiency with values published by Wolfrum [52] presented in Figure 3.9. It was found that the temperature window for the reduction efficiencies was much more narrow for the reaction constants from Brouwer (See Figure 3.14), which explains the lower than expected reduction efficiency in the simulation [89].

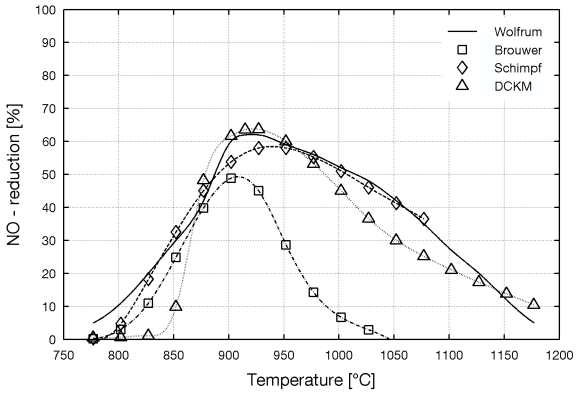

Figure 3.14.: SNCR reduction efficiency investigated in a plug flow reactor for different models (adapted from [58])

New reactions constants have been determined to adapt the SNCR efficiency to the literature values. The programming language "Scheme", can be used to overwrite the values implemented in Fluent [90]. Schimpf investigated different sets of reaction constants for Equations 3.72 and 3.73 [86]. The best values he found are presented along the constants of Brouwer in Table 3.4.

As final investigation on the SNCR performance, Angerer used a detailed chemical kinetic model based on a combined model of Miller and Bowman for normal NO_x chemistry [31] and Glarborg for the SNCR chemistry [38] [58]. The reduction efficiency is also shown in Figure 3.14 labeled with DCKM and a good correspondence with the values from Wolfrum and Schimpf can be seen.

To model the fuel NO formation two different approaches are possible. The first one is the so called "gas phase approach" (GP). This approach is extensively investigated by Dürrschmidt [82]. The second approach is the "waste bed approach" (WB).

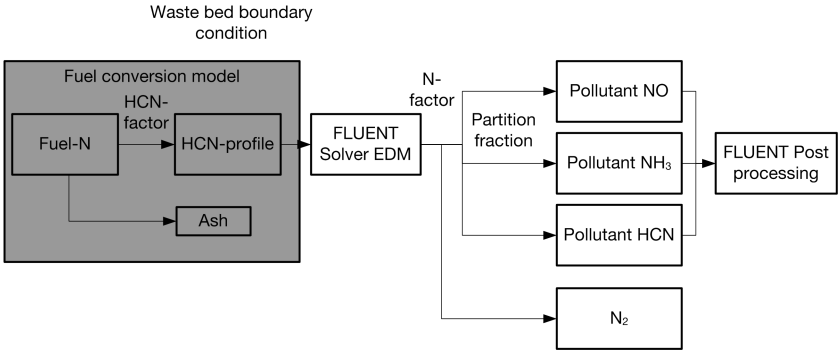

Figure 3.15.: Calculation scheme for the gas phase NO_x modeling approach (adapted from [82])

The gas phase approach was derived from the Fluent tutorial on NO_x formation and reduction. HCN is defined as nitrogen carrier species. It is used to have a controllable and independent concentration of TFN in the flue gases entering the furnace from the waste bed. As shown in Figure 3.15, the HCN factor controls the ratio of fuel nitrogen being converted into the gas phase. Some small fractions of nitrogen remains in form of ammonium in the bottom ash, their concentration can be quantified by elution tests [91]. On the simulation boundary condition "waste bed inlet", a species distribution profile for HCN is applied, defining the quantity and the location of the release of fuel nitrogen fixed as HCN. At the location where it reacts, source terms are set for the pollutant species NO, NH_3 and HCN according to Equations 3.67 and 3.66. A conversion factor called N factor is used as a multiplier to account the part of the TFN reduced to N_2 directly. The distribution for the different species is defined by the partition fraction. As shown by Dürrschmidt, the gas phase approach works well for processes where the HCN is oxidized in a single stage. Since the total fixed nitrogen is released in a small fraction of the furnace and starts to interact from there on [82]. For a strongly staged combustion, this approach does not work since the pollutant source terms are distributed over the furnace. Therefore the waste bed approach was developed.

The waste bed approach is shown in Figure 3.16. The same factors and multipliers are used as for the gas phase approach. However now they are used directly as multiplier on the HCN profile. Three individual profiles are generated, one for

each pollutant species. With this approach, the total mass flow rate of fixed nitrogen is directly introduced in the waste bed and its reduction can be observed along the flue gas path.

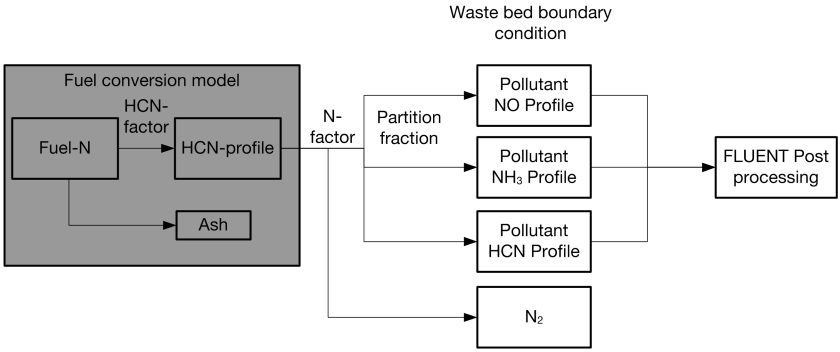

Figure 3.16.: Calculation scheme for the waste bed NO_x modeling approach

To investigate the influence of the partition fraction, 10 calculations were performed on an EFW boiler geometry with a conventional combustion system. The partition fraction of NO and NH_3 was varied according to Figure 3.17b. Both approaches (GP and WB) described above have been investigated. The resulting NO_x concentration have been analyzed on dry basis (See Equation 3.75) at the beginning of the second pass of the boiler geometry. All NO_x concentration in this work are given on dry basis, since it is the highest value, compared to raw NO_x and referenced by an oxygen concentration of 11 vol.%. In Germany, the NO_x concentration has to be corrected according Equation 3.76 by the oxygen concentration only if the oxygen content in the flue gas exceeds the reference concentration ($x_{O_2,ref}$) of 11 vol.% on dry basis as discussed in Section 2.1;

$$\rho_{NO_x dry} = \frac{\rho_{NO_x}}{1 - x_{H_2O}} \tag{3.75}$$

$$\rho_{NO_x ref} = \rho_{NO_x dry} \cdot \frac{21 - x_{O_2,ref}}{21 - x_{O_2,actual}} \tag{3.76}$$

Figure 3.17a shows the results of this investigation. For the gas phase approach, the NO_x emissions drops from 1250 mg/Nm^3 for 0 NH_3 to 350 mg/Nm^3 at the partition fraction of NH_3 set to 0.6. From there, it stays at this level for all other

settings. The drop in the graph can be explained by reaction of NH_3 with NO. With higher NH_3 concentration, however, NO is not reduced according Equation 3.69 but is newly formed due to Equation 3.68 in the post combustion zone, thus keeping the NO concentration high.

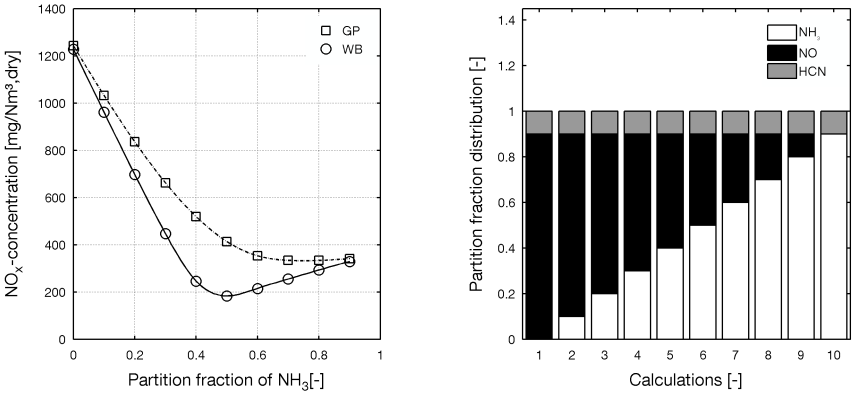

(a) NO_x concentration depending on the partition fraction of NH_3

(b) Partition fraction distribution for the different calculations

Figure 3.17.: Influence of different partition fraction settings on the NO_x formation, HCN is kept constant at 0.1. HCN factor is set to 0.9 and N factor to 0.52

For the waste bed approach, the drop in NO_x emissions is stronger and a minimum is reached for a NH_3 partition fraction of 0.5. From there, the emission starts to raise again until it reaches the same level as the GP approach for a NH_3 partition fraction of 0.9. The lower emissions are caused by the fact that the pollutants are released directly at the waste bed and therefore have time to react in a fuel rich environment until the post combustion zone. So, depending on the availability of NO and NH_3, the emissions are reduced. With an increased partition fraction for NH_3, not enough NO is available for a reduction of the TFN.
Expected NO_x emissions for such a combustion system are 350 mg/Nm^3 to 400 mg/Nm^3. This is achieved for high partition fractions of NH_3 for both approaches, which corresponds to the data published by Hunsinger and Seifert [48]. The partition fractions from Seifert and Merz are gained from an experimental setup [87], which represents the combustion setup of a grate based combustion system poorly.

Frank investigated partition fractions of 100 % for NO, NH_3 and HCN using the GRI3.0 mechanism on an EFW boiler. The resulting NO_x concentration was in the same range for all three cases [92]. This implies a near complete conversion of the precursors to NO in the boiler. This is only possible if they are oxidized fast without the chance to be reduced by NH_i radicals.
Nonetheless both settings presented in Figure 3.13 for the partition fractions are used for further investigations to cover a broader range of possible values. However, for the gas phase approach, only setting 1 is used since it gives the slightly higher values, while for the waste bed approach both settings are used.
The influence of the HCN factor and the N factor on the NO_x concentration was investigated for the gas phase approach by Dürrschmidt [82]. Additional calculations using settings 1 and 2 for the waste bed approach have been performed as part of this thesis.
A validation of the NO_x model is a variation for the N factor . This factor can vary in a range from 0 to 1. For 0, no fuel NO is formed, since no NO, NH_3 and HCN are released into the furnace. This implies that all NO_x emissions are formed by the thermal NO mechanism. Figure 3.18 shows the result of an investigation of the N factor. The N factor is increased in steps of 0.05 from 0 to 1, while the HCN factor is kept constant at 0.9. This implies that for a N factor of 1, a conversion factor of 0.9 is set, which is much higher than the values found in literature. The results for the single calculations along with trend lines are shown. The gas phase approach results in the highest NO_x emissions, with nearly 600 mg/Nm^3 for a N factor of 1. Second highest emissions are determined for the waste bed approach with a partition fraction of 0.9 for NH_3 (WB-0.9). For an N factor of 1, the emissions are just below 500 mg/Nm^3. The lowest emissions (around 250 mg/Nm^3 for an N factor of 1) are calculated for the WB-0.5 cases with a partition fraction of 0.5 for NH_3. At an N factor of 0, all cases have a NO_x concentration of 10 mg/Nm^3, which is the contribution of thermal NO_x formed during the combustion process. The GP and WB-0.9 approach show NO_x emissions which are in the expected range for this type of combustion process.
A second investigation was performed to understand the influence of the HCN factor. This is a parameter set already during the generation of the inlet conditions for the simulation in the fuel conversion model and therefore it depends on the modeling of the waste bed, which is described already more in detail in Section 3.3.2.2.
Again, a preliminary investigation on the HCN factor using the gas phase approach was performed by Dürrschmidt [82]. However some unexpected anomalies made a more detailed investigation necessary. During this work, the waste bed approach was added for the HCN factor investigation.

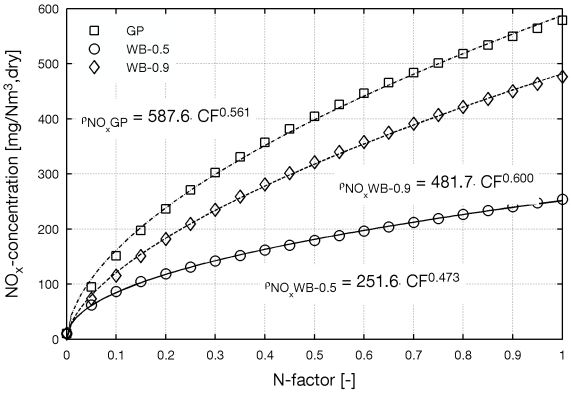

Figure 3.18.: NO_x concentration depending from the N factor, for a setting 1 and 2 and for a HCN factor of 0.9 (adapted from [82])

The HCN factor determines how much of the fuel nitrogen is transferred into the gas phase. The rest of the nitrogen remains in the bottom ash. Calculations are performed for HCN factors of 0.2, 0.4, 0.6, 0.7, 0.8, 0.9 and 0.99. The N factor is set to 0.52 according to the upper range of the conversion factor found by Sørum et al. [37].

During the generation of the inlet profiles, the inhomogeneous composition of the waste is accounted for by applying a random algorithm, which changes the waste composition. This has a significant effect on the NO_x formation since locally under and over stoichiometric zones can be present. In these zones NO is either formed or reduced to N_2. To be able to get a clear dependence for the NO_x emissions from the HCN factor four sets of profiles are calculated for each HCN factor, resulting in a total of 28 calculations.

The order of the NO_x emissions for the different modeling approaches is again the same as found during the investigation of the N factor, with the gas phase showing the highest values, as shown in Figure 3.19.

It is interesting to see that there is a spread on the calculated NO_x emissions for the different profiles at the same HCN factor. For the gas phase approach and the WB-0.5 approach this is in the range of 30 mg/Nm^3, while for the WB-0.9 approach it increases to 100 mg/Nm^3. These high spreads seam realistic since the stationary combustion a 7 hour NO_x trend (5 min averages) is presented by Dürrschmidt for the investigated boiler [82]. This trend shows fluctuations between 230 mg/Nm^3 and 450 mg/Nm^3, with most of the values in the range

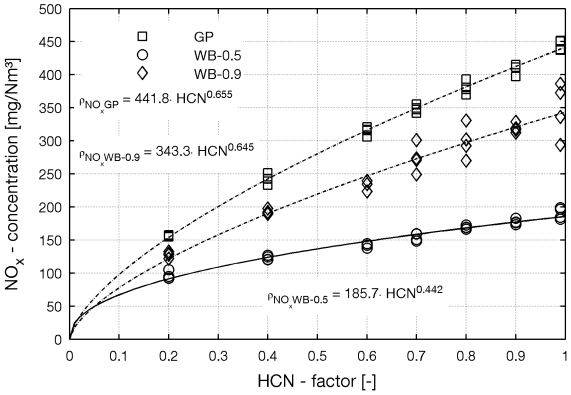

Figure 3.19.: NO_x concentration depending from HCN factor, for setting 1 and 2 and a N factor of 0.52

of 280 mg/Nm^3 to 380 mg/Nm^3. This is exactly the range where the results for the HCN factor of 0.99 are located for a conversion factor of 0.52.

This implies the partition fraction with nearly only NH_3 published by Hunsinger and Seifert along with the conversion factor (HCN factor times N factor) from Sørum et al. of 0.52 give the most realistic results. Additionally the randomizing of the waste composition reproduces a spread similar to the one observed in a real trend.

Dürrschmidt additionally investigated the influence on the main location where NO, NH_3 and HCN are released. This can be adjusted using the waste bed model presented in Section 3.3.2.2. An increase of NO_x emission by 100 mg/Nm^3 was seen if the main release was moved more to the end of the main combustion zone where more O_2 is available [82].

4. Energy efficiency optimization

The transition to a sustainable energy system is not only achieved by replacing fossil fuels with renewable sources but also, by improving the efficiency of processes and components. This Chapter deals with increasing the energy efficiency of EFW plants and shows what steps can be taken to improve the efficiency as well as methods for a better understanding and optimization of the process. Technical data for a theoretical EFW plant was chosen to design an efficient energy conversion process. First some thermodynamic principals are discussed focusing on the water steam cycle. After optimizing the water steam cycle, different measures to influence the heat availability in the flue gas are discussed. Some of these measures are combined to improve the heat in the flue gas. As a last step the overall plant is optimized.

4.1. Plant design parameters

The plant size is an important factor for the design of an EFW plant. Many plants are designed with several small combustion lines, to reduce the loss in combustion capacity during boiler downtime. The tendency however goes toward bigger plant sizes, with fewer combustion lines. More than 170 combustion units with more than 60 MW_{th} gross heat input were in operation already in 2007 [93]. New plants, such as built in Amsterdam [12] and designed for Copenhagen [94], process 500000 t waste per year and are equipped with only two lines. This results in boilers with a gross heat input close to 100 MW_{th}.

Bigger plants are generally more efficient due to more efficient components like turbines and pumps. Additionally a bigger plant size allows investing in more sophisticated plant concepts, since the cost of control system and sensors as well as personnel costs are nearly independent from size [95].

More efficient plants can accept waste from more distant locations. Otten and Bergsma showed in terms of avoided CO_2 emissions and energetic efficiency: it is more beneficial to transport waste from greater distances and burn it in a more efficient plant than to burn it in a closer but less efficient plant. The calculated distance is about 200 km per percent point efficiency increase [96].

Parameters for an EFW plant are selected considering the facts presented above and are included in the following Table 4.1:

Table 4.1.: Plant design parameters

Throughput	403000	t/a
Lower heating value	10	MJ/kg
Availability	92	%
Lines	2	-
Throughput / line	25.00	t/h
Gross heat input / line	69.45	MW_{th}

The plant throughput of 400000 t/a is chosen to meet the demand of a large central European city and the surrounding rural areas (approximately 1.8 million citizens). The availability is set to 92 %, which is a value achievable for modern plants as demonstrated by the plant in Amsterdam [20].

Electricity and heat is generated from waste with a thermal process based on the Rankine cycle, operated as water-steam cycle. The water steam cycle is the main component of the process and operates between two separate systems. (See Figure 4.1)

$$\eta = \frac{\text{useful output}}{\text{input}} = \frac{Q_{in} - Q_{out}}{Q_{in}} \tag{4.1}$$

Equation 4.1 defines the efficiency η, which depends on the heat input Q_{in} and heat leaving the system Q_{out}. The efficiency is used to evaluate the performance of the overall process, as well as the individual systems in interaction.

The first system is the heat source or combustion system in the case of EFW plants. To optimize the overall system it is necessary for the heat source to supply as much heat as possible at high quality to the water steam cycle. The second system in interaction with the water steam cycle is the heat sink system. This system absorbs the waste heat from the process and transfers it to the environment. The technical optimization potential for the heat sink system is limited, since it is only a heat exchanger discharging waste heat to the environment. Figure 4.1 shows the ideal interaction between the three systems.

Heat should be transferred only in one direction from the heat source to the heat sink. The steam cycle in the middle has to be designed in such a way to minimize the heat transferred to the heat sink and as a result generate as much work as possible out of the heat input.

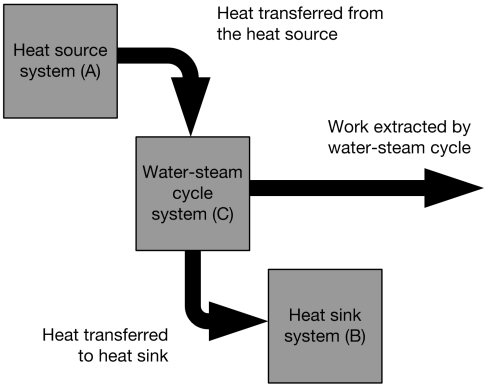

Figure 4.1.: Integration of a thermal process (System C) in interaction with a heat source (System A) and a heat sink (System B)

4.2. Water steam cycle optimization

The water steam cycle is the central component of the power generating process. Its design is influenced by the heat source and heat sink system. The effects imposed by these systems are however low compared to the optimization potential, which is still present in the water steam cycle of EFW plants itself. First some basic thermodynamic principles are presented to clearly explain the possible options.

4.2.1. Carnot cycle and T-s diagram

The efficiency of the water steam cycle can be compared with the Carnot cycle, the ideal thermodynamic process, operating between an isothermal heat source and an isothermal heat sink. Thermal processes are best described in a temperature entropy diagram. In these diagrams the heat input and output of the cycle process is defined by the area under the temperature curves. In Figure 4.2 the added heat of the Carnot cycle is given by the gray hatched area, the points s_1-2-3-s_4-s_1, or Equation 4.2. The heat transferred from the Carnot cycle to the heat sink corresponds to the black hatched area or the points s_1-1-4-s_4-s_1.

Using Equation 4.1 in combination with Equation 4.2 results in the formulation of the Carnot efficiency. (See Equation 4.3) In other words, the efficiency of the cycle process can be seen as the ratio of the difference between the gray hatched

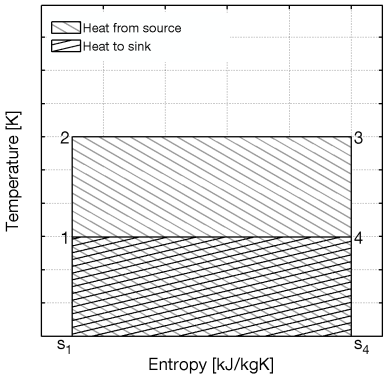

Figure 4.2.: Carnot cycle in the T-s diagram

area and the black hatched area to the gray hatched area.

$$q = T \cdot \Delta s \tag{4.2}$$

$$\eta_{Carnot} = 1 - \frac{T_c}{T_h} \tag{4.3}$$

The Carnot efficiency (η_{Carnot}) depends on the temperature level at which heat is added (T_h) and the colder temperature level at which heat is removed (T_c). These considerations can be transferred to a Rankine cycle as shown in Figure 4.3. The area of the heat supplied to the process is characterized by the points s_1-1-2-2'-3-s_4-s_1. Due to irreversibility of the expansion in the turbine the heat transferred to the heat sink is increased. The area is not s_1-1-4-s_4-s_1, but rather s_1-1-4'-$s_{4'}$-s_1. After calculating the thermodynamic average temperature using Equation 4.4, the efficiency can be calculated using Equation 4.5, which is the adaption of the Carnot efficiency for general cycle processes.

$$\bar{T}_{th} = \frac{Q}{\Delta S} = \frac{\Delta h}{\Delta s} \tag{4.4}$$

The thermodynamice average temperature ($\bar{T}_{th}$) depends on the entropy change ($\Delta S or \Delta s$) during the heat transfer ($Q or \Delta h$). The thermodynamic average temperature is evaluated for the heat added $\bar{T}_{thh}$ and removed heat $\bar{T}_{thc}$ to calculated

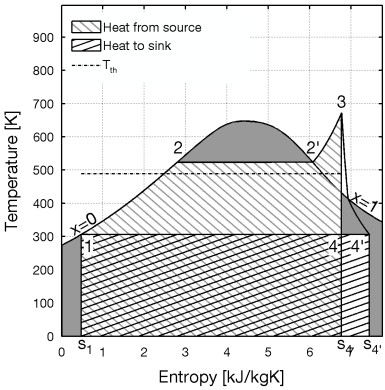

Figure 4.3.: T-s diagram of a simple steam cycle

the cycle efficiency η.

$$\eta = 1 - \frac{\bar{T}_{thc}}{\bar{T}_{thh}} \tag{4.5}$$

The heat sink system is used to transfer heat from the water steam cycle to the environment. Exhaust steam from the turbine is condensed isothermally and slightly sub cooled, before it is fed back into the feed water system.

4.2.2. Plant concepts

In this section different plant concepts are compared. First, a state of the art plant with moderate efficiency is presented along with suggestions for improving the efficiency. Then, the HRC concept implemented in Amsterdam is presented. Finally, an optimized water steam cycle is discussed, which is based on the Amsterdam concept, but has additional components implemented known from coal power plants.

4.2.2.1. State of the art plant: 40 bar 400 °C

Today the typical water steam cycle design of an EFW plant is rather simple and designed for high availability and not high efficiency.
The key parameters for such a plant are:

- 400 °C - 425 °C live steam temperature
- 40 bar - 50 bar live steam pressure

- 130 °C - 150 °C feed water temperature
- 1 - 2 feed water preheating stages
- 70 mbar - 150 mbar pressure at turbine outlet, due to air cooled condensers
- 1.5 -1.8 excess air ratio
- 25 °C - 150 °C primary air temperature
- no secondary air preheating
- 180 °C - 250 °C flue gas temperature at boiler outlet

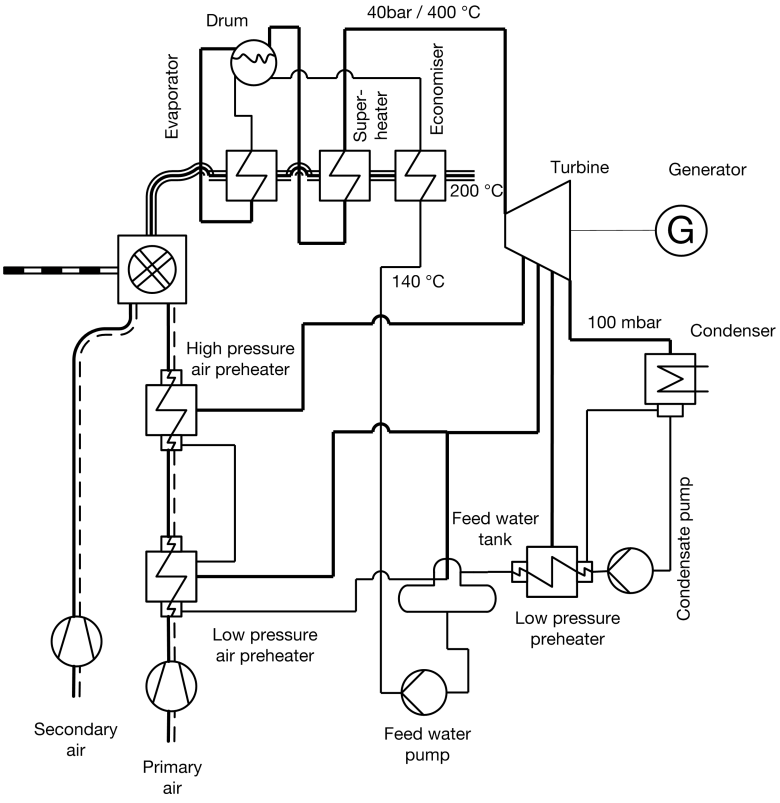

Figure 4.4.: Plant scheme for a typical state of the art EFW-plant

These plants have a net electric efficiency of 19 % to 22 %, if they are operated in condensing mode. A plant scheme of such a plant is shown in Figure 4.4 and

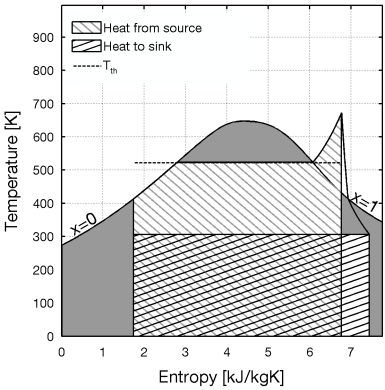

Figure 4.5.: T-s diagram of a 40 bar and 400 °C plant, with a feed water temperature of 150 °C

the water steam cycle is shown in a T-s diagram in Figure 4.5. These plants are labeled by Kamuk as "well documented" since there is a low risk of reduced availability in operating such a plant [100].
These plants have feed water preheating temperatures up to 150 °C, therefore the ratio between the heat from the heat source and the heat to the heat sink shown in Figure 4.5 is not completely correct. Steam containing more heat is extracted during the expansion process for the preheating, while in the diagram only the heat below the condensing temperature is accounted for in the graphical efficiency estimation. Therefore, in reality the heat which goes to the sink is even lower, since the changes in the steam mass flow rate can be properly represented in this type of diagram.
Different aspects of the water steam cycle can be changed to optimize the efficiency of the water steam cycle.

4.2.2.2. Condensing pressure

The heat sink system in EFW plants is mainly implemented in two different ways. In northern Europe the heat sink is normally a district heating system. This implies condensing pressures of 500 mbar to 1500 mbar, depending on the temperatures of the district heating system and the exact heat exchanger arrangement.
The rest of Europe uses mainly air cooled condensers for back cooling, which operate at 70 mbar to 150 mbar, depending on the size and average air tem-

perature. Some exceptions like Amsterdam use direct sea water cooling, which allows a condensing pressure of 30 mbar.

Weber and Maschke investigated different back cooling options for EFW plants with regard to complexity, investment and operational cost. They show that the seldom used wet cooling tower with forced draft has actually lower investment cost compared to a direct air cooled condenser. The electricity demand for operation is slightly increased due to the operation of fans and pumps, but it is overcompensated by the additional electricity production due to the achievable condensing pressure of 40 mbar. The main disadvantages are the continuous replacement of cooling water, which is approximately 2 % of the circulated water and the visibility of the plume caused by the evaporated water [97].

The plume visibility can be reduced by using a hybrid cooling tower instead of a wet cooling tower. The hybrid cooling tower has about 1/3 of its cooling capacity by air cooling, the rest by evaporation. The warm air produced is mixed with the wet air and therefore prevents early plume formation [15].

The big advantage of water cooled condensers is the additional water circuit. The steam can condense directly at the outlet of the turbine. The waste heat is transported in form of warm water outside of the plant to be transferred to the environment. For air cooled condensers steam has to be piped outside of the plant. Due to the low operating pressure the steam volume is huge and the pressure drop in the pipe has a big effect on the achievable condensing pressure.

In modern coal power plants with wet cooling tower the flue gas is released into the cooling tower. This helps in the dispersion of the flue gases, since wet air has a lower density compared to the surrounding air [98]. For EFW plants it is more likely to have small cell cooling towers, but they can be arranged close to the stack to help in the dispersion of the flue gases.

Table 4.2.: Condensing pressures and corresponding temperatures

Condensing pressure mbar	Temperature °C	Temperature K
30	24.1	297.2
40	29.0	302.1
50	32.9	306.0
70	39.0	312.2
150	54.0	327.1
500	81.3	354.5
1500	111.4	384.5

The condensing pressure is an important parameter for the efficiency, since it directly determines the condensing temperature. Musil suggests in 1966 the condensing temperature of process to be used as T_c in the Carnot efficiency (See Equation 4.3) as well as environment temperature for exergy calculations [99]. Since the Carnot efficiency is linearly dependent to the temperature of the heat sink, small changes in the condensing pressure have a big effect on the efficiency. (See Table 4.2)

For a state of the art EFW plant the change in electrical efficiency is about $1\,\% - \text{point}$ for every 5 °C in condensing temperature change. So, by changing from a well-designed air cooled condenser with a turbine outlet pressure of 70 mbar to a hybrid cooling solution with 50 mbar at the same position leads to an increase in net electric efficiency of 1.2 %.

4.2.2.3. Increased live steam parameters

Increasing the live steam parameter raises the thermodynamic average temperature $\bar{T}_{thh}$ at which heat is added to the system. As can be seen in Equation 4.3 raising the temperature results in an increase in efficiency. Wünsch showed that increasing the live steam temperature does not have such a strong effect as raising the live steam pressure [15]. Increasing the pressure raises the evaporation temperature; more heat is therefore transferred at a higher average temperature level, which has a stronger impact on the average heat transfer temperature level, than raising the superheating temperature. This implies 1 °C change in evaporation temperature has a stronger impact on the efficiency than 1 °C change in live steam temperature.

Dräger et al. presents different concepts, where the live steam pressure and temperature are raised from a typical 40 bar 400 °C configuration stepwise up to 90 bar and 500 °C. This live steam temperature is necessary due to the risk of erosion of low pressure turbine blades since the moisture content in the low pressure turbine rises if only the pressure is increased. These concepts lead to a relative increase in the necessary superheater surface area, since more heat for superheating is necessary. Also, the flue gas temperatures at which the superheaters are arranged are elevated. This results in an increased area with corrosion risk [101]. Kailbauer et al. suggest the use of platen superheaters in the second pass completely covered with tamped concrete as protection for corrosion while increasing the superheater surface [102]. Schu and Leithner finally, suggest the use of supercritical steam parameters in EFW plants to push the efficiency even higher [103], this is however only possible if the EFW plant can feed steam into a coal power plant due to the necessary steam turbine size.

Kamuk shows a typical plant (throughput 20 t/h) with different live steam parameters and estimates how many days of downtime the additional sold electricity can compensate. For a raise from 40 bar and 400 °C to 70 bar and 480 °C this is 10 days for an electricity revenue of 55 €/MWh [100].

4.2.2.4. Steam reheating

As discussed before with increasing live steam pressure, the live steam temperature has to be increased as well. An alternative for reducing the risk of droplet erosion in the low pressure turbine is to reheat the steam after the high pressure turbine. For coal power plants, reheating of steam is state of the art. For EFW plants only two different examples are implemented.

The first concept is internal reheating and is implemented in Rüdersdorf. The steam with 25 bar is piped back into the boiler and is heated up to the same temperature as the live steam (420 °C). The pressure drop for this reheater is 2 bar, the achieved net electric efficiency is 27.4 % [104]. The disadvantage of this concept is the extra need of high temperature heat above evaporation temperature. The superheater and reheater have to be placed at a flue gas temperature with increased risk of corrosion.

The second concept is external reheating and is implemented in the HRC concept in Amsterdam (HRC Hoog Rendement Centrale (High efficient EFW plant)). Exhaust steam at 14 bar leaves the high pressure turbine with a moisture content of up to 2 %. It then passes a droplet separator and is reheated to 320 °C with condensing heat of saturated steam extracted from the drum [105], [12]. This is possible since the evaporation pressure is between 135 bar and 145 bar, which results in a condensing temperature of 330 °C to 340 °C. The resulting condensate is pumped back into the drum at more than 300 °C. A T-s diagram for this process is shown in Figure 4.6.

The disadvantage of this concept is the need to pump nearly saturated water back into the drum. The pressure drop on the reheating side of the heat exchanger is in the range of 0.5 bar, since the reheater can be located close to the turbine. This kind of reheater actually decreases the average temperature level of the heat added to water steam cycle system and thereby also, the efficiency, since the reheat temperature is rather low. However it is a simple possibility to operate the boiler at high pressures without risk of erosion in the low pressure turbine. An additional benefit is the extra demand of saturated steam, which increases the demand for evaporation heat transfer surface, which is less affected by corrosion, compared to superheater bundles. Combining this type of reheater with other improvements results in an efficiency of 30.6 % as discussed in Section 4.2.2.7.

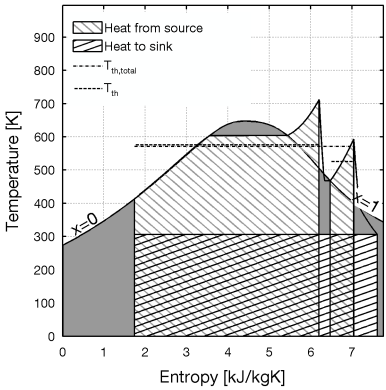

Figure 4.6.: T-s diagram of the Amsterdam plant concept (130 bar and 440 °C) with external steam reheating at 14 bar to 320 °C

4.2.2.5. Use of low temperature heat

In recent years exploitation of low temperature heat is an often used option to increase the efficiency of EFW plants. Additional heat exchangers can be arranged between the various stages of the flue gas treatment equipment to extract some heat by cooling the flue gas. Normally the temperature is reduced by quenching the flue gas by injecting water. In Section 4.2.2.1 it is mentioned, that the flue gas temperature at the boiler outlet is in the range of 200 °C. With this temperature more than 10 % of the gross heat input is dissipated into the atmosphere by the flue gas. The efficiency of the heat source system (See Figure 4.1) can be improved by reducing the heat loss according to Equation 4.1.

New plants are designed with lower flue gas temperatures at the boiler outlet. The heat can be used for various objectives like feed water preheating, district heating and primary air preheating [102]. More on air preheating with low temperature heat is discussed in Section 4.3.2.5. The use of this low temperature heat for feed water preheating is common.

Boilers with lower boiler outlet temperature are presented by Dräger et al. and Aleßio and Mück [101], [106]. The size of the economizer increases drastically when the flue gas temperature is reduced and the feed water temperature stays constant. An option is to decrease the feed water temperature as well.

Villiani and de Greef investigated the corrosion risk for feed water temperatures as low as 90 °C.They found no risk for corrosion down to 105 °C and presents several plants operating with this feed water temperature [107].

The HRC lines in Amsterdam have an external economizer called ECO2, which cools the flue gas from 180 °C down to 130 °C. The heat is used to preheat the feed water before the feed water tank [12].
Murer et al. performed an exergy analysis of the boilers investigated by Dräger et al. [101]. The boiler with lower flue gas temperature at boiler outlet transfers 4.8 % more heat to the water steam cycle, but the net electric efficiency of the plant rises only by 1.3 % [108]. The water steam cycle is not able to convert the additional heat efficiently into work, since it is added with low quality. Most of the heat loss is moved from the heat source system to the water steam cycle system. The losses leave the overall plant through the condenser instead of the stack. At the same time both the boiler and condenser become more expensive.

4.2.2.6. Feed water preheating

The feed water temperature of EFW plants ranges from 105 °C to 150 °C. The state of the art is to use the feed water tank as the final step for the feed water preheating. Before only one additional steam heated feed water preheater is installed, preheating the feed water to 85 °C to 100 °C. Additional stages for feed water preheating are implemented with waste heat available in various stages of the process. These are low temperature heat of the flue gas, heat from the grate cooling and flue gas condensing.
In coal power plants on the other hand up to 10 steam heated feed water preheaters can be installed [105], with 8 to 9 preheaters being state of the art. The feed water temperature is in the range of 300 °C to 330 °C for modern concepts. Steam heated feed water preheaters are also, called regenerative feed water preheaters, since they use internal heat available in the water steam cycle. Steam is extracted at different pressure levels from the turbine and then condensed at the respective condensing temperatures. This allows a stepwise heating of the water.
The steam extracted does not end up in the condenser, but is fed in the form of water or steam to the feed water system at different stages. Therefore less heat (Q_{out}) has to be transferred to the heat sink. Equation 4.1 shows why this increases the efficiency. Another way of explaining the increase in efficiency due to feed water preheating is to look at the Carnot efficiency of the process with and without regenerative feed water preheating. The average temperature of heat transfer can be increased significantly by preheating the feed water.

4.2.2.7. The HRC concept Amsterdam: 130 bar 440 °C

In 2007 an additional block was commissioned at the Amsterdam EFW plant. The plant was designed for high availability and efficiency.

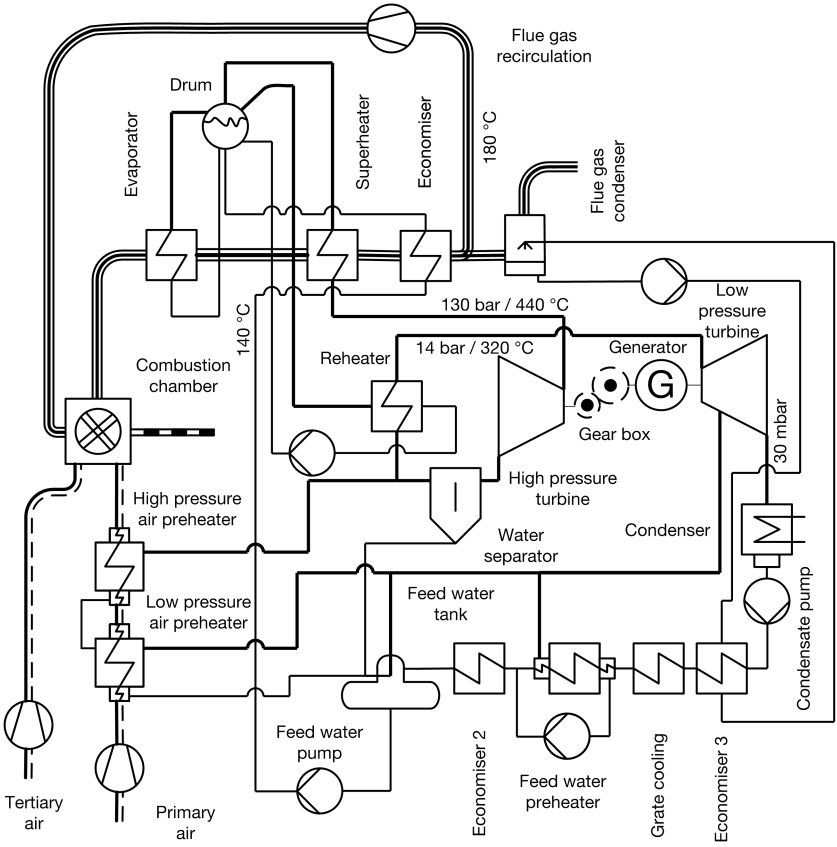

Figure 4.7.: Plant scheme for the HRC block in Amsterdam

The plant's key parameters are:

- 440 °C live steam temperature
- 130 bar live steam pressure
- external steam heated reheating (see Section 4.2.2.4)
- 140 °C feed water temperature
- 2 stage steam heated feed water preheating
- 3 stage waste heat feed water preheating, (flue gas condensing, grate cooling, second economizer)
- 30 mbar pressure at turbine outlet

- 1.39 excess air ratio
- flue gas recirculation 25 %
- up to 150 °C primary air temperature, depending on grate zone
- no secondary air preheating
- 180 °C flue gas temperature at boiler outlet

The plant has a design electric efficiency of 30.6 %, which could also, be reached during continuous operation [80]. The achieved availability reaches 91.5 % for the year 2010 [20]. The T-s diagram for this plant is shown in Figure 4.6 and a plant scheme is shown in Figure 4.7. Two equal combustion lines incinerate a total of 530000 t/a of waste and feed steam to a Siemens 74 MW SST-700RH extraction condensing turbine in reheater configuration [109].

Compared to the state of the art plants an increase in efficiency from 22 % to 30 % is significant, while the same high availability as in state of the art plants can be maintained.

4.2.2.8. Next step in EFW efficiency: high efficient boiler concept: 177 bar 500 °C

Five years of operational experience with the Amsterdam plant show additional potential for increasing the energy efficiency even further. The steam cycle offers still some potential, which is investigated in a new design concept as follows:

As a first step the live steam parameters of the plant are raised to the technically reasonable limits. The pressure is mostly limited by the available turbines on the market. Of the main steam turbine suppliers Siemens is the only one to offer smaller turbines for pressures higher than 140 bar. These turbines can have a live steam pressure of up to 165 bar. For turbines with 90 MW mechanical output turbines with a pressure up to 177 bar are available [110], [111].

Selecting the right turbine is a problem and depends on the desired efficiency. With 400000 t of waste per year, a plant with 24 % gross electric efficiency needs a 32 MW turbine. So looking for a more efficient turbine in this power range and optimizing the process from there on is difficult. Starting from the assumption that a gross electric efficiency of 34 % can be achieved the resulting turbine has a size of 47 MW. There are more turbine models available in this power range and therefore the selection of the right turbine is easier.

As a second step the live steam temperature is raised to a higher value. A reasonable value is 500 °C, even though the available turbines can handle up to 565 °C. There are several EFW plants which already operate at 500 °C. Most of them however suffer from increased corrosion. Therefore the use of a wall superheater, where the pipes are protected by rear ventilated tiles is planned as

final stage of the superheater (445 °C to 500 °C). More details on the layout of the wall superheater are given in Section 3.1.1.5.

The biggest improvement in the water steam cycle can be achieved by increasing the feed water temperature to levels known from coal power plants. For this reason the process must operate at high pressures and the turbine must offer the possibility to have multiple extractions at pressures up to 90 bar.

The design feed water temperature for the high efficient EFW water steam cycle is set to 300 °C. The feed water is preheated to this temperature with steam extractions in 5 steps. Additional waste heat is added at two levels where it is available. More on the use of waste heat is given in Sections 4.3.2.5, 4.3.2.6 and 4.4.1. Setting the limit to 300 °C for the feed water preheating is done for a

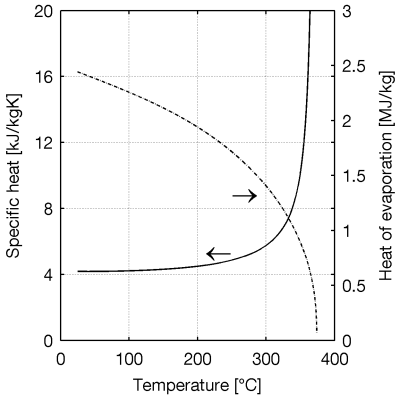

Figure 4.8.: Specific heat capacity and heat of evaporation for water vs. temperature range for feed water preheating

practical reason. The heat of evaporation or condensation drops continuously with increasing temperature as can be seen in Figure 4.8. The specific heat capacity of the feed water starts to increase significantly at arround 300 °C. This implies the mass flow rate of steam which needs to be extracted for preheating the feed water above 300 °C raises drastically. For the Carnot efficiency on the other hand there is no temperature optimum for feed water preheating, simply spoken: the hotter the better for the efficiency. Here only the main parameters of the water steam cycle are listed, all other parameters are discussed in Section 4.3:

- 500 °C live steam temperature
- 177 bar live steam pressure

- external steam heated reheating (See Section 4.2.2.4)
- 300 °C feed water temperature
- 5 stage steam heated feed water preheating
- 2 stage waste heat feed water preheating, (flue gas condensing, second economizer)
- 50 mbar pressure at turbine outlet, with hybrid cooling tower

Figure 4.9 shows the T-s diagram of the optimized steam cycle. Comparing the thermodynamic average temperatures shows the significant improvement to the other processes. This is mainly caused by the high feed water temperature. A plant scheme of this concept is shown in Figure 4.28 after the discussion of the overall plant optimization in Section 4.4, since some features have not yet been discussed so far.

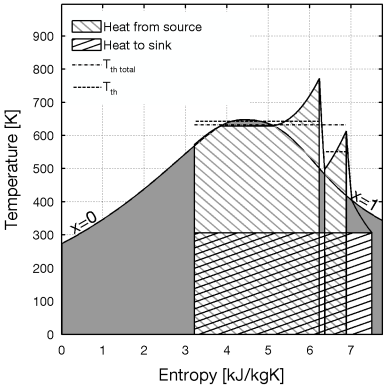

Figure 4.9.: T-s diagram of an optimized steam cycle with high steam parameters (177 bar and 500 °C) with external steam reheating and 300 °C feed water temperature

4.2.3. Concept comparison

Finally, all three discussed concepts are compared for a better understanding of the implications on the boiler by the efficiency improvement.

4.2.3.1. Heat distribution

For designing the heat transfer surface the heat distribution is needed. This is shown in Figure 4.10a. In Figure 4.10b the temperature change of water

and steam in the three components (economizer and superheater) is shown. Of special interest is the ratio of heat needed for superheating and evaporation, since it significantly influences the boiler design. The heat for water preheating in the economizer is secondary since the water should enter the drum sub cooled. The additional heat needed is then simply added to the evaporator. The heat

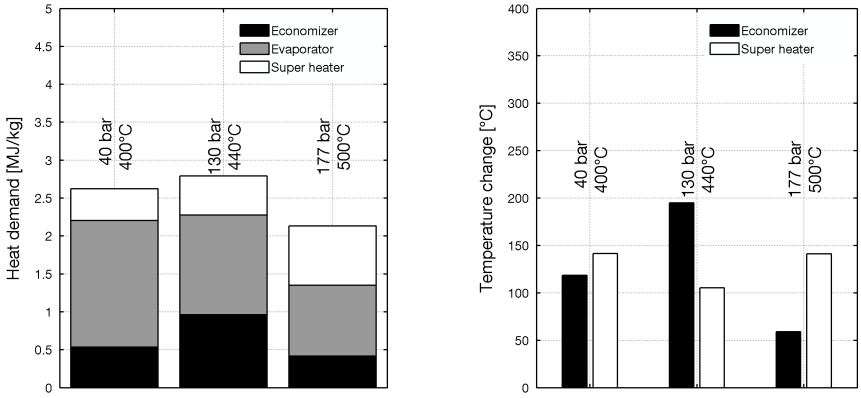

(a) Heat needed to reach saturation temperature, for evaporation and superheating

(b) Theoretical temperature changes in economizer and superheater

Figure 4.10.: Plant comparison in respect to heat distribution and temperature changes in the main boiler components

demand in the evaporator drops by half comparing the evaporation at 40 bar to the evaporation at 177 bar. The typical 5 bar to 6 bar pressure drop between drum and turbine is neglected in this investigation. The heat needed in the economizer is biggest in the 130 bar concept since the difference between feed water temperature and saturation temperature is highest.

The heat needed for superheating at the 130 bar concept is only slightly higher than for the 40 bar concept, since the temperature difference in the superheater is about 40 °C less. For the 177 bar concept the temperature difference in the superheater is similar to the 40 bar concept. The needed heat for superheating however is more than double. This is explained by the higher specific heat capacity of steam at higher pressures. (See Figure 4.11). It can be seen that per kg of live steam the high pressure boiler concept needs one fifth less heat. This is mainly caused by the higher feed water temperature. Less heat demand per kg of live steam implies more steam can be produced for the same gross heat

input. This results in higher efficiency since more steam is available for the same fuel input.

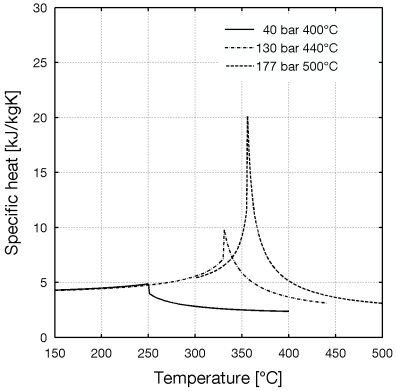

Figure 4.11.: Specific heat vs. temperature for the three different concepts

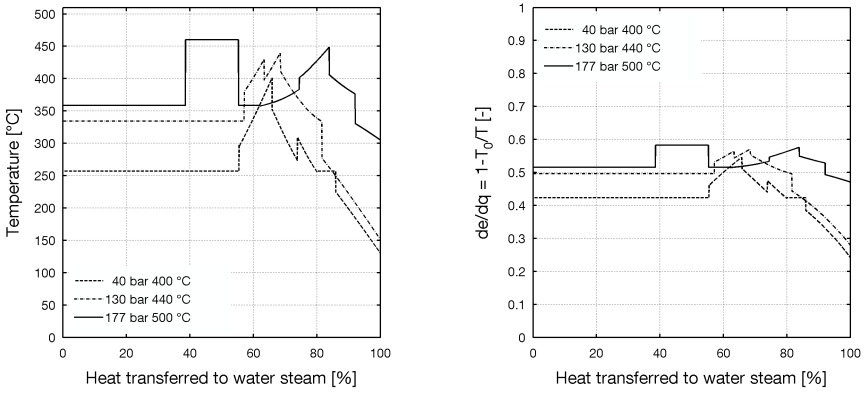

(a) Temperature-heat diagram

(b) Quality-heat diagram

Figure 4.12.: Temperature and heat quality distribution for different boiler concepts

A more detailed distribution of the needed heat is also, shown in the temperature-heat (t-q) diagram 4.12a, a quality analysis of the transferred heat is presented

by a quality-heat (de/dq-q) diagram shown in Figure 4.12b. The afore mentioned wall superheater applied in the 177 bar concept is shown as the rectangular block with its thermodynamic average temperature t_{th}, since due to its size it cannot be implemented in a clear co or counter current arrangement. (See Equation 4.4) Also, in this representation the higher average temperature of the heat transferred to the steam cycle can be seen. The quality of the heat transfer is calculated by means of a numerical exergy analysis, which is described in Section 4.3.1.

4.3. Heat source optimization

The heat source in an EFW plant is the flue gas generated during combustion. Depending on combustion settings the available temperature profile of the heat can be influenced and optimized.

In Section 4.2 it is shown how the water steam cycle of an EFW plant can be optimized. In Figure 4.12 a detailed distribution of the needed heat and its quality is presented. As a next logical step to optimize efficiency, the combustion system has to be optimized in such a way, to make as much of the heat input available at the temperatures required by the water steam cycle. This is done by a numerical analysis of exergy and temperature distribution. Parameter variations are performed for different settings influencing the combustion. Finally, different measures are combined stepwise to achieve an optimized heat source for the given water steam cycle.

4.3.1. Numerical exergy analysis

It is possible to produce shaft work from any lack in mutual equilibrium between a system and the environment. This is defined by the concept of exergy (e) and anergy (b). Exergy, unlike energy does not obey a conservation law. Exergy is destroyed (transformed to anergy) during irreversible processes, therefore exergy analysis makes inefficient process steps as well as the direction for improvement clearly visible [112]. The Carnot efficiency gives the ideal efficiency with which heat can be converted into work. As discussed in section 4.2.1 this is only valid for isothermal heat sources. To determine the ideally available work of a non-isothermal heat source in respect to a defined reference temperature T_0 exergy can be used. Equation 4.6 shows that the Carnot efficiency gives for the exergy the quality of the heat defined as de/dq. By integrating over the quality of the

heat from T_0 to T the exergy e is determined (See Equation 4.7).

$$\eta_{carnot} = \frac{de}{dq} = 1 - \frac{T_0}{T} \tag{4.6}$$

$$e = \int_{T_0}^{T} 1 - \frac{T_0}{T} dq \tag{4.7}$$

$$b = q - e \tag{4.8}$$

The two following equations are obtained by solving this integral. For water and steam it is mostly used in the form of Equation 4.9, using a enthalpy (h) and entropy (s) difference. While for flue gases with assumed constant average specific heat capacity (c_p) Equation 4.10 can be used.

$$e = h - h_0 - T_0 \cdot (s - s_0) \tag{4.9}$$

$$e = c_p \cdot (T - T_0) - T_0 \cdot c_p ln(\frac{T}{T_0}) \tag{4.10}$$

The exergy for both water steam and for flue gases with a non-constant c_p can be computed numerically in a simple way. The integral of the heat quality for determining the exergy can be solved numerically by using the Newton-Cotes formula for degree 1, also, known as trapezoid rule [113]. The numerical equation is shown below (See Equation 4.11). This type of analysis was already used by Murer et al. in 2010 to analyze different boiler concepts for EFW plants [108].

$$E = \sum_{n(T_0)}^{n(T)-1} (1 - \frac{T_0}{\frac{T(n)+T(n+1)}{2}}) \cdot (Q(n+1) - Q(n)) \tag{4.11}$$

For this analysis steps of constant transferred heat (Q) are used, although steps with constant temperature are also, possible. It is more practical to use steps of constant heat if a combined analysis of the flue gas and water steam side of a boiler is performed. The step size for these investigations is set to 1 kW_{th}.

$$T(n+1, i+1) = T(n) + \frac{Q(n+1) - Q(n)}{c_p(T(n+1, i)) \cdot \dot{m}_{fg}} \tag{4.12}$$

The flue gas temperature is determined after each step iteratively to compensate for the temperature dependence of the specific heat capacity (See Equation 4.12

with iteration indices n and i). Iterations are performed until the change in temperature is smaller than 0.001 °C. The chosen step size of 1 kW_{th} results in temperature steps of 0.02 °C at the flue gas side.

The temperature - heat diagram The data generated by the numerical exergy analysis can be used to generate expressive diagrams. Typical for boilers is to show the temperatures of the flue gas and water steam in a temperature-heat (t-Q) diagram. An example for such a diagram is shown for a state of the art EFW boiler in Figure 4.13. The transferred heat is normalized with the gross heat input. This allows for a better comparison with other boiler concepts and makes the effect of air preheating and grate cooling better visible. As can be seen, the flue gas contains slightly more heat than the gross heat input (graph goes to more than 100 %), this is caused by the air preheating. The heat content of the flue gas is decreased due to heat losses by high temperatures at the removal of bottom and fly ash as well as radiation and convection losses at the outside of the boiler. Therefore plants with no combustion air preheating have energy content in the flue gas which is slightly lower than the energy in the fuel (gross heat input). The heat in the flue gas is based on a reference temperature of 25 °C, this can also be seen in Figure 4.13 since the temperature curve for the temperature drops to 0, when reaching 25 °C.

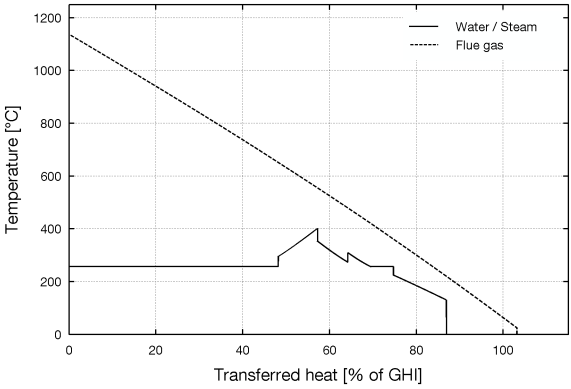

Figure 4.13.: Temperature-heat diagram for a state of the art EFW plant

The energy quality - heat diagram Murer et al. presented in 2010 the energy quality - heat diagram (See Figure 4.14b), which is an derivation of the tradi-

tionally used $\frac{1}{T}$-Q diagram [108]. In the $\frac{1}{T}$-Q diagram (See Figure 4.14a) the exergy destruction due to the heat transfer is proportional to the area between the graphs of the cold and hot medium. Multiplication of the $\frac{1}{T}$ values with T_0 shows then the anergy ratio directly in the diagram. The graphs can be flipped by subtracting all values from 1, as a result the diagram shows directly the quality of the transferred heat: $\frac{de}{dq} = 1 - \frac{T_0}{T}$. (See Figure 4.14b)

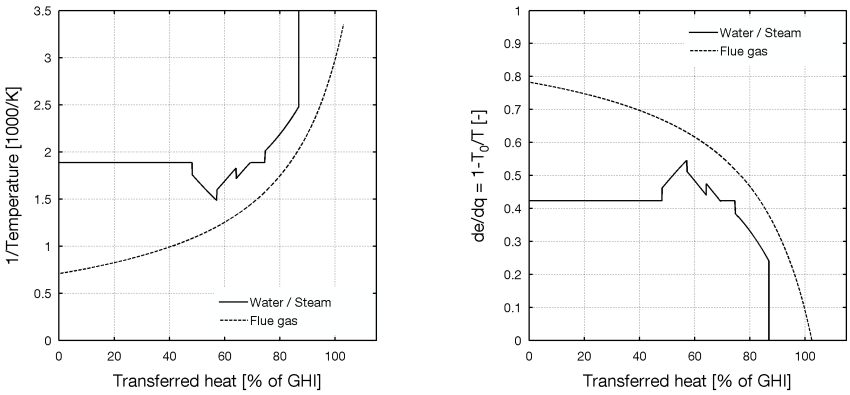

(a) 1/temperature-heat diagram for a state of the art EFW plant

(b) Heat quality - heat diagram for a state of the art EFW plant

Figure 4.14.: Different representation methods for the quality of the transferred heat in a boiler

The y-axis of the heat quality-heat diagram ranges from 0 to 1. 0 means the transferred heat is 100 % anergy and 1 implies the transferred heat is 100 % exergy. On the x axis the transferred heat is shown in percentage of the gross heat input. The full square between the corner points (0,0) and (100 %, 1) gives the exergy available in the fuel, neglecting the exergy available in a possible flue gas condenser.

The exergy available in the flue gas is characterized by the area spanned by the flue gas temperature curve, which starts at the adiabatic temperature and finishes at the reference temperature of 25 °C. The exergy transferred from the flue gas to the water steam cycle is represented by the area under the water steam curve. The difference in exergy between the exergy available in the flue gas and the exergy originally available in the fuel is destroyed during the combustion process in the form of irreversibilities and heat losses with the ashes and grate cooling (if installed). The heat quality of the flue gas decreases slowly to the level

of 0.5, which corresponds to a temperature of approximately 325 °C. Quality of 0.5 implies an exergy content of 50 % in the transferred heat. More than 75 % of the heat in the flue gas has a higher quality than 0.5. For the optimized steam cycle this percentage has to be improved further, since it can only use heat above 300 °C. After the heat quality in the flue gas decreased to 0.5 it starts to drop drastically. The heat quality of the losses (no heat is transferred to the water steam site) is in average below 0.2. Therefore the unused heat in state of the art EFW plants is of low thermodynamic value.

4.3.2. Influencing the heat source system

After describing the methods for analyzing the heat source system, different combustion parameters and other parameters are studied to see how the effect on both the temperature profile and the available heat quality are influenced. The main settings for this investigation are shown in Table 4.3.

Table 4.3.: Main combustion settings for the investigation on the heat source

Excess air ratio	1.35	-
Combustion air temperature	25	°C
Air humidity	0.63	vol.%
t_0	25	°C

4.3.2.1. Condensing pressure

As mentioned before, Musil uses the condensing temperature as T_0 for exergy calculation [99]. The condensing temperature depends on the condensing pressure as shown by the values listed in Table 4.2. A variation of condensing pressure is performed to make the change in heat quality visible (See Figure 4.15). The condensing pressure has no effect on the temperature of the flue gas (See Figure 4.15a). The heat quality is however, influenced drastically (See Figure 4.15b). Lower condensing pressures make the heat in the flue gas more valuable. The effect is actually caused by the more efficient heat sink system, since the temperature drop between heat source and sink of the same heat becomes bigger with lower condensing pressures. The efficiency can be increased by reducing the condensing pressure since the temperature difference between heat source and sink is increased.

For all following investigations T_0 is set to 25 °C which corresponds to a condensing pressure of approximately 0.03 bar.

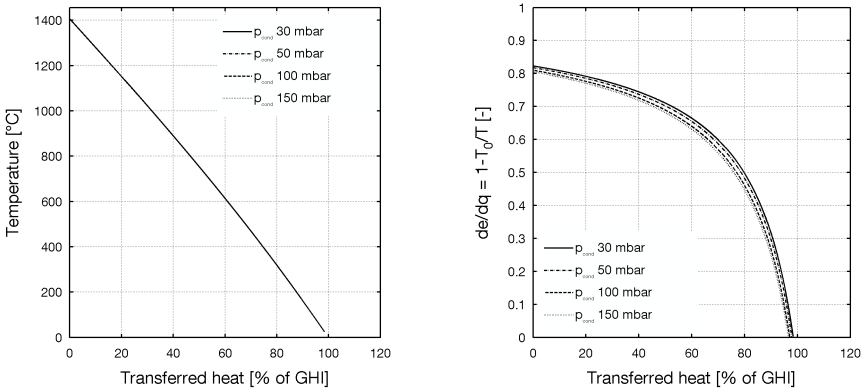

(a) Temperature-heat diagram

(b) Quality-heat diagram

Figure 4.15.: Influence of different condensing pressures on temperature and heat quality distribution

4.3.2.2. Excess air ratio

One of the main combustion parameters is the excess air ratio λ, defined by Equation 4.14. The air to fuel ratio (AFR) is needed before hand to determine the excess air ratio (See Equation 4.13). λ defines the surplus air added to the combustion to guarantee complete burnout and low emissions. Traditionally EFW plants are operated with an excess air ratio of 1.5 to 1.8. With flue gas recirculation the excess air ratio is often reduced to 1.4. Schu and Leithner as well as Aleßio and Mück suggest both a reduction of the excess air ratio to 1.2; however, the mixing has to be improved. This can be done by the injection of recirculated flue gas, steam or by constructive mixing elements [114], [106]

$$AFR = \frac{\dot{m}_a}{\dot{m}_f} \tag{4.13}$$

$$\lambda = \frac{AFR}{AFR_s} \tag{4.14}$$

The air fuel ratio (AFR) is the current ratio of the oxidizer mass flow rate ($\dot{m}_a$) to the fuel mass flow rate ($\dot{m}_f$). From the air fuel ratio the excess air ratio can be calculated, if the stoichiometric air fuel ratio (AFR_s) is known. For this investigation the excess air ratio is varied from 1.35 - 1.8 in steps of 0.15. Decreasing

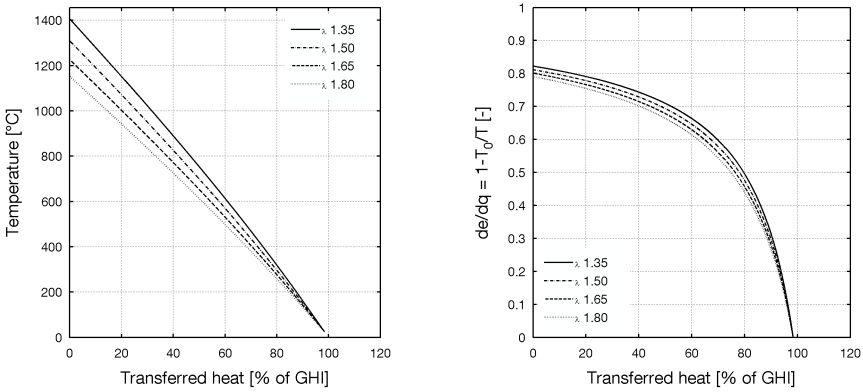

(a) Temperature-heat diagram

(b) Quality-heat diagram

Figure 4.16.: Influence of different excess air ratios λ on temperature and heat quality distribution

the excess air ratio decreases the oxygen concentration (x_{O_2}) in the combustion, however, also, the mass flow rate of nitrogen going through the boiler decreases. Nitrogen is thermal ballast, which decreases the flame temperature. By reducing the excess air ratio, the flame temperature is increased. Also, less flue gas passes the boiler resulting in steeper temperature gradients for the same heat flow. Less flue gas subsequently passes the flue gas treatment plant, which can therefore be designed smaller. The thermal loss of the flue gas depends on the flue gas mass flow and can therefore be reduced by reducing the excess air ratio.

As can be seen in Figure 4.16a the adiabatic flame temperature (T_{ad}) increases by more than 200 °C, if the excess air ratio is changed from 1.8 to 1.35. The exergy content is slightly higher for low excess air ratios. However, most gain is achieved at a heat quality above 0.5, where the exergy is destroyed by the heat transfer to the water steam cycle. The total heat flow available in the flue gas does not change with the excess air ratio. However, the heat flow contained in the flue gas at the boiler outlet is reduced if the boiler outlet temperature stays constant, since the flue gas mass flow rate is reduced and thus the boiler efficiency increased.

All following investigations are performed with an excess air ratio of 1.35.

4.3.2.3. Grate cooling

The possibility to cool the grate not only by the combustion air, but by water as and additional cooling medium offers an additional degree of freedom in the combustion control [115]. The grate cooling allows to keep the metal temperature of the grate bars low and thereby improves the grates lifetime [26]. Aleßio states that on average about 1.6 % of the gross heat input is extracted by the grate cooling system [106]. During the performance of a sensitivity study of a boiler energy balance it was noticed that the extracted heat can reach up to 3 % for the gross heat input for longer periods [116]. The heat extracted by the grate cooling system is downgraded to 80 °C to 120 °C and can only be used for water or air preheating and has therefore low thermodynamic quality. The heat extracted fluctuates with the inhomogeneous combustion process on the grate; this makes the continuous use of the heat more difficult. An additional steam heated preheater can be installed to compensate for the fluctuations [12]. Other grate systems, like the reverse acting grate of Martin, do not need grate cooling since it operates in such a way that it is continuously covered with a layer of waste and slag [117].

For this investigation the ratio of grate cooling (gc) is varied from 0 % to 3 % of the gross heat input.

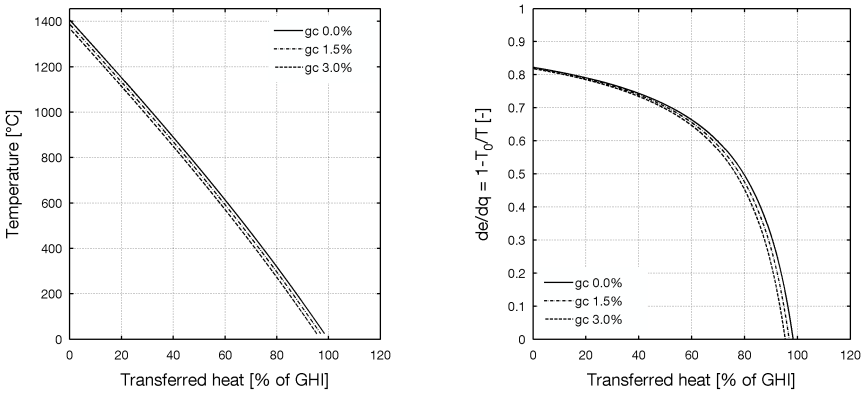

(a) Temperature-heat diagram

(b) Quality-heat diagram

Figure 4.17.: Influence of different percentages heat extracted by grate cooling (gc) on temperature and heat quality distribution

The missing heat in the flue gases decreases the combustion temperature and therefore the available heat in the flue gas. (See Figure 4.17a) For 3 % grate cooling the adiabatic flame temperature decreases by 40 °C. The temperature, as well as the heat quality graphs is moved to the left by the ratio of heat extracted by the grate cooling. If the temperature at the boiler outlet is kept constant, the heat removed by the grate cooling is directly missing in the flue gas. This implies the live steam mass flow rate drops by exactly the ratio of the grate cooling, which finally, reduces the net electric efficiency (See Equation 4.15).

$$\frac{\dot{m}_{ls,gc}}{\dot{m}_{ls}} = \frac{\dot{Q}_{ghi} + \dot{Q}_{aph} - \dot{Q}_{los} - \dot{Q}_{gc}}{\dot{Q}_{ghi} + \dot{Q}_{aph} - \dot{Q}_{los}} \tag{4.15}$$

In Equation 4.15 $\dot{m}_{ls}$ is the live steam mass flow rate, $\dot{m}_{ls,gc}$ is the mass flow rate with grate cooling, $\dot{Q}_{ghi}$ is the gross heat input, $\dot{Q}_{aph}$ is the heat input by the air preheater, $\dot{Q}_{los}$ represents all general boiler losses and $\dot{Q}_{gc}$ is the heat extraced by the grate cooling.

4.3.2.4. Flue gas recirculation

Flue gas recirculation is a good method to reduce the temperature of the combustion and allows for additional mixing. NO_x, CO and O_2 can be reduced by a good mixing in the post combustion zone [118]. The lower oxygen of the recirculated flue gas especially favors the decomposition of NO_x. Recirculated flue gas circulates some oxygen, which results in a locally higher excess air ratio, compared to the design excess air ratio of the plant. This extra oxygen helps additionally in maintaining a good burnout.

Recirculation rate The recirculated flue gas has nearly the same composition as the gas at the boiler outlet. The recirculated flue gas is extracted normally after the dedusting step in the flue gas treatment plant to avoid deposits and erosion in the recirculation duct. It is common to recirculate at least 20 % to 25 % of the flue gas flow. Equation 4.16 shows how the flue gas recirculation rate (FRR) is defined, calculated from the recirculated flue gas mass flow rate ($\dot{m}_{reci}$) and flue gass mass flow rate at the stack ($\dot{m}_{stack,ideal}$).

$$FRR = \frac{\dot{m}_{reci}}{\dot{m}_{stack,ideal}} \tag{4.16}$$

For this investigation the FRR is varied from 0 % to 40 % in steps of 10 % and the recirculation temperature is kept constant at 160 °C. A flue gas recirculation

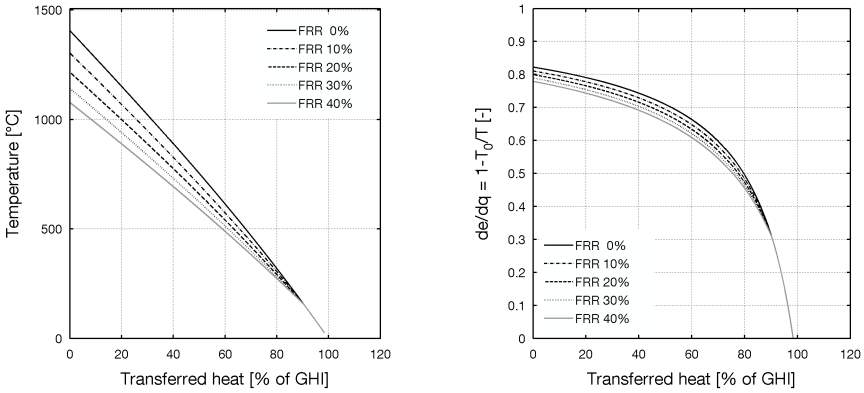

(a) Temperature-heat diagram

(b) Quality-heat diagram

Figure 4.18.: Influence of different rates of flue gas recirculation on temperature and heat quality distribution

rate of 20 % decreases the adiabatic flame temperature by 200 °C. (See Figure 4.18a) The cooling effect is not linear since it is a dilution effect. With increasing FRR the mass flow rate of the flue gas through the boiler is increased, this reduces the temperature gradient of the flue gas since more heat has to be transferred for the same temperature change. Depending on the boiler geometry this increases the residence time. This is good for reactions, which take place in defined temperature windows, like selective non catalytic NO_x reduction.

Recirculating flue gas influences the exergy content of the flue gas significantly, but only above the recirculation temperature. Therefore it is possible to reduce the exergy especially in the part of the boiler where it is destroyed anyway due to the heat transfer to the water steam cycle.

Recirculation temperature Flue gas recirculation changes not only the adiabatic flame temperature but also, the flue gas flow through the boiler. It is not necessary to have this increased flue gas flow through all low temperature components. Additionally it can be better to decrease the adiabatic flame temperature only slightly. To achieve this, the location and therefore the temperature at which the flue gas is piped back can be changed. There are plants where the flue gas is taken rather cold directly before the stack, while other plants recirculate the flue gas after an electro static precipitator at 200 °C and more. For

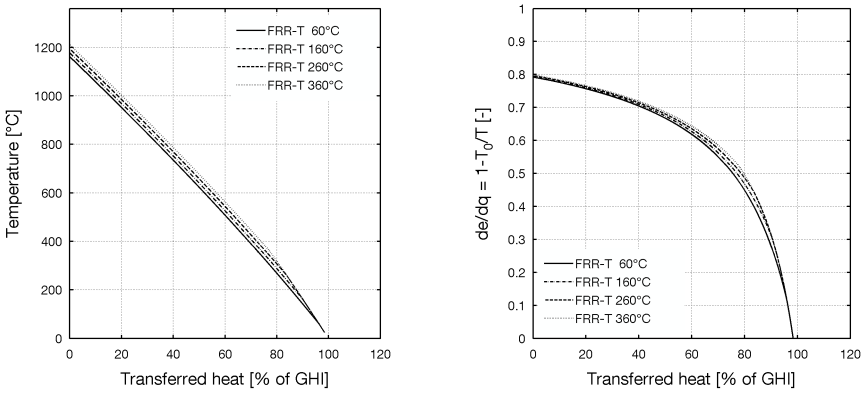

(a) Temperature-heat diagram

(b) Quality-heat diagram

Figure 4.19.: Influence of different temperatures of recirculated flue gas on temperature and heat quality distribution

this investigation the flue gas recirculation rate is kept constant at 25 % and the recirculation temperature is varied from 60 °C to 360 °C in steps of 100 °C. The adiabatic flame temperature changes only by 50 °C depending on the recirculation temperature.(See Figure 4.19) The heat flow at a quality above 0.5 increases, however, by about 5 % for higher recirculation temperatures. To reduce the combustion temperature and at the same time keep the available heat above a certain temperature level high, this temperature level has to be chosen as design temperature for the flue gas recirculation.

4.3.2.5. Air preheating

In EFW plants air is preheated mainly for improving the combustion process and not for efficiency reasons. Preheated air helps for the drying and ignition of the fuel. Grate based combustion systems are preheated up to 200 °C [28]. Depending on the moisture content of the fuel, up to 260 °C air temperature has been reported for the reverse acting grate.

For state of the art EFW plants air is preheated with steam. This implies heat is transferred from the water steam cycle system back to the heat source system. As shown in Figure 4.1 for an efficient operation heat should only flow from the heat source system to the heat sink and not in the opposite direction. The efficiency decrease occurs since high quality heat was used to produce the

steam. Therefore it should be used inside the boundaries of the water steam cycle for example in the turbine as efficiently as possible. As discussed below low temperature heat of the flue gas is the favorable heat source for efficient air preheating.

Markovic et al. performed tests with wood chips. They found out that at air temperatures higher than 230 °C the wood chips self-ignite in the combustion system [119]. High air temperatures ensure that all of the fuel ignites and additionally increase the combustion speed and improves the burnout.

Low temperature heat of the flue gas can be used to preheat the combustion air. This allows for a beneficial use of flue gas heat at temperatures below 200 °C [114]. Aleßio and Mück suggest a direct heating of the air at the boiler end. Hot air has a lower density; therefore investment in bigger duct cross sections has to be made from the outlet of the boiler to the combustion system [106].

However, the heat can also be transported by one or two additional water circuits from the boiler outlet to the combustion system. This implies additional heat exchangers, however, the air can be preheated as close to the combustion system as possible. This gives more degrees of freedom in the design of the plant layout.

To improve combustion most of the time only the primary air is preheated. Preheating the secondary air can ensure that the temperature in the post combustion zone is high enough for good burnout and destruction of dioxins [26]. A plant planned with secondary air preheating is the new EFW plant for Copenhagen presented by Kamuk [120].

An additional low temperature heat source is made available by dry discharge of the bottom ash. Air is sucked through the ashes to filter out the fine fraction; thereby it cools the ash particles and absorbs their heat. A dust removal system removes most of the particle and the warm air is injected along with additional air as secondary air in the post combustion zone [121]. This is a unique method for recovering heat normally quenched away in a wet ash discharger.

For this investigation the total combustion air is preheated to different temperature levels (APT) between 50 °C and 300 °C. 25 °C is selected as reference case. Where the heat comes from is irrelevant for this investigation. Only small part of the air is added at the end of the grate, therefore the influence of higher air temperature on the bottom ash temperature is neglected. Increasing the air temperature from 25 °Cto 300 °C raises the adiabatic flame temperature by only 180 °C. For 100 °C air temperature the change is only 50 °C (See Figure 4.20a). This is caused by the higher specific heat capacity of the combustion gases at high temperature compared to the specific heat capacity of air at low temperature. Additionally also, the gases released from the waste bed absorb some of the heat. The extra heat supplied shifts the graphs in both the temperature-heat

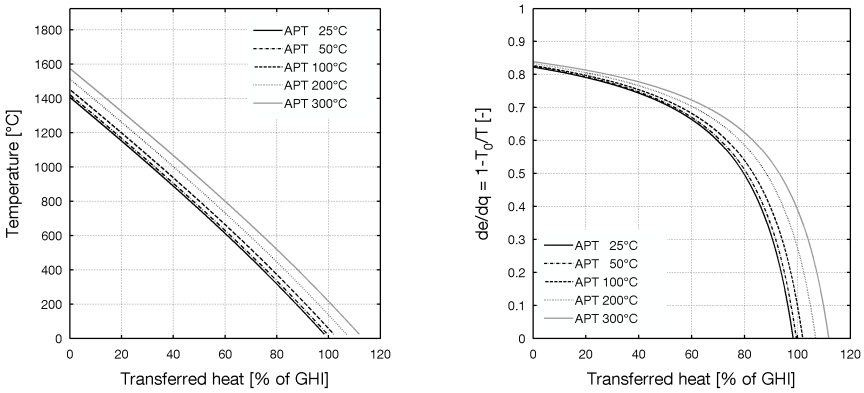

(a) Temperature-heat diagram

(b) Quality-heat diagram

Figure 4.20.: Influence of different temperatures for air preheating on temperature and heat quality distribution

diagram and the heat quality-heat diagram to the right (See Figure 4.20). In total there is more heat available which consists of the heat input by the fuel as gross heat input plus the heat from the air preheater. The positive effect on the heat quality in the flue gas can be seen by comparing the effect on the heat quality (See Figure 4.20b). Low quality heat in form of hot air is added to the system and more high quality heat is obtained in the process. Of course gain in efficiency is highest if the heat of the air comes from a respective low temperature heat source like the flue gas at the boiler outlet.

4.3.2.6. Air humidification

An option discussed in biomass fired boilers is the humidification of the combustion air. A patent of Åbyhammar uses preheated combustion air to dry biomass with high moisture content. The air is preheated with low temperature heat available in a flue gas condenser. The air with increased moisture content is later injected as combustion air into the boiler [122]. The desired effect is mainly a faster and better combustion of the fuel. Gaderer shows a concept for air humidification indirectly with heat from a flue gas condenser as well as other heating applications for low temperature heat [123]. Westmark also has a patent on combustion air preheating and humidification with warm water of the flue gas condenser with the sole purpose of improving the boiler performance [124].

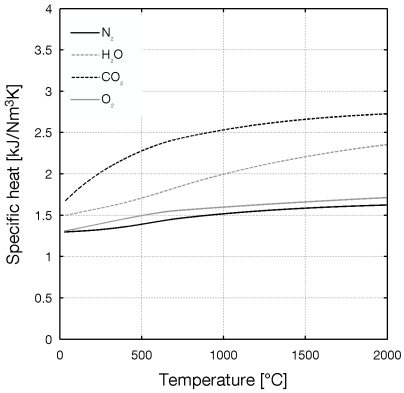

Figure 4.21.: Specific heat capacity for the 4 major flue gas species

Becker investigated in 2012 the use of humidified air in an EFW boiler from a thermodynamic point of view. The combustion air can be heated and humidified directly with warm water up to 55 °C [125]. The water content at this temperature for saturation conditions is 15.8 vol.%. This results in an increased mass flow rate, which, similar to flue gas recirculation has a cooling effect. Advantages of increased moisture content in the combustion air are:

- high specific heat capacity of water vapor (H_2O) (See Figure 4.21), small additional mass significantly reduces the combustion temperature.
- waste bed is kept colder, more air preheating is possible
- lower partial pressure of oxygen, results in reduced NO_x formation
- increased partial pressure of H_2O, results in higher concentration of OH radicals, which accelerate the burnout of CO and other chemical reactions
- H_2O is along with CO_2 the dominant species for gas radiation [60], more radiation from the post combustion zone is available to ignite dry fuel faster
- additional mixing impulse for secondary air for the same mass of oxygen added to the combustion
- dry flue gas cleaning works better for increased relative humidity [126]
- dew point of the flue gas is raised; heat form flue gas condenser is available at a higher temperature level [125]

For this investigation water contents from 0 vol.% to 15 vol.% in steps of 5 vol.% are investigated. These correspond to saturation temperatures of 0 °C, 33 °C,

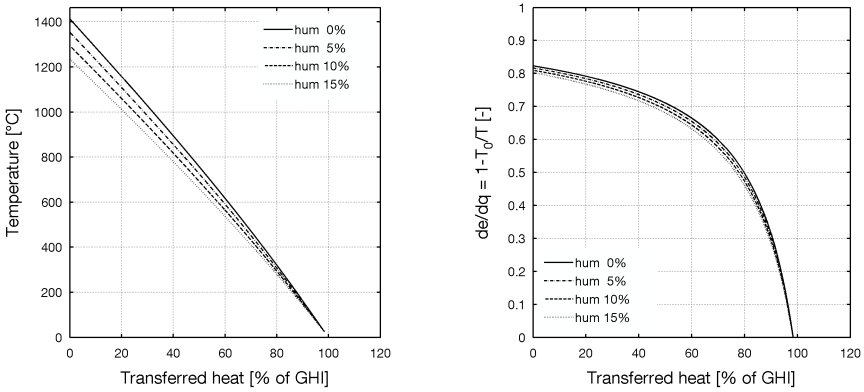

(a) Temperature-heat diagram

(b) Quality-heat diagram

Figure 4.22.: Influence of different combustion air humidification's on temperature and heat quality distribution

46 °C and 54 °C. The air is added to the combustion system at 25 °C and humidified internally. Increasing the combustion air humidity from 0 vol.% to 15 vol.% decreases the adiabatic flame temperature by 180 °C. Similar effects as for the flue gas recirculation can be observed. (See Firuge 4.22) Heat quality is also, reduced mainly above 0.5.

Process implementation of air humidification At the HRC plant flue gas condensers are installed after the flue gas treatment plant. They are of the same design as the HCl and SO_2 scrubbers upstream of the flue gas condensers. The warm water is used locally to preheat the main condensate.
The air humidification can be implemented in a similar way, as shown in Figure 4.23. Warm water of the flue gas condenser has a temperature of 70 °C and is pumped close to the grate. There a similar scrubber is installed. Combustion air sucked from the bunker is blown through the scrubber. The warm water first passes a small air preheater, before it is sprayed into the scrubber. The air is dusty since it comes from the bunker. This dust is washed out; while at the same time the air is humidified and preheated to 55 °C. The air enters finally, the small air preheater where it is heated from 55 °C to 65 °C with a finned tube heat exchanger. During the process of humidification the water cools down and is loaded with dust. The dust is removed in the form of sludge from the water.

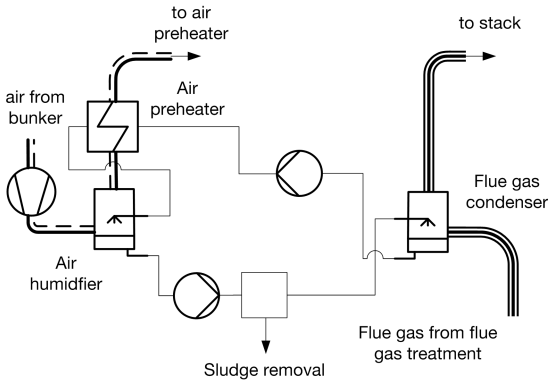

Figure 4.23.: Scheme for arrangement of an air humidifier operated with warm water from the flue gas condenser

The water is then pumped back to the flue gas condenser to close the cycle. The sludge is also, incinerated in the combustion system. It can be mechanically dried and added to the waste chute or directly pumped by a nozzle in the wall onto the grate.

4.3.2.7. Overview on methods to influence the heat source

Tabel 4.4 presents a summary of the tendencies of the individual measures for influencing the heat in the flue gas. The flame temperature is an important

Table 4.4.: Tendencies for different combustion settings on the heat source

	T_{ad}	x_{O_2}	$\dot{V}_{fg}$
↓ Excess air ratio	↑	↓	↓
↓ Grate cooling	↑	-	-
↑ Flue gas recirculation rate	↓	-	↑
↑ Flue gas recirculation temperature	↑	-	-
↑ Air preheating	↑	-	-
↑ Air humidification	↓	↓	↑

factor for the combustion. Higher temperatures increase the heat transfer rate and therefore reduce the boiler size of the empty passes. On the other hand high temperatures also, increase the risk for ash melting and corrosion. It is therefore

important to combine different process changes to get a good combustion along with high quality heat in the flue gas.

Most measures which decrease the combustion temperature result in an increase of the flue gas volume flow, since the heat is simply distributed over more mass flow. Reduced grate cooling and increased air preheating have a direct influence on the available heat in the flue gas without changing the volume flow rate. These measures can be used to adjust the combustion process to optimal parameters. The effect of these measures is mainly limited to the furnace, while measures like air humidification, flue gas recirculation and changed excess air ratio affect also, the rest of the boiler.

4.3.3. Optimizing the available heat in the flue gas

The combustion settings described above can be combined to optimize the available heat and the use of the heat of the flue gas to meet the requirements of the optimized water steam cycle. The feed water temperature is set to 300 °C and the live steam temperature is 500 °C. A pinch point temperature of 25 °C is chosen, which implies that only heat above 325 °C can be transferred into the water steam system. With t_0 set to 25 °C only heat with a quality of more than 0.5 is transferred to the water steam cycle. The heat with lower quality can be used for air preheating and other measures.

Stepwise changes in the combustion settings are performed to optimize the heat quality in the flue gas. The optimization starts with the combustion parameters presented in Table 4.5. To keep as much as possible of the released heat in the flue gas a grate system without grate cooling is used in this investigation.

Table 4.5.: Combustion settings before the heat source optimization: step 0

Excess air ratio	1.65	-
Combustion air temperature	25	°C
Adiabatic flame temperature	1225.5	°C

4.3.3.1. Step 1 reducing excess air ratio to 1.35

As a first step the excess air ratio is reduced from 1.65 to 1.35. The adiabatic flame temperature increases by nearly 200 °C (See Figure A.1 in the Appendix A). The cooling gradient of the flue gas increases; this reduces the losses at the boiler outlet assuming constant boiler outlet temperature of 325 °C. About 3 % more heat is available at a quality over 0.5. The combustion can be staged,

which implies a heat release in several stages, this allows an intermediate cooling and keeps the flue gas temperature in the real combustion process far below the adiabatic flame temperature. More on staged combustion is discussed in Sections 3.2.2.2 and 5.1.

4.3.3.2. Step 2 implementing flue gas recirculation

The next step is to introduce flue gas recirculation to reduce the adiabatic flame temperature again and especially to improve the mixing due to the lower oxygen available for the combustion. To reduce the adiabatic flame temperature back to the adiabatic temperature of step 0 25 % of the flue gas mass flow at the stack has to be recirculated. The flue gas is extracted at the boiler outlet. This implies a flue gas temperature of 325 °C, which can be controlled by a drum preheater. The flue gas has to be cleaned by a high temperature ESP or baghouse filter to keep the dust load of the recirculated flue gas low. More on the topic of high temperature dust removal is discussed in Section 4.4.2. Fans for this high temperature are available from other industrial sectors, but are not yet used with flue gas from waste incinerators. Also, the duct for the recirculated flue gas should be made of higher quality materials to ensure high availability. The adiabatic flame temperature drops by 200 °C as shown in Figure A.2a in the Appendix A. A corner can be seen in the temperature graph, where the flue gas is recirculated. This is caused by the lower mass flow available for lower temperatures, due to the flue gas recirculation. Along with the flame temperature also, the quality of the heat drops, but only above the desired value of 0.5 (See Figure A.2b in the Appendix A).

4.3.3.3. Step 3 preheating the combustion air to 275 °C

The heat available below 325 °C has to be used efficiently. As discussed in Section 4.3.2.5 the low temperature heat can be used for air preheating. In total about 20 % of the gross heat input is available as low temperature heat. Not all of it can be used for air preheating, since the flue gas cannot be cooled down to 25 °C. Also, the flue gas flow is slightly higher and has due to its composition a higher specific heat capacity than the air flow. As also, discussed in Section 4.3.2.5 air can be heated with an intermediate water loop. Using the same pinch temperature as at the boiler outlet the air can be preheated up to 275 °C. This is no problem for the secondary air. For the primary air, however, the waste bed temperature is increased drastically. This results in higher wear of the grate bars and reduced lifetime, depending on the waste incinerated on the grate. The adiabatic flame temperature is increased by 130 °C. The preheated combustion

air contains about 11.5 % of the gross heat input, when heated to 275 °C. This is exactly the distance the graphs in both Figures A.3a and A.3b (In the Appendix A) move to the right. This implies 11.5 % more heat is available with a quality of more than 0.5. The same increase is transferred directly to the water steam cycle. So air preheating with low temperature heat of the flue gas is very efficient, since it converts low value heat to high value heat. The heat is circulated inside the heat source system; therefore it is more efficient than using steam for preheating and transfer the low temperature heat into the water steam cycle.

4.3.3.4. Step 4 humidification of combustion air

Preheating the combustion air leads to high temperatures at the grate. Additional flue gas can be recirculated to reduce the temperature. Traditionally recirculated flue gas is only used in the post combustion zone and not used as under fire air, since it is more corrosive than air. A suitable alternative to decrease the temperature of the waste bed is to humidify the combustion air. The optimization step is to use 70 °C warm water from the flue gas condenser to saturate the combustion air at a temperature of 55 °C. This is a very useful way of using extremely low value heat. At this temperature the air is saturated with a water content of 15.8 vol.%. Air humidification to more than 15 vol.% reduces the adiabatic flame temperature down to 1190 °C. This is 140 °C lower compared to the previous step (See Figure A.4a in the Appendix A). Due to the warm water vapor added the total available heat in the flue gas is further increased. However, the heat quality slightly drops for the heat above the quality of 0.5. Below this limit the value is slightly increased due to the increased mass flow rate.

4.3.3.5. Step 5 reduction of excess air to 1.25

Flue gas recirculation and air humidification lead both to additional mixing for the same amount of oxygen. This consideration offers the possibility to decrease the excess air ratio further to 1.25 as the final step in the heat source optimization. The effect of this change is only minimal. The adiabatic flame temperature increases by about 50 °C (See Figure A.5a in the Appendix A). However, this is no problem for the combustion on the grate, since the ratio of primary to secondary air can be set independently from the excess air ratio. So the waste bed temperature of a furnace operated with an excess air ratio of 1.25 can be the same as for one with 1.35 or even lower.

The only purpose of this change is to reduce the total mass flow rate of flue gas and thereby the size of the flue gas treatment equipment.

Table 4.6.: Combustion settings after the heat source optimization

Excess air ratio	1.25	-
Combustion air temperature	275	°C
Flue gas recirculation at 325 °C	25	%
Air humidification	15.8	vol.%
Adiabatic flame temperature	1239.7	°C

Tabel 4.6 presents the combustion settings after the optimization.

The temperature profile before and after the optimization is compared in Figure 4.24a. The adiabatic flame temperature is nearly the same. Due to flue gas recirculation and air humidification the temperature decreases more slowly and more heat is available at high temperature levels. At 325 °C a corner marks the point of the flue gas recirculation. In total the flue gas contains about 11.5 % more heat, which is recirculated from low temperature heat to the air preheating and then back into the combustion system.

The heat quality however, is improved with the focus on improving the heat flow with a quality higher than 0.5. An increase from 76.5 % to 91.5 % of this high value heat was achieved (See Figure 4.24b). This implies that 91.5 % of the gross heat input can be transferred to a water steam cycle at a temperature of more than 300 °C. Recalling the Carnot efficiency (See Equation 4.3) the positive effect of this improvement is obvious. The biggest improvement in the heat source optimization is achieved by air preheating (step 3). Preheating of combustion air is mainly seen in the EFW business as a method to improve the combustion process with moist fuel and not as an option to improve the efficiency. This investigation however, showed that air preheating is the key option for improving the energy efficiency. All other options are only used to tune the combustion process and allow for it to be operated in an efficient way.

It is important for the air preheating, that it is done with low value heat from the flue gas and not with steam. Combustion air temperature of 275 °C is a thermodynamic based choice due to the chosen feed water temperature of 300 °C and the resulting boiler outlet temperature of 325 °C. Nowadays the feed water temperature is as high as 150 °C. This would imply a combustion air temperature of about 125 °C for both primary and secondary air. From here on heat has to be used for air preheating which is normally used for feed water preheating in the economizer. Therefore the air temperature should only be raised if the feed water temperature is increased accordingly and the feed water is preheated using extracted steam from the turbine. The heat transfer surface

of the economizer decreases, while heat transfer surface for the air preheater has to be installed at the same position.

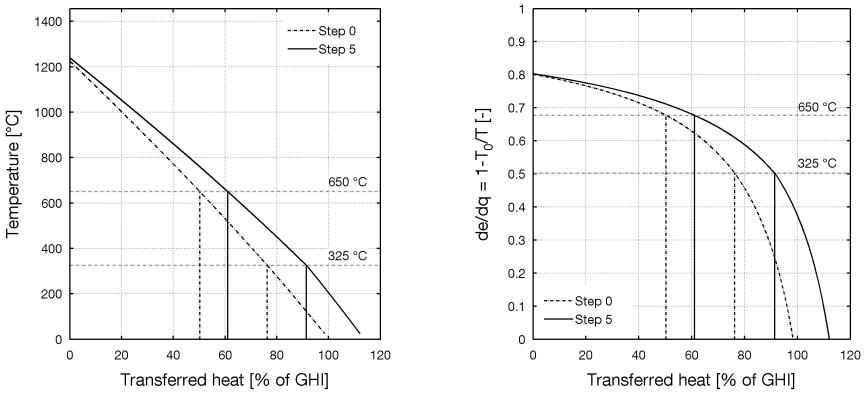

(a) Temperature-heat diagram

(b) Quality-heat diagram

Figure 4.24.: Step 0 compared with step 5

The heat in the flue gas can be classified in three different groups: high temperature heat, high value heat and low temperature heat.

High temperature heat is all heat available over 650 °C. This heat can be used in membrane walls for evaporation without problems and has high quality. The risk of corrosion in the convective heat transfer bundles is rather high when using this method of heat transfer for this heat.

High value heat is the heat between 650 °C and 325 °C. It is most valuable since it can be used for steam superheating with reduced risk of corrosion.

Low temperature heat is all heat with a temperature of less than 325 °C. For a high pressure boiler the heat cannot even be used to evaporate water, but only for preheating of water or combustion air.

The distribution of these three types of heat in the flue gas for the initial set of combustion with an excess air ratio of 1.65, called step 0 and the final step of the heat source optimization step 5, from now on called HEB (high efficient boiler) is shown in Figure 4.25. The HEB has slightly less low temperature heat, about 5 % more high value heat and about 11 % (based on the gross heat input) more high temperature heat. The heat in the flue gas in step 0 differs from the gross heat input, since some heat is removed with the bottom ash and also, the outside convection and radiation of the boiler is accounted for. These heat losses

for the HEB are not directly visible in Figure 4.25, since it is not visible how much heat is added by the air preheater.

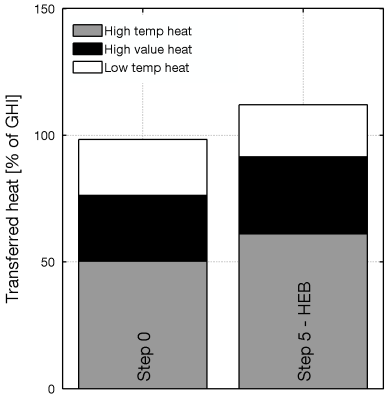

Figure 4.25.: Comparison of available heat at different temperature levels

Not only the changes in the temperature profile and quality of the heat in the flue gas is important, but also, other changes imposed by the optimization steps. These are changes in volume flows shown in Figure 4.26 and flue gas composition shown in Figure 4.27.

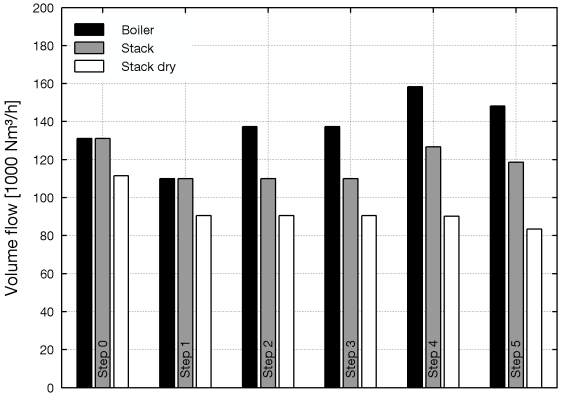

Figure 4.26.: Comparison of flue gas flows for the different optimization steps

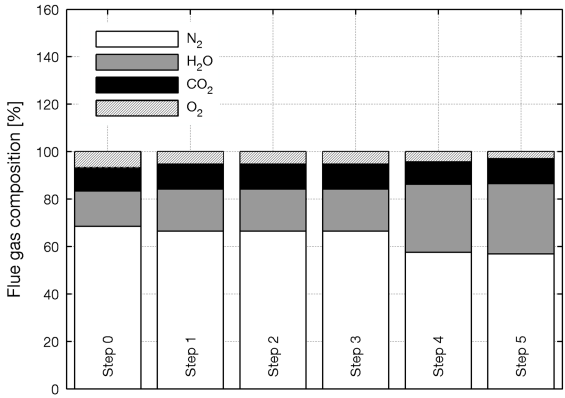

Figure 4.27.: Flue gas composition of the 4 main species for the different optimization steps at the stack

The volume flow going through the boiler, the volume flow at the stack (without considering false air, flue gas condensing or quenching) and the dry volume flow at the stack are compared for the different steps. Decreasing the excess air ratio (step 1) reduces the volume flow by about 20000 Nm^3/h. The volume flow through the boiler is still the same as at the stack. For step 2 flue gas recirculation increases the volume flow through the boiler. At the stack the volume flow stays the same. Only the dust removal before the extraction of recirculated flue gas must be designed bigger. Air preheating in step 3 imposes no change in the volume flow. For the air humidification (step 4) the volume flow is increased further. The flow at the stack is nearly as big as for step 0. The flow through the boiler is approximately 20000 Nm^3/h higher than for the other cases with recirculation. This results in an unnecessarily big flue gas treatment plant. Therefore the excess air ratio is reduced further (step 5). The difference in flue gas volume flow going through the boiler for step 5 compared to step 0 is still 10000 Nm^3/h. For normal plants with wet flue gas treatment the flue gas is saturated at a temperature of 65 °C to 70 °C by a quench anyway and the volume flow increases respectively. This implies a moisture content in the flue gas between 25 vol.% and 31 .% The moisture content in the flue gas is therefore in the same order as for the HRC concept, therefore a wet flue gas treatment system for the HEB concept would build smaller, due to the lower excess air ratio, although the air is humidified. It is also important to have a look at the dry volume flow. All emissions are based on this volume flow,

which is reduced significantly. Since the emission limits are the same the flue gas cleaning efficiency must be increased. On the other hand the total emissions are reduced when a boiler is operated with lower excess air ratio.

As can be seen in Figure 4.27 changes in the flue gas composition tend to lower oxygen and nitrogen values, especially while the water vapor fraction increases, increasingly so for the step with air humidification.

4.4. Overall efficiency optimization and plant design

After the selection of the water steam cycle main parameters and the optimization of the heat availability in the flue gas the focus is brought to the optimization of the overall plant.

4.4.1. Feed water preheating optimization

So far the feed water system is only determined by the temperature at the outlet of the condenser and the design feed water temperature. The plant is however designed with five steam heated feed water preheaters. Also some waste heat available in the flue gas has to be used in the water steam cycle efficiently.

Müller suggests the use of a pinch analysis to optimize the use of available heat and needed heat [127]. He uses heat from different sources in the plant and redistributes them depending on the temperature of the available heat.

As discussed in Section 4.3.3.3 combustion air is preheated to 275 °C using low temperature heat. There is, however, more low temperature heat available in the flue gas than needed for the air preheating, since the additional mass of the burnable part of the waste is contained in the flue gas and due to the different composition also the specific heat is higher. Additionally at the flue gas condenser much more warm water is available than needed in the air humidifier. These two low temperature heat sources are therefore available to be transferred to the water steam cycle system.

The heat for air preheating is transferred with a water loop from the flue gas to the air. This method is suggested to avoid large ducts for hot air running through the plant and enables the use of surplus heat in the water steam cycle in an simple way. Practically the heat transport should be implemented in 2 separate loops: a high pressure loop and a low pressure loop.

The high pressure loop has to be operated at a pressure above 90 bar to avoid evaporation. It cools the flue gas from 325 °C to 235 °C. At the same time the

air is heated from 160 °C to 275 °C. The temperature difference at the cold side is much higher due to the higher heat capacity discussed above.

In Section 4.3.3.4 it is described that the combustion air is heated and saturated with water vapor at a temperature of 55 °C. This is done with 70 °C warm water from the flue gas condenser. Using a finned tube heat exchanger the 70 °C warm water can be used in a final stage to preheat the saturated air to 65 °C. The warm water can also be used in a platen heat exchanger to preheat the main condensate from condensing temperature to 65 °C. This kind of preheater is implemented in the HRC concept as ECO 3 [12].

The low pressure loop operates at about 20 bar and cools the flue gas down to 100 °C. Part of the heat transfer surface in the flue gas has to be double coated with enamel and finally covered with perfluoroalkoxy (PFA) as suggested by Wandschneider [105] or made directly from weldable polytetrafluoroethylene (PTFE) material as suggested by Hoffmann to avoid corrosion [128]. This loop has to close the gap between 65 °C from the air humidifier and the 160 °C where the high pressure loop starts with the air preheating. In the plant design this leaves about 2.7 MW_{th} per combustion line of hot water with a temperature between 170 °C and 210 °C, which can be used in the water steam cycle. In Figure 4.28 a scheme of the whole process is presented. The second economizer is fed with the waste heat from the low pressure preheater loop. The piping is not drawn.

Now, how shall the 5 steam heated preheaters be arranged to optimally preheat the feed water from 65 °C to 300 °C? The waste heat from the low pressure air preheating loop should be included and, at the same time, the steam turbine must be kept as simple as possible. This implies that one steam extraction must be implemented at the reheat pressure, since all the steam leaves the turbine at this point anyway.

Musil presents a graphical method to optimize extractions points of a steam turbine, based on a condensing heat graph and heat demand graph. This depends mainly on the type of preheaters used [99].

However, this task can also be performed numerically. In 2007 a Matlab code using water steam tables implemented by Holmgren [129] was developed at the Royal Institute of Technology (KTH) to optimize the water steam cycle of a supercritical water reactor [130]. This cycle was designed to operate at 250 bar and 500 °C and in addition it had an external reheater system similar to the suggested cycle for the HEB.

This code was used to implement the water steam cycle with additional heat sources for the heat from the flue gas condenser and the low pressure air preheating loop, as well as all five feed water preheaters. (See Figure 4.28). The

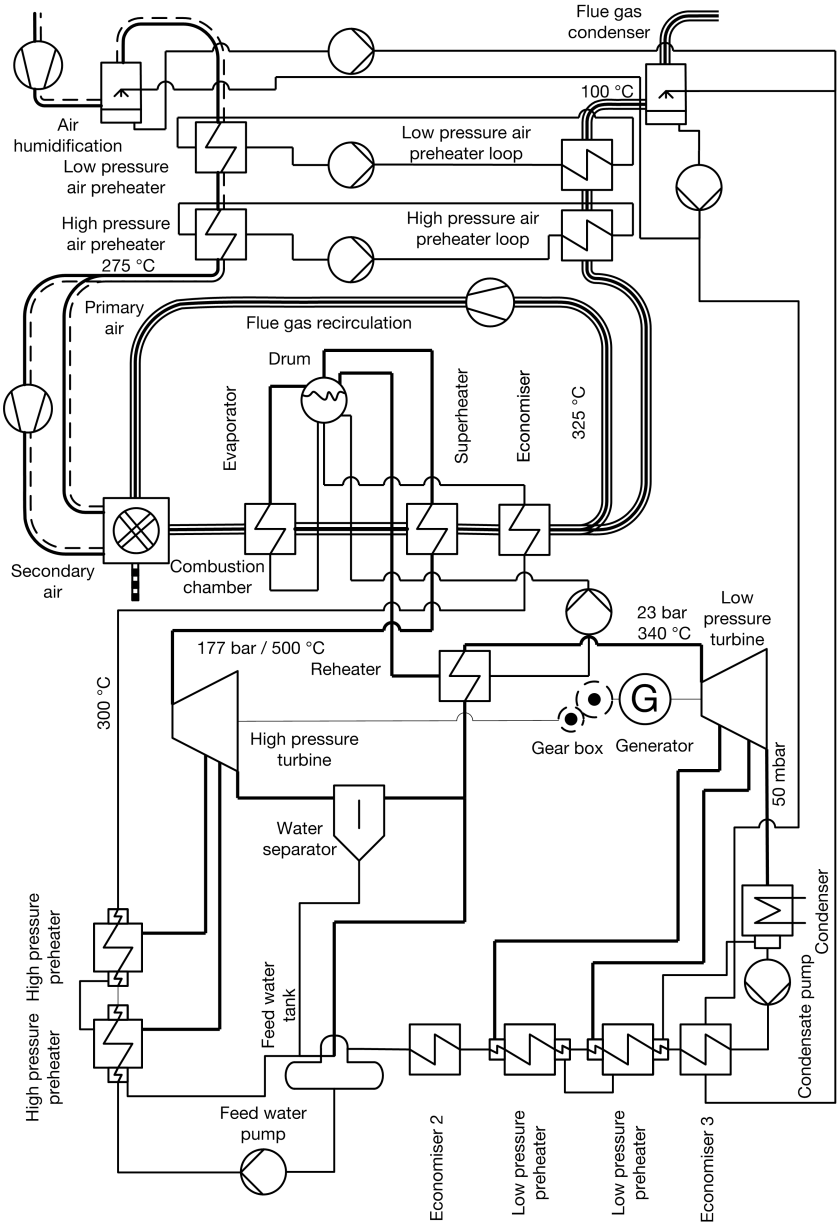

Figure 4.28.: Plant scheme for an HEB concept EFW plant

Matlab function "$fminsearch$" was finally used to find the minimum of a defined function [131]. As optimization parameters the temperatures after the first four steam heated feed water preheaters are chosen. The temperature after the fifth preheater is set to 300 °C. The function for minimization contained as main parameter the formulation $1 - efficiency$, additional terms checked the validity of the input variables. The temperature after a preheater cannot be lower than the temperature of the previous preheater. An additional term keeps the steam quality at the low pressure turbine outlet at acceptable values.

As starting values equal temperature steps over each preheater are set, neglecting the additional waste heat completely. The algorithm takes about 80 iterations to converge to the highest efficiency with this configuration. The resulting pressure for the feed water tank is 23 bar, which is therefore also the pressure of the reheater. This pressure is higher than the 14 bar for the HRC concept. This is possible since the reheater outlet temperature is 20 °C higher due to the higher saturation temperature of the HEB concept. Table 4.7 presents the design data for the feed water preheating

Table 4.7.: Feed water preheating system design parameters

Preheater stage	Heat source	Outlet temperature	Extraction pressure
		°C	bar
ECO 3	waste heat	65	
Low pressure preheater 1	steam	97	0.96
Low pressure preheater 2	steam	140	3.8
ECO 2	waste heat	168	
Feed water tank	steam	217	23
High pressure preheater 1	steam	258	46.7
High pressure preheater 2	steam	300	88

The optimized feed water preheating temperatures were transferred back in the commercial thermodynamic balancing software. An improvement of 0.5 % in efficiency for the HEB concept was achieved. This results in a plant net electric efficiency of 37.1 %, which is more than 1 MWh_{el}/t of waste. Figure 4.29 shows the water steam process in a T-s diagram after optimization. The two sections where waste heat is used for the feed water preheating are marked separately, as well as the low thermodynamic value they provide (low thermodynamic average temperature). In any case it is available heat in the plant and should therefore be used. The temperature heat diagram of the HEB concept is shown in Figure 4.30. Also, the temperature of the air during preheating is shown, as well as

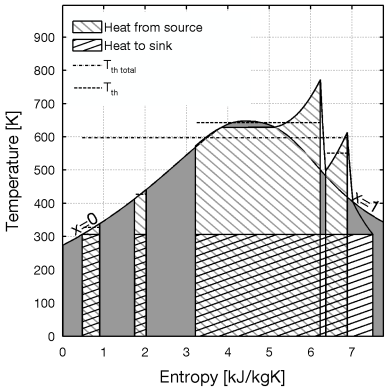

Figure 4.29.: T-s diagram for the optimized steam cycle with 5 stage feed water preheating

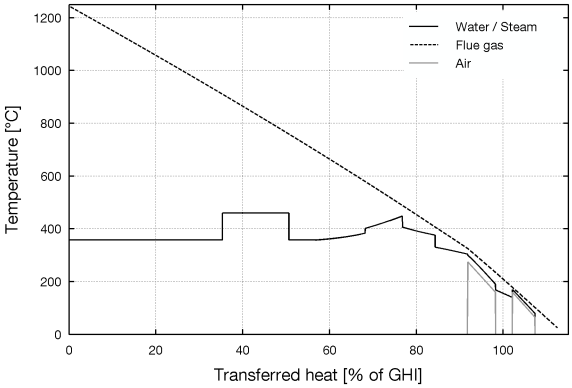

Figure 4.30.: Temperature-heat diagram of the HEB plant for flue gas, water and steam and air

the low temperature heat transferred to the water steam cycle. In the heat quality heat diagram (See Figure 4.31) it can be seen how efficiently the heat is used. Here the T_0 is adjusted to the design condensing temperature of 33 °C. (0.05 bar condensing pressure). This explains the reduction in quality of the heat, compared to the quality-heat diagrams shown in section 4.3.

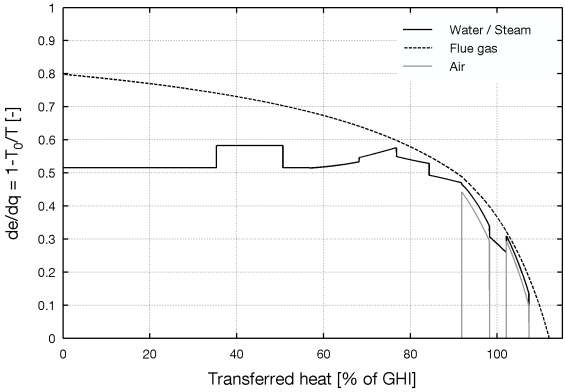

Figure 4.31.: Quality-heat diagram of the HEB plant for flue gas, water and steam and air

4.4.2. High temperature dust removal

The plant design uses flue gas recirculation at a temperature of 325 °C. The flue gas should be as dust free as possible. Therefore a high temperature electrostatic precipitator (ESP) or bag house filter has to be installed upstream of the extraction point for the flue gas. The reference document for the best available technique in waste incineration gives a temperature range of 150 °C to 350 °C for the use of ESP's [26]. Therefore the concept should be feasible. However details from different ESP suppliers where checked. Balcke Dürr offers precipitators for corrosive gas applications for temperatures up to 450 °C [132]. Air Clean Technologies offers ESP for temperatures up to 430 °C with a removal efficiency of 99 % for particles down to 0.5 µm [133].

In the HRC plant the ESP is combined with a bag house filter. Activated carbon and limestone are injected before the filter to remove dioxins and furans as well as heavy metals [12]. This is also possible at higher temperatures. 3M offers high temperature filter bags for applications like cement industry or incineration processes, which can be operated at temperatures up to 371 °C [134]. This is high enough to work for the HEB plant concept.

A disadvantage to use an ESP and bag house filter at higher temperatures is the size. The flue gas velocity is one of the main design criteria. The velocity depends on the operational volume flow rate, which depends on the temperature, due to the influence on the density. Compared to 250 °C, which is a state of the art design temperature of an ESP or a bag house filter in EFW plants

the volume flow increases by about 15 %. Having a dust removal at higher temperatures, however allows for a more efficient design of the downstream heat transfer surfaces due to the lower dust load. Francisco investigated the use of a high temperature ESP at temperatures up to 400 °C for the HRC concept, followed by a finned tube economizer. For a fin pitch of 12 mm, a fin thickness of 2 mm and the same flow cross section the economizer is reduced by two thirds compared to bare tube bundles [135]. Finned tubes are suggested also for the heat exchangers downstream of the dust removal, which extract the heat for the air preheaters. Finned tube heat exchangers can also be used on the air side of the air preheaters, since the air is cleaned by the air humidifier. This reduces the construction size of the total air preheating system, even though the heat flow transferred is much higher compared to state of the art plants.

4.4.3. Superheater corrosion assessment

The risk of corrosion of different heat transfer surfaces can be estimated in a corrosion diagram. The temperature of the flue gas and the water steam side of the boiler are used as parameters in the diagram. Zones for corrosion are marked for different materials. Such a diagram is shown in Figure 4.32, representing the HRC (130 bar 440 °C) and HEB concept (177 bar 500 °C). The corrosion areas are marked due to experience at the Amsterdam EFW plant published by van Berlo and Simoes [20]. The hatched areas with dotted lines in the corrosion diagram mark the area for transitional corrosion, where only slight corrosion occurs. Compared to the HRC concept the evaporation temperature of the HEB concept is increased by 20 °C. This imposes a risk for the membrane walls close to the grate and the post combustion zone. This implies the walls have to be covered with ceramic tiles, additionally; it can be cladded below it. An alternative could be to influence the combustion in such a way so that the temperature stays below 1150 °C in the furnace and therefore cladding can be enough. Temperature profiles after optimizing the combustion process are discussed in Section 5.7. Compared to other boiler concepts like the HRC concept the HEB concept needs more heat for superheating the steam (See Figure 4.10a). There is not enough heat available at flue gas temperatures with low risk for corrosion. Therefore heat at higher temperatures must be used. This can be done with low risk for corrosion by the use of a wall superheater (WSH) as patented by Rüegg and Ziegler [24]. After that there is a membrane wall for evaporation; it can be made of uncladded membrane wall due to the slow cooling rates of the flue gas in the wall superheater section. The first convective superheater is installed at rather high flue gas temperatures, but since it is the coldest of the convective superheaters and arranged in parallel flow it is just outside the

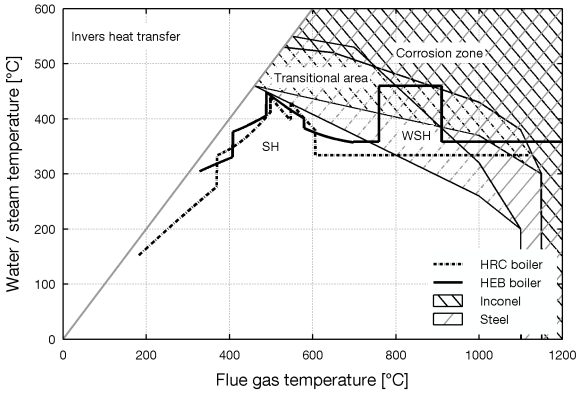

Figure 4.32.: Corrosion diagram with steam cycles for the high efficient boiler and HRC boiler (adapted from [20])

corrosion zone. The next superheater in flue gas direction is the final convective superheater also arranged in parallel flow, which reaches a steam temperature of 450 °C and is just outside the corrosion zone. The last superheater is arranged in counter flow and operates completely in the low corrosion zone.

4.4.3.1. Increased wall thickness

Additionally the availability of the superheater can be improved by increasing the wall thickness of the superheater. In a traditional design the superheater tubes for a pressure of 177 bar have a wall thickness of 5 mm to 7 mm. This can be increased to 9 mm for the superheaters (SH1 and SH3) (See Figure 4.33) with highest corrosion risk. (See Figure 4.32) For an average corrosion rate of 0.5 mm/a, this implies four extra years of life-time. Only the thickness of the pipes has to be increased. The thickness of the headers, which in the HRC boiler form the roof of the horizontal pass, is already big enough. The change in wall thickness increases the weight of the pipe by 35 %. This increases mainly the material cost of the superheater bundles, while the cost for engineering, manufacturing and installation is nearly the same. The extra weight is nearly negligible compared to the weight of the fly ash deposits on the superheater accumulated during operation. This implies that minimal extra reinforcement in the steel construction has to be considered.

The additional wall thickness has an effect on the heat transfer and the temperature at the outside of the tube. Calculations for the hottest wall temperature

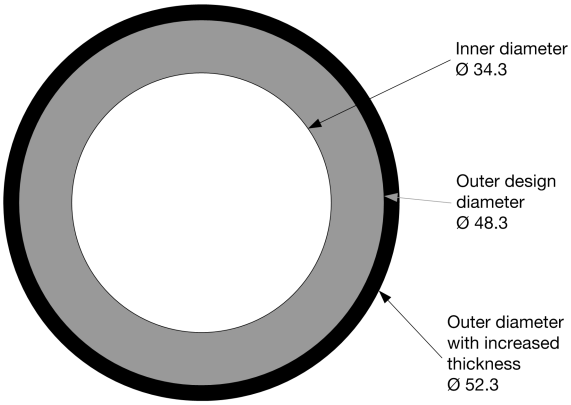

Figure 4.33.: Superheater pipe cross section with increased wall thickness

in the convective pass show, that the wall temperature increases by only 0.2 °C, when the wall thickness is increased by 2 mm. The heat transfer per pipe however is increased by about 4 %. This is caused by the increase in circumference of the pipe. The limiting factor in the heat transfer is not the heat conduction inside the pipe but the heat transfer on the outside.

4.4.3.2. Inner heat transfer of superheater pipes

As a final step the heat transfer on the inside of the pipes is investigated to assure sufficient cooling, by the change of live steam temperature and pressure. The inner heat transfer is calculated using Equation 4.17 taken from "Kraftwerkstechnik" of Strauß [136].

$$\alpha_i = 0.0224 \cdot \lambda\left(p,t\right)^{0.58} \cdot \mu\left(p,t\right)^{-0.38} \cdot c_p\left(p,t\right)^{0.42} \cdot \Phi^{0.8} \cdot d_i^{-0.2} \tag{4.17}$$

Figure 4.34 shows the heat transfer over the temperature for superheaters with 40 bar, 130 bar and 177 bar. A 5 bar pressure drop is assumed for all superheaters. The heat transfer is larger by a factor 2 or more for higher pressures. This improves the cooling of the pipes. The heat transfer coefficient of 3.5 $\mathrm{kW/m^2K}$ is rather high along with the high specific heat at the same temperature as shown in Figure 4.11. The cooling rate in SH1 is similar to that of a convective evaporator. Therefore no pre-evaporator is specified in the HEB concept.

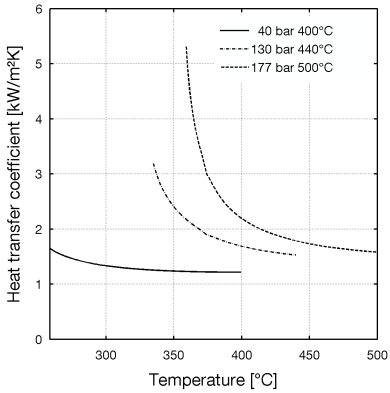

Figure 4.34.: Inner heat transfer coefficient vs. temperature for the three different concepts

4.4.4. Plant design

Combining all the design features discussed in this section allows making a first picture of the plant. This is shown in Figure 4.35.

The wall superheater (WSH4) is responsible for the long first and second pass. Only a small part of the boiler is designed as membrane wall evaporator (EVAP). In the convective pass only four superheaters (SH1, SH2.1, SH2.2 and SH3) and two economizers (ECO1.1 and ECO 1.2) bundles are needed to transfer the heat to the water steam side. After the economizer the flue gas has a temperature of 325 °C. At this temperature it is cleaned and a part of it is recirculated, before the rest enters the finned tube heat exchangers needed for the two air preheaters.

4.4.5. Combined heat and power generation

The high efficient boiler concept is designed for maximum electric efficiency. However modern EFW plants operate in combined heat and power mode, since this improves the economy of the plant significantly. Prices for electricity are about 55 €/MWh, while the easier produced heat can be sold for 20 €/MWh [120]. These prices make the investment in plants with higher electric efficiency uneconomic, if there is a large district heating system available. For central Europe, where heat is only needed during the winter producing more electricity during the rest of the year can be economical.

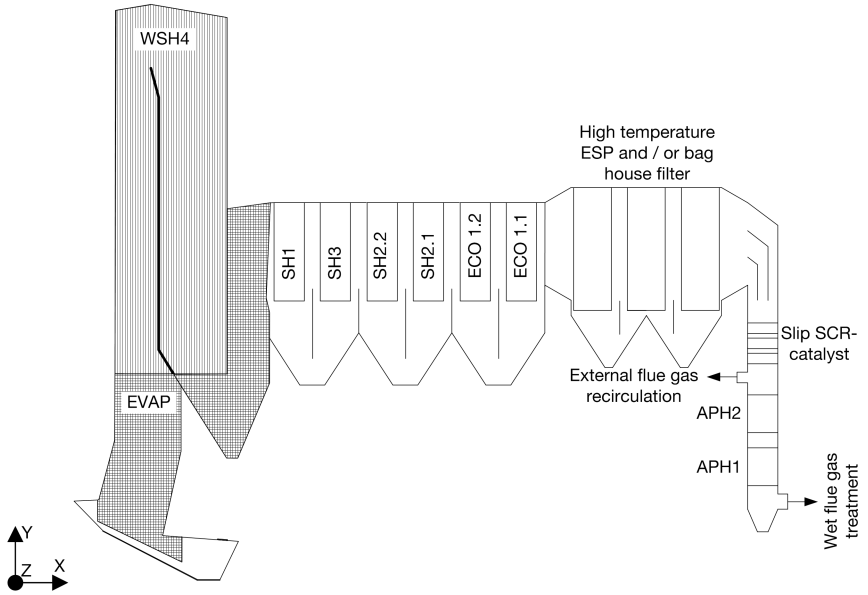

Figure 4.35.: Plant design with arrangement of the main heat transfer surfaces, dust removal and NO_x reduction equipment

The European directive 2010/31/EU on the energy performance of buildings states that from 31st December 2020 all buildings must be nearly zero energy buildings [137]. This might reduce the heat demand in district heating networks in the future. The study "Varmeplan Danmark" estimates for 2030 an average heat demand of 50 kWh/m^{2}a for buildings. Then the district heating networks in Denmark will operate with design feed temperature of 90 °C, however the yearly average will be only 70 °C and the return temperature is estimated to be 30 °C. These temperatures allow EFW plants to operate even more efficiently and have an overall efficiency of 104 % based on the lower heating value [138] compared to up to 99 % achieved today [3].

4.4.5.1. Flue gas condensation

Flue gas condensing was already discussed in Section 4.3.2.6. Normally, however, flue gas condensing is neither used for air humidification nor feed water preheating, but as additional heat source for district heating. In the countries

of northern Europe the flue gas condenser is combined with a steam heated absorption heat pump to produce warm water for the district heating systems.

With increasing moisture content of the fuel the lower heating value is decreased, the latent heat in the flue gas increases [128]. Using flue gas condensers nearly 20 % additional heat can be extracted from the flue gas [139], however only at very low temperature.

A negative effect of flue gas condensing is reduced buoyancy forces of the dryer and colder flue gas at the stack [140].

Becker investigated the combined use of warm water for air humidification and feed water preheating. There is however more warm water left, which he used once to reheat the now dryer flue gas before the stack to increase the buoyancy forces again. The rest is made available for district heating [125]. This is 24 % of the condensing water, or approximately 2.7 MW_{th} per combustion line. An

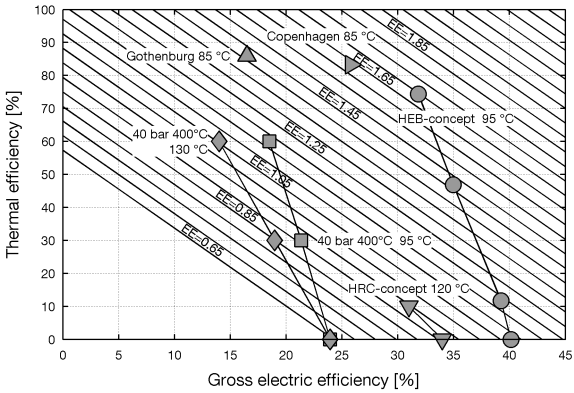

Figure 4.36.: Gross electric efficiency - thermal efficiency diagram (adapted from [3], with data added from [94])

investigation for the HEB concept in combined heat and power operation was performed. Stepwise changes from maximum power production to highest possible heat production have been performed. (See Figure 4.36) The temperatures of the district heating network are set to 40 °C return temperature and 95 °C feed temperature. The warm water from the flue gas condenser is primarily used for air humidification and flue gas reheating at the stack, only the rest can be used directly or via absorption heat pumps. The extraction (0.96 bar) for the first low pressure feed water preheater is used as final stage of the heat extraction. Steam from the extraction (3.8 bar) for the second low pressure preheater is used for

operation of the absorption heat pumps. At maximum heat production the HEB plant concept is able to deliver 74.4 % of its gross heat input into the district heating system, while the net electric efficiency is still at 28.8 %. This results in a fuel utilization of 103.2 %, based on the lower heating value (LHV).

Poulsen presented the concept for the new EFW plant in Copenhagen with flue gas condensing and absorption heat pumps. The net electric efficiency given by him is 22.3 % and the possible heat supply is 83.2 % of the gross heat input, which results in an overall efficiency of 105.5 % [94], which is significantly higher than for the HEB plant concept. However less electricity is produced. Combined heat and power generation makes it harder to compare plant concepts. In the end an economical study including predictions of heat and electricity prices will decide the concept selected.

5. Combustion optimization

In Section 4.3, the combustion parameters for an optimized heat source were defined. In this Chapter, the design of the furnace and nozzle arrangement in the post combustion zone is discussed followed by a parameter studies for different combustion settings using CFD. Finally, an optimization of the combustion process based on the findings of the parameter study was performed. The previous Sections 3.2, and 3.3, give the methods and theory on how to optimize the combustion.

5.1. Aim of investigation

The combustion process has to be optimized according to three design criteria:

- high availability of the combustion system
- low NO_x emissions
- good burnout of the flue gas and the ash

High availability is the key for the economic operation of EFW plants. The combustion system and the boiler are the most critical components responsible for the down time of the plant. Fouling and corrosion of the membrane wall, as well as broken ceramic tiles in the furnace are the main reason for the down-time. All these effects can be linked to elevated temperatures. This implies the temperature in the waste bed as well as the flue gas temperature in the lower furnace must be kept as low as possible to guarantee high availability. This can be difficult if uneven combustion on the grate occurs, which generates strands of high temperature flue gas. This strands can be up to 300 °C hotter than the average flue gas temperature [81] and increase the local wall temperature significantly due to the increased radiation heat transfer.

The heat release during the combustion process can be influenced by using staged combustion. The heat can be released in different stages, allowing the flue gas to cool in between the stages. This allows influencing the temperature profile to avoid high temperatures peaks [114], which cause melting of deposits and corrosion. Also, the use of recirculated flue gas can be combined with staged combustion. It can be used to reduce the temperature and convert only part of

the chemical bound energy in the flue gas, since compared with air, less oxygen is added at the same mixing impulse.

NO_x emissions are not a problem at the moment since the use of SCR systems is enough to keep the emission limits low. However, as discussed in Section 3.2.2.2, there is still much unused potential in combustion engineering measures. This can be used to reduce the investment and operational costs of post combustion reduction systems. As for the temperature, also for the NO_x emissions, the key approach is to stage the combustion process and improve mixing in the lower furnace.

The CO emissions of conventional plants are well below legal limits. The same or even better values must be achieved also for new combustion concepts to be accepted by the market. Flue gas burnout can become a problem if the excess air ratio is reduced and the post combustion takes place at too low of a temperatures. The 3Ts: temperature, (residence) time and turbulence are important for the burnout of CO [51]. The combustion process has to be designed accordingly.

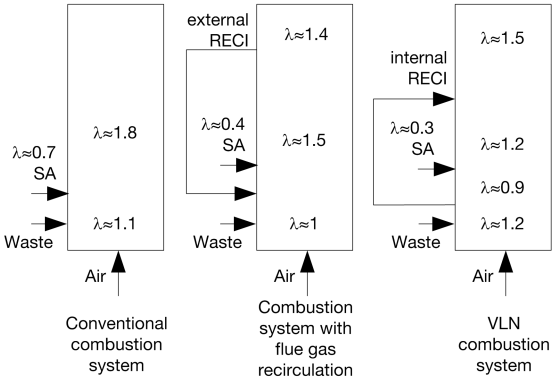

Figure 5.1.: Different typical combustion systems with excess air ratios to show the oxygen supply

A combustion system has to be designed to meet all these criteria defined above. Typical state of the art combustion systems with air ratios for various locations in the combustion process are presented in Figure 5.1. To meet the first design criterion, an external flue gas recirculation is necessary to keep the temperature low. For the second criterion, a staged combustion process as for example the very low NO_x (VLN) combustion system is necessary. (See Section 3.2.2.2) The third criterion just needs good mixing of the flue gas. Therefore the combustion

process is designed with a staged combustion according the VLN scheme with an internal flue gas recirculation, additional an external flue gas recirculation system is implemented in the design. Out of a combustion calculation the oxygen demand and the needed air supply is determined. The division of the combustion air to primary and secondary air is chosen in such a way to have an excess air ratio on the grate of 0.85. In real combustion systems unwanted air enters the boiler since it is operated with lower pressure than the ambient pressure. This air is called false air. False air enters already at the grate and is therefore added to the primary air for the simulation. For false air, an share of 10 % of the stoichiometric air flow is assumed. This value is higher than expected for a new plant. As a simplification, the false air is added to the primary combustion air for the simulation. This results in an overall excess air ratio on the grate of 0.95. The low oxygen content results in the release of the fuel nitrogen mainly in the form of NH_3 [48], which increases the degree of freedom for combustion engineering measures for NO reduction. The volume flow rate of external flue

Table 5.1.: Gas volume flows and temperatures for the different gas streams influencing the combustion, for step 3 and step 5 of the heat source optimization

	Temperature	Volume flows Step 3	Volume flows Step 5
	°C	Nm^3/h	Nm^3/h
Primary air	275	58464	68968
False air	25	6878	8114
Secondary air	275	27512	24341
Internal recirculation	325	20634	20634
External recirculation	325	27512	28922

gas recirculation (RECI) was determined by the heat source optimization and should be in the range of 25 % to 30 %. The internal recirculation should be designed for a volume flow in the range of 30 % of the air volume flow needed for an excess air ratio of 1. According to these design criteria, the volume flows for the different gas streams added to the combustion are determined. These are presented in Table 5.1 for step 3 and step 5 of the heat source optimization process. The volume flow rate of secondary air is reduced due to the reduction of the overall excess air ratio for step 5. Also, the volume flow rate of external

flue gas recirculation is slightly increased to keep the recirculated mass constant, since the flue gas density changes with air humidification.

5.2. Boiler design

The boiler engineered using the above mentioned design criteria is presented in Figure 5.2. It is designed with a Martin reverse acting grate called Vario, since the reverse acting grate is the only grate type which has proven there is no need for water cooling, when operated at the required conditions. It keeps the temperature of the grate bars low when operated with oxygen enriched air as well as during the combustion of high caloric waste with a heating value up to 18 MJ/kg [117], [141].

However, the grate for this boiler is operated with air preheated to 275 °C, therefore the design thermal load is decreased from typical 1.1 MW/m^2 to 0.8 MW/m^2. This should keep the lifetime of the grate bars to typical values, and so the availability of the plant is high.

As discussed before, the excess air ratio for the primary combustion stage is about 0.85 to 0.95, this is lower than normal which reduces the combustion temperature and the mass flow rate of fly ash particles carried away with the combustion gases [142].

In Figure 5.2, in the first pass, four levels are marked with arrows for the injection of gas in the post combustion zone. The first level is about 3.5 m above the grate and is used for the injection of externally recirculated flue gas. This stage is mainly used to mix the burnable gases with the unused oxygen from the primary combustion. This ensures a clear under stoichiometric zone in the whole cross section of the furnace.

The second injection level is at 5 m and it is used for the secondary air (SA). Most of the gases from the furnace are oxidized in this stage.

Levels 3 and 4 at 7 m and 8 m above the grate are used for the injection of the internal flue gas recirculation. The internal recirculation is no recirculation in the traditional sense, since no gas is transported from a downstream location to a more upstream location. Instead gas is first extracted from an opening at the ceiling on the rear part of the grate and then reinjected further downstream. Two levels are used for the injection to improve the mixing at the end of the furnace, which should homogenize temperature distribution and counteract the bypassing of CO strands. Only by mixing the flue gas in several stages low excess air ratios are possible for EFW boilers [114].

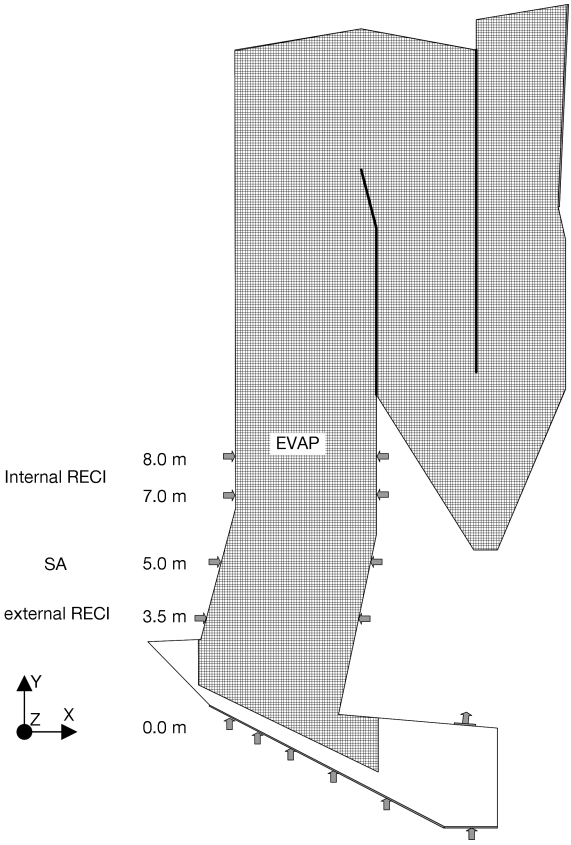

Figure 5.2.: Boiler cross section seen from the right side

5.3. Nozzle arrangements

The nozzle arrangement and diameters chosen for the external flue gas recirculation and secondary air are shown in Figure 5.3. The distance between two big nozzles on one wall is set to nearly 1.2 m, this is so close that the jets from the opposite walls interact in the middle of the furnace cross section, creating a large mixing zone. The recirculated flue gas is designed with a stitching arrangement with additional small nozzles between the big nozzles on the front wall. This results in more intense mixing on the front wall and cools the flue gas locally. On the rear wall, two small nozzles are arranged close to the corners, since the

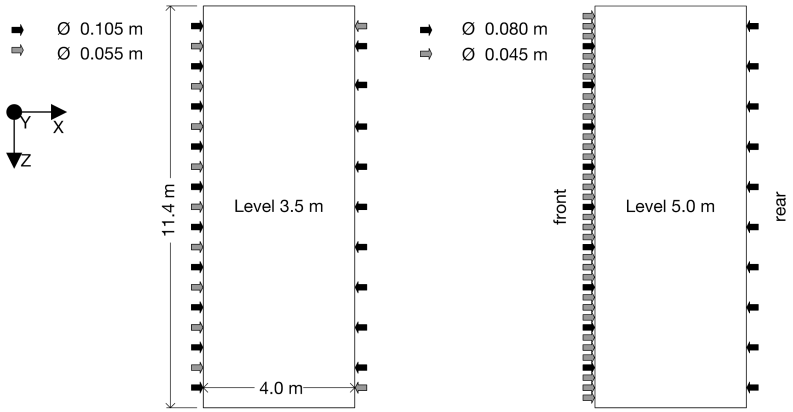

Figure 5.3.: Nozzle arrangement for external flue gas recirculation (left) and secondary air (right) level

outermost injection is not decelerated by the shear stress imposed by the jet from the opposite directions. Such an arrangement was first investigated for the combustion improvement in the HRC boilers [143].

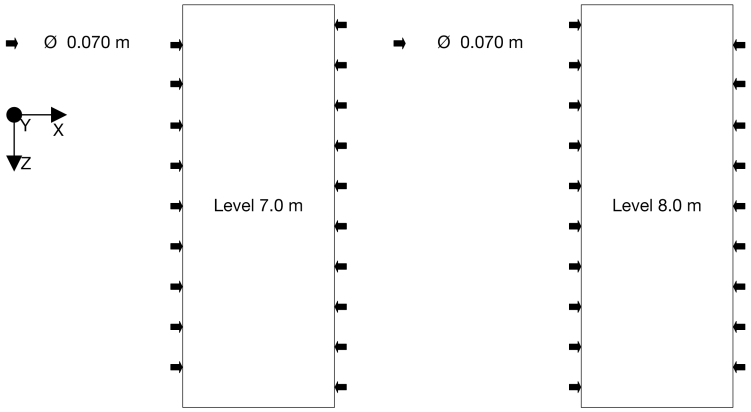

Figure 5.4.: Nozzle arragenemnt for injection of the two internal recirculation (left lower, right upper level) levels

At the secondary air level, the position of the big nozzles is switched between front and rear wall to get a better mixing effect due to the interaction with

the injection level below. On the front wall, three small nozzles are arranged between each big nozzle. The waste on the grate does not combust when it enters the furnace. It first partially pyrolysis and gasifies at the beginning of the grate. Only after the main combustion zone, a complete oxidation is achieved already in the waste bed. This fact is underlined by measured data presented in [77], [72] and [74]. This implies the oxygen demand in the front part of the furnace cross section is higher than in the rear. The small nozzles supply the oxygen directly in this zone with high oxygen demand and mix it with the flue gas. The nozzle arrangement and diameter chosen for the injection of the internal flue gas recirculation is presented in Figure 5.4. For these two levels, a simple stitching arrangement is chosen. The arrangement is again switched compared to the level below, to improve the overall mixing.

5.4. Data evaluation

CFD simulations allow reproducing complex processes numerically. This gives valuable inside knowledge of the process, which can be used to optimize it; however the limitations of the used models must be kept in mind at all time. A good validation of the models used as presented in section 3.3.2.4 for the NO_x model has to be performed before new models are used. Measurements for different cases and geometries also improve the confidence in new models. Each investigation itself should be followed by a sensitivity study, like the use of two sets for the partition fraction, to confirm trends and values. This increases the trustworthiness of the results obtained significantly. CFD simulations give a huge amount of information, with a resolution which can never be achieved by measurements. To draw the right conclusions from this broad range of data is an art itself. In this section, different possibilities for data evaluation are presented and discussed.

5.4.1. Visual data assessment

The most well-known presentation method for CFD data is visual presentation. Data are presented as contour plots for various variables, vector fields, flow path lines, or particle trajectories. As any visual representation of data, the range used of the data and its units is of great importance, especially if different cases are compared. Even planes or iso surfaces can be generated inside the geometry to show profiles on specific locations. The pictures generated can be used only to get an overview on what is taking place inside the boiler. To obtain actual values, the numerical data assessment is more valuable.

5.4.2. Numerical data assessment

Numerical data are easier to analyze and compare than pictures. Results from simulations offer different possibilities to export numerical values. On different geometries or cross sections, the minimum (min), maximum (max), area weighted average (awa) or mass weighted average (mwa) can be determined. For flow problems, the use of the area weighted average is critical since each part of the cross section has the same weight. Therefore it is better to use the mass weighted average. To determine values on a boundary condition such as a wall, it is on the other hand logical to use the area weighted average. For example, the average surface temperature of a membrane wall can only be obtained using the area weighted average, while the average temperature of the flue gas flowing through a cross section of the boiler can be only determined when the mass weighted average is used.

CFD programs allow also the export of data along lines placed inside the geometry. These data sets can be used to show the changes in temperature or species. However, these lines are limited in dimension and represent therefore only a small part of the geometry. The data from several lines can be combined to generate a more representative profile of the boiler cross section as shown in the works of Dürrschmidt [82] and [66].

5.4.3. Vertical Profiles

A better way to account for the whole cross section of the boiler is to use several planes of the boiler cross section and evaluate mass weighted average, minimum or maximum of the variable of interest in each plane. For EFW boilers, a vertical distance between the planes of 0.05 m was found to be suitable. Also the mass flow rate can be balanced for each plane. This allows the calculating the flow rate of different species. Some basic profiles of variables for resulting from the simulation with the volume flows presented in column "Volume flows Step 3" of Table 5.1 are discussed in the following section. Combining information of different variables to get additional knowledge for a better understanding of the combustion process in EFW plants is presented in section 5.4.3.2.

5.4.3.1. Basic profiles

Profiles which can be directly extracted from the CFD results without performing further calculations are termed basic profiles. Showing the maximum and minimum value of a variable in each cross section along with the mass weighted average allows estimating the inhomogeneous distribution over the cross section.

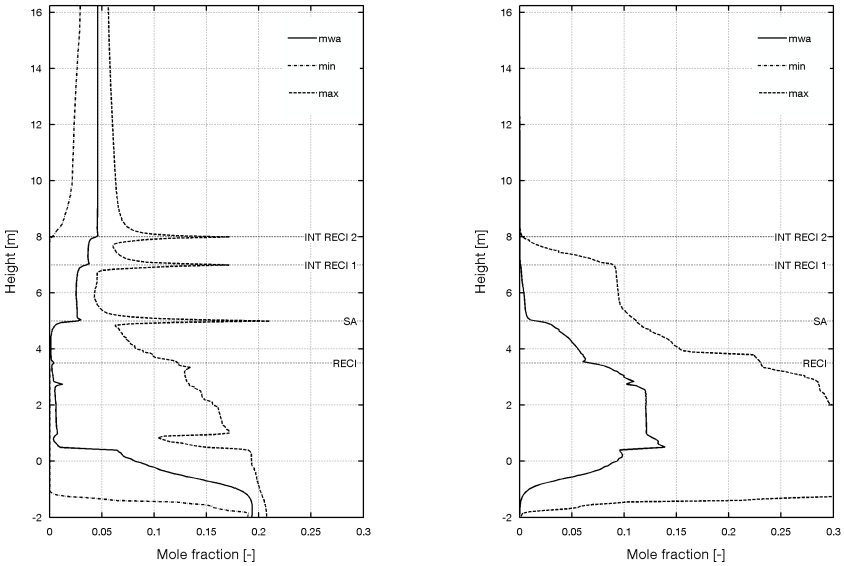

(a) O_2 concentration

(b) CO concentration

Figure 5.5.: Vertical profiles for O_2 and CO, minimum (min), maximum (max) and mass weighted average (mwa)

Species profiles The profile for the species O_2 (See Figure 5.5a) and CO (See Figure 5.5b) is used to understand the combustion process and monitor the burnout of the flue gas.

The profiles start at the lower edge of the grate at -2 m, since the reference coordinate system is set on first step of the grate. This must be kept in mind when interpreting the graphs shown. The oxygen concentration starts rather high and is constantly reduced while taking more of the grate into account. Suddenly there is a nearly horizontal drop. At this altitude, the internal recirculated flue gas is extracted which has a high oxygen concentration. The CO profile on the other hand starts at 0 and increases continuously. At the same level as for the oxygen there is a horizontal jump in the positive direction, since the flue gas remaining in the furnace has a higher CO concentration. At 3.5 m, the CO concentration drops drastically and the O_2 concentration drops as well. This is the effect of the mixing caused by the external flue gas recirculation. The oxygen concentration stays low until 5 m. The graph showing the maximum peaks at

this point since the secondary air is injected here. The average CO concentration drops significantly at this level and is close to zero. The maximum graph for CO decreases faster again at a height of 7 m to 9 m. Internal recirculated flue gas is injected for additional mixing at 7 m and 8 m. The oxygen concentration increases at these two levels accordingly. From there on, all 3 graphs converge since the flue gas gets more homogeneous.

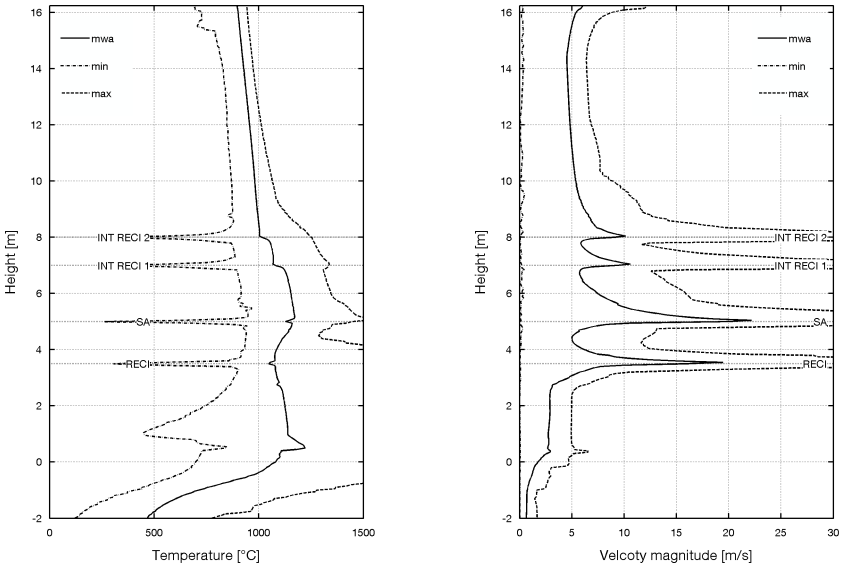

(a) Temperature

(b) Velocity

Figure 5.6.: Vertical profiles for temperature and velocity, minimum (min), maximum(max), and mass weighted average (mwa)

Temperature and velocity profile Figure 5.6a shows the vertical profile for the temperature and Figure 5.6b shows the profile for the velocity magnitude.

The average temperature in the cross section rises with height up to 0 m . Also, here the jump caused by the extraction of the internal gas recirculation can be seen. Peaks in the minimum graphs mark the injection of the colder gas streams. The temperature increases 5 m above the grate due to the post combustion taking place at this level. While at 3.5 m, no change in temperature can be

seen, here the cold injection of the recirculated flue gas keeps the balance with the heat released by the combustion initiated by the mixing. This implies a very good design since the average temperature has no sharp peaks. At the level for the injection of internal recirculated flue gas, the temperature drops for a few degrees. The maximum for the average temperature is around 1180 °C.

The velocity profile also shows the peaks for the gas injections. The sudden increase of the average velocity makes the relative impulse visible added by the injections. This impulse is highest for the lowest level and decreases for the higher levels. This depends mainly on the mass flow rate of gas injected and secondly by the mass flow rate of flue gas already present in the furnace, which is higher in the upper levels. At the end of the first pass, the flue gas accelerates since the cross section is reduced to improve the flow in the second pass.

5.4.3.2. Advanced profiles

The advanced profiles use data provided by the CFD program and calculates additional values of interest out of them. One of the most interesting values is the volumetric heat release during the combustion process, calculated out of the reaction enthalpy and the volume of the respective cell (See Equation 5.1). This profile is best discussed along with the temperature profile as shown in Figure 5.7a. In the waste bed about 40 % of the energy in waste is released for this combustion settings, the rest is released in the post combustion zone. Heat is mainly released at the injection level for external recirculated flue gas and secondary air. As discussed above, a lot of heat is released in the cross section where external recirculated flue gas is injected, but the average temperature stays constant. For the second heat release peak, the temperature increases. The higher oxygen concentration of air is responsible for high heat release values. The mixing induced by the injection of the internally recirculated flue gas is also responsible for some heat release, but it is not much since there is little combustible gas left and therefore the temperature drops.

In Figure 5.7b, the net mass flow rate and the total mass flowing upward are plotted next to each other. The net mass flow rate can be exported from Fluent directly and is the net sum of all mass passing a cross section (See Equation 5.2), where mass flowing in one direction is positive and mass flowing in the other direction is negative. For recirculation zones, the mass passes the cross section twice and is therefore not counted. Equations 5.3 and 5.4 determine the flow in only one direction, for a vertical cross section. Comparing the net mass flow rate with the total flow rate flowing upward shows where recirculation zones exist in the boiler. The graph for the net flow rate has several jumps. The first is a decrease in mass flow rate which is caused by the extraction for the internal

flue gas recirculation. The following jumps are caused by the various injection levels. The difference between the total upward flow rate and the net flow rate below the first injection is caused by the blocked cross section due to the gas injection discussed further in Section 5.6.2.

$$q''' = \frac{Q_{chem.reaction,cell}}{V_{cell}} \tag{5.1}$$

In Equation 5.1 q''' is the volumetric heat release rate, $Q_{chem.reaction,cell}$ the heat released in a single cell and V_{cell} the cell volume. The mass flow rates $\dot{m}$ are calculated using the velocity in y direction (v), the desnity (ρ) and the area (A).

$$\dot{m} = \int v \cdot \rho \cdot dA \tag{5.2}$$

$$\dot{m}_{up} = \int \frac{(v + |v|)}{2} \cdot \rho \cdot dA \tag{5.3}$$

$$\dot{m}_{down} = \int \frac{(v - |v|)}{2} \cdot \rho \cdot dA \tag{5.4}$$

The gas released from the waste bed is burnable. Using the mole fraction and the enthalpy of formation of the species and their oxidized products, the lower heating value of the gas can be determined. The graph of this value is presented in Figure 5.8a and can also be used to determine the combustion progress. Below, the start of the post combustion zone, the flue gas has an average heating value of about 1.5 MJ/Nm^3. The post combustion process starts already some distance below the first injection level, due to the remnants effect of the injection. Another important value to understand the NO_x and burnout performance of a combustion system is the oxygen demand, the oxygen availability and the resulting net oxygen demand in a cross section. Oxygen is added with the gas injections. However, the oxygen is not directly distributed where it is needed most. This is made visible by these two profiles. The oxygen demand can either be given in mole or mass fractions or in a flow rate. The net oxygen demand flow rate is negative if there is not enough oxygen available in the cross section for a complete oxidation of all burnable components. The approach to zero should

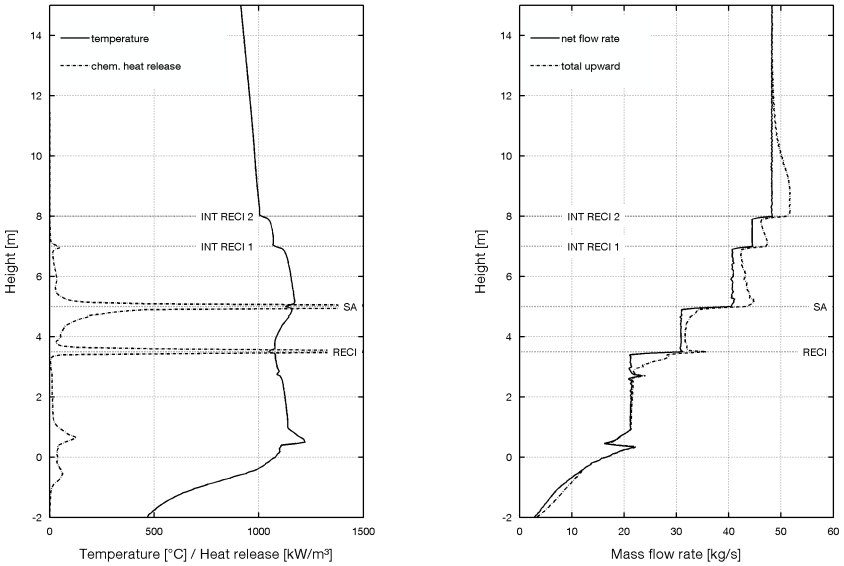

(a) Temperature and chemical heat release

(b) Mass flow rates

Figure 5.7.: Vertical profiles for temperature, chemical heat released and mass flow rates

occur in smaller steps which imply staged burnout. In this case, a small step is performed at around 3.5 m, while a rather big step occurs at 5 m.

$$LHV_{gas} = \frac{\sum(x_{ed} \cdot h_{for_{ed}}) - \sum(x_{pro} \cdot h_{for_{pro}})}{22.414 \frac{Nm^3}{kmol}} \tag{5.5}$$

The lower heating value of the gas from the waste bed LHV_{gas} is calculated with the mole fraction of the various species (x) and their enthalpy of formation (h_{for}). Also for the oxygen demand the mole fraction of the gas components is used multiplied by their stoichiometric ratio for oxidation. The oxygen demand mass flow $\dot{m}_{O_2 demand}$ is calculated from the oxygen demand mole fraction and

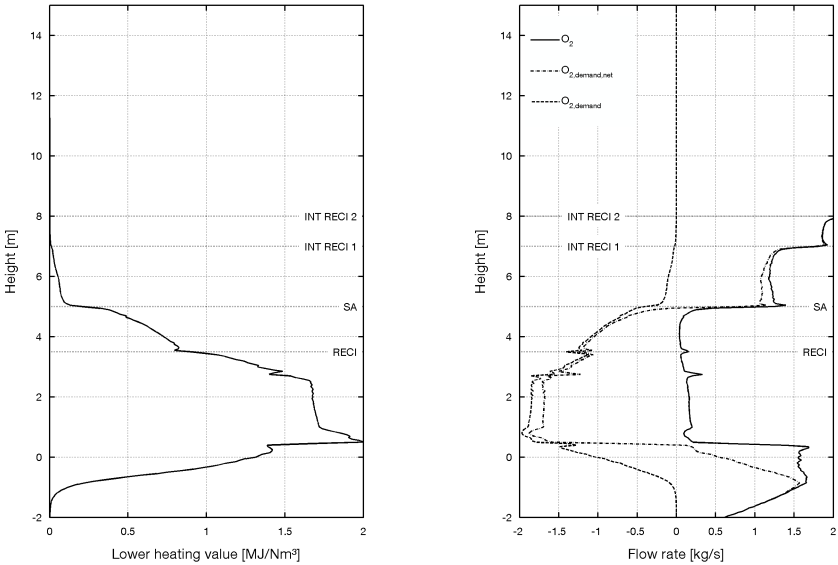

(a) Lower heating value

(b) Oxygen and oxygen demand

Figure 5.8.: Vertical profiles for lower heating value, oxygen flow rate and oxygen demand

the molecular weight of oxygen MW_{O_2} and the flue gas MW_{mix},as well as the flue gas mass flow rate.

$$x_{O_2,demand} = -(\frac{x_{CO}}{2} + \frac{x_{H_2}}{2} + \sum(x_{C_mH_n} \cdot (m + \frac{n}{2}))) \tag{5.6}$$

$$x_{O_2,demand,net} = x_{O_2} + x_{O_2,demand} \tag{5.7}$$

$$\dot{m}_{O_2demand} = x_{O_2demand} \cdot \frac{MW_{O_2}}{MW_{mix}} \dot{m} \tag{5.8}$$

5.5. Parameter study on combustion settings

Using this combustion system, different investigations were performed to see the effect on the NO_x formation. The varied parameters are the internal recirculation rate in combination with the excess air ratio on the grate and the external recirculation rate. In total, 83 different settings are simulated. A table with the main settings for the simulation is presented in Table B.1 in Appendix B. The most important results are presented and discussed in the Sections 5.5.1 to 5.5.3. These tests are performed only for the gas phase approach described in Figure 3.15. The HCN factor is set to 0.99 and the N factor to 0.52. The partition fraction for NO is 0.4 and for NH_3 is 0.5. The results of these simulations led to the implementation of the waste bed approach with different partition fractions discussed in Section 3.3.2.4. All investigations are performed with the gas flows for step 3, presented in Table 5.1. Except the air humidification test which is performed with the gas flows for step 5. The following trends presented here are calculated with a bug in the code influencing the result of Equation 3.64. The error results in about 20 °C lower temperatures in the furnace, which however has little effect on the trends presented in the Sections 5.5.1 to 5.5.3. The bug was fixed for the more important calculation presented in Section 5.6 and 5.7.

5.5.1. Internal recirculation

As a first parameter the internal recirculation rate is varied in steps of 3000 Nm^3/h from 0 Nm^3/h to 27000 Nm^3/h, which corresponds to about 25 % of the flue gas volume flow at the stack. This test is performed for five different excess air ratios from 0.85 to 1.05, in steps of 0.05. Due to the false air the excess air ratio is increased by 0.1 for all cases. The volume flow rate of secondary air is decreased accordingly to keep the overall excess air ratio of the combustion process constant at 1.35. Since the diameter of the secondary air nozzles is not adapted, the injection velocity increases by 50 % from the lowest to the highest grate excess air ratio. The typical oxygen concentration in the lower part of the furnace with a state of the art combustion system is shown in Figure 5.9.

An under stoichiometric zone is formed on the front side of the grate. Excess oxygen is available on the rear side and enters the first pass along the rear wall. NO is formed from NH_i radicals on the transitional area between $\lambda < 1$ and $\lambda > 1$. The idea of the internal recirculation is to remove the oxygen rich gas in the rear of the boiler and thereby changing the stoichiometry in the post combustion zone [50]. This effect is made visible by increasing the internal recirculation rate. Figure 5.10a shows the simulated NO_x emissions for the five different excess air ratios and ten different internal recirculation rates. The NO_x

Figure 5.9.: Exemplary representation of the stoichiometry in the lower furnace of a state of the art EFW plant

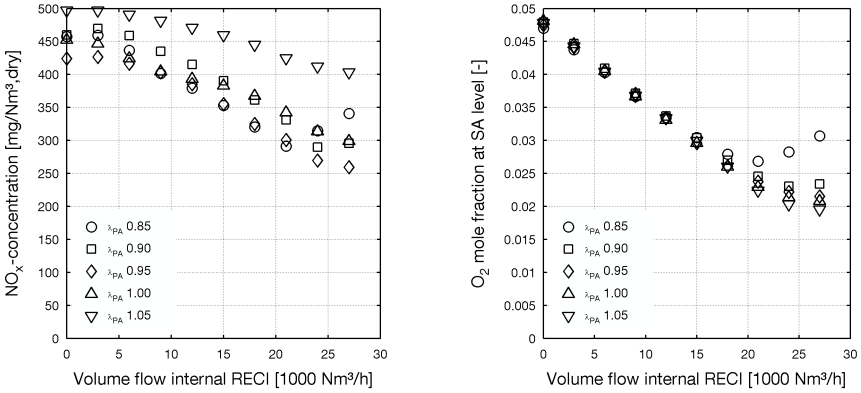

(a) NO_x concentration vs. volume flow of internal recirculation

(b) O_2 concentration at secondary air (SA) level vs. volume flow of internal recirculation

Figure 5.10.: Influence of internal recirculation rate on NO_x and O_2 concentration

emissions of all cases are determined in the middle of the second pass as mass weighted average in the cross section and this location is used for all NO_x values

reported in this Chapter. At this position, the combustion is completely finished and effects from the outlet of the geometry are negligible. Up to a volume flow rate of 10000 Nm^3/h for the internal recirculation, the NO_x emissions for all cases stay at the constant level. A clear order depending on the grate excess air cannot be determined this is caused by the simulation of the inhomogeneous waste composition affecting the NO_x formation, as discussed in Section 3.3.2.4. However, a slight tendency toward lower NO_x emissions for lower excess air ratio on the grate can be estimated.

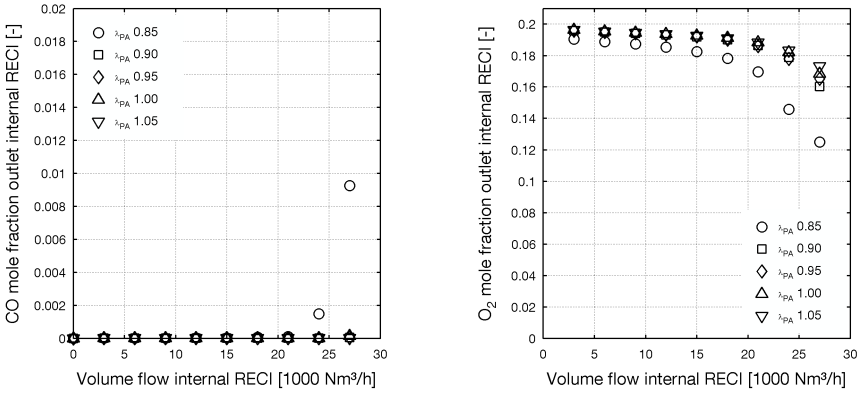

(a) *CO* concentration of the internal recirculated flue gas vs. volume flow of internal recirculation

(b) O_2concentration of the internal recirculated flue gas vs. volume flow of internal recirculation

Figure 5.11.: Influence of internal recirculation rate on gas composition at the outlet for the internal recirculated flue gas

For internal recirculation rates higher than 10000 Nm^3/h, a linear reduction in NO_x emissions can be seen. At the design point of roughly 21000 Nm^3/h, the NO_x emissions range from 280 mg/Nm^3 to 440 mg/Nm^3. This is rather high compared to the NO_x emissions reported for staged combustion which are 113 mg/Nm^3 [82] to 250 mg/Nm^3 [50]. This can be explained by the improved oxidation at the secondary air level in this new combustion concept compared to the St. Gallen plant investigated by Dürrschmidt. The NO_x emissions trend for the lowest excess air ratio increases again for internal recirculation rates higher than 21000 Nm^3/h. This effect is explained by the trends shown in Figure 5.10b, 5.11a and 5.11b. Figure 5.10b shows that the mass weighted oxygen concentration in the furnace at the secondary air level starts to increase again.

This implies more oxygen is added at this level than is needed since part of the burnable gases is extracted by the internal recirculation. This can be monitored by the CO (See Figure 5.11a) and O_2 (See Figure 5.11b) content of the extracted gas. Since more oxygen is already available, less oxygen is needed for the post combustion and the NH_i radicals are oxidized as well.

5.5.2. External flue gas recirculation

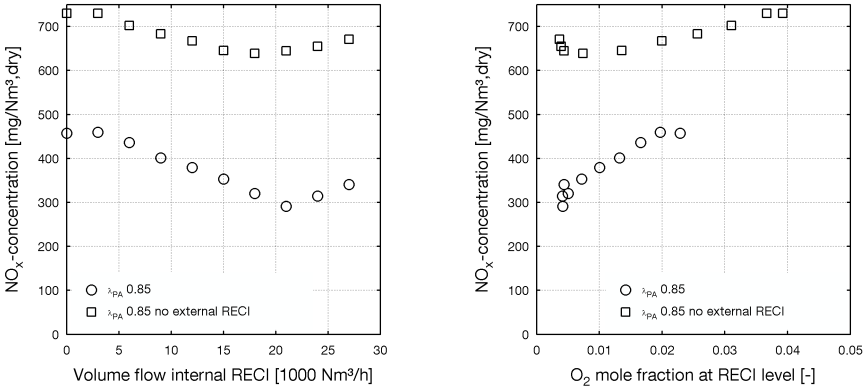

(a) NO_x concentration vs. volume flow of internal recirculation

(b) NO_x concentration vs. O_2 concentration at external recirculation level

Figure 5.12.: Influence of internal recirculation rate on NO_x and O_2 concentration for cases with and without external recirculation

The case with no external flue gas recirculation and a grate excess air ratio of 0.85 is compared to the corresponding data gathered for the case with flue gas recirculation. The trend for NO_x emissions and internal recirculation rate (See Figure 5.12a) and oxygen concentration at the level for the flue gas recirculation (See Figure 5.12b) are compared. The oxygen concentration at the flue gas recirculation level gets down to 0.05 for both trends, while the NO_x emissions differ by up to 300 mg/Nm^3.
With no flue gas recirculation, no mixing occurs before the secondary air is added. The calculated values for the case without external flue gas recirculation are in the range of 650 mg/Nm^3. They are much higher than the typical values expected for such an furnace. This occurs due to more unburned gas entering the improved post combustion zone.

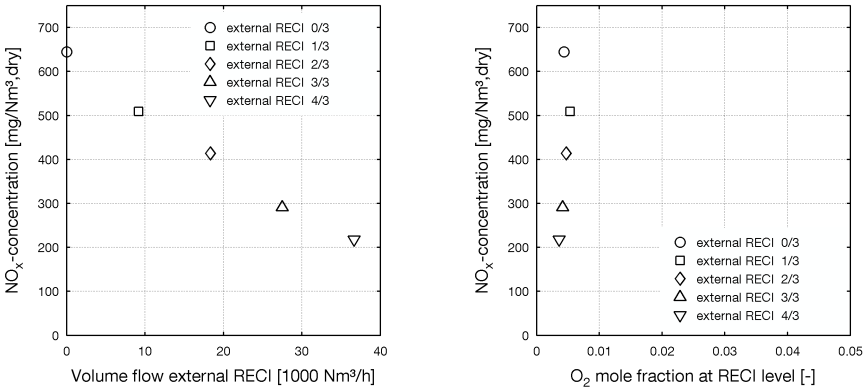

(a) NO_x concentration vs. volume flow of external recirculation

(b) NO_x concentration vs. O_2 concentration at external recirculation level

Figure 5.13.: Influence of internal recirculation rate on NO_x and O_2 concentration for cases with different external recirculation

Different volume flow rates for the external flue gas recirculation are tested for an excess air ratio at the grate of 0.85 and an internal recirculation volume flow of 21000 Nm^3/h, which is close to the design value. The external recirculation rate is increased in equal steps of 1/3 of the design external flue gas recirculation rate from 0 to 4/3 of the design value. Figure 5.13a shows a strong linear decrease of the NO_x emissions, while the O_2 concentration at recirculation level is unchanged. The reduction in NO_x emissions is caused by the good mixing and increased oxidation in this level and not by the reduced oxygen content. This concludes that good mixing at low oxygen levels is of main importance for low NO_x emissions. This was experimentally confirmed by Beckmann and Spiegel [118].

5.5.3. Air humidification

As a last test the settings for step 3 and step 5 are compared for different internal recirculation rates. The main difference between both sets is the overall excess air ratio and the partial pressure of oxygen in the combustion air. The excess air ratio is reduced from 1.35 to 1.25, while the moisture content is increased from 0.6 vol.% to 15.8 vol.%. The overall NO_x performance for the case with the humidified combustion air is significantly better. For the best case without

air humidification there is still an improvement of 150 mg/Nm^3 possible for similar settings with air humidification. It is smaller than for the case without air humidification. Comparing the O_2 concentration in the internal recirculation case the change for different recirculation rates is not so large for the case with air humidification. (See Figure 5.14b) About 10000 Nm^3/h are additionally supplied into the primary combustion zone, this reduces the volume flow rate of gas from the main combustion zone sucked in by the internal recirculation. There is not improvement for NO_x emissions above an internal recirculation rate of 21000 Nm^3/h (See Figure 5.14a) which corresponds to about 17 % of the volume flow at the stack for combustion with humidified air. This value is selected in the design of the combustion system since it keeps the necessary duct diameter and fan small. The design for the internal recirculation system has to be similar to the external flue gas recirculation system.

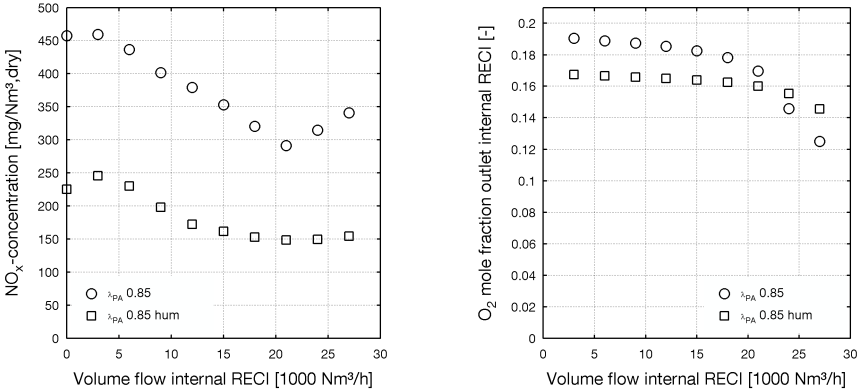

(a) NO_x concentration vs. volume flow of internal recirculation

(b) O_2 concentration at outlet of internal reci vs. volume flow of internal recirculation

Figure 5.14.: Influence of internal recirculation rate on NO_x and O_2 concentration for cases without external recirculation

5.6. Improved geometry and geometry variations

In Section 5.5 different parameters influencing the combustion are investigated. For some investigations, an optimum NO_x level was achieved due to a change in

local chemistry. The design point with roughly 21000 mg/Nm^3 for the internal recirculation and a grate excess air ratio of 0.85 gave good results for cases with and without air humidification. These are however, optima for a particular geometry. Changing the geometry may hold the potential to improve the NO_x performance even further. These changes imply not the change of the lower furnace but mainly nozzle arrangements and injection directions. To get a more general picture on the NO_x performance of the cases, all cases are investigated with the gas phase approach and with both settings using the waste bed approach described in section 3.3.2.4. NO_x emissions for all approaches are evaluated in the middle of the second pass to get a general trend on the effects achieved by the geometry changes. The geometry was also changed so that the wall superheater needed to reach a live steam temperature of 500 °C could be incorporated in the first and second pass of the boiler.

5.6.1. Wall super heater and improved first and second pass design

The first change in geometry was to modify the first and second pass, so that the complete surface needed to superheat the steam from 450 °C to 500 °C can be implemented as a wall superheater. An alternative option is for example the use of radiation superheaters with rear ventilated tiles which hang directly in the empty passes. These options keep the volume of the boiler low. However the cost of boiler volume is rather low compared to the cost of the heat transfer surfaces surrounding this volume. Therefore it is possible to design the radiation passes in such a way to fulfill specific targets. One target is increased residence time in the temperature range between 880 °C to 800 °C as discussed in Section 3.1.1.2. This can be achieved due to the lower heat transfer of the wall superheater compared to a membrane wall used as an evaporator. The HRC boilers in Amsterdam are designed with a large first pass with low flow velocities to increase the residence time. Simulations have however shown that this design does not work under all operational conditions. With an uneven heat release on the rather wide grate, temperature strands are formed. Due to buoyancy forces the hot gas of the strands move faster upward, compared to the colder gas in the rest of the cross section. This leads to the formation of significant recirculation zones [143]. The recirculation zones occupy part of the boiler cross section since the volume flow passes in the cross section several times. This reduces the available cross section for the rest of the gas, which results in higher velocities of the gas, reducing its residence time. This implies only part of the gas reaches the desired residence time. A simple solution to this problem is possible due to the lower cooling rate of the wall superheater. The first pass is made narrower, starting somewhere

above the last gas injection at the end of the furnace. This increases the flue gas velocity, and therefore the upward impulse, eliminating the risk for backflows in the first pass completely. In the second pass, where the flue gas flows downward, the buoyancy forces work in the direction opposite to the flow. For a downward flow, no back flow can occur and the flow is stable under any condition. Due to the buoyancy forces high temperature strands tend to move slower and have more time to cool down. This homogenizes the temperature profile at the entrance of the convective part of the boiler, and reduces therefore the risk of corrosion even further. Using this reasoning the design for the first and second pass is implemented as shown in Figure 5.15. The positive effect of the narrow first pass can be seen by the fact that both lines are on top of each other in the vertical mass flow rates profile shown in Figure C.1 in Appendix C.

The furnace up to the beginning of the wall superheater is exactly the same as for the previous geometry (See Figure 5.2); therefore the risk of more fly ash carried with the flue gas due to higher velocities is not given. In Table 5.2 the most important results for the flue gas flow through the part of the boiler equipped with the wall super heater are presented. The flue gas velocity is reported from the horizontal cross section in the middle of the respective pass. For the second pass, the flue gas velocity can be further decreased by optimizing the transition points between first and second pass. CFD simulation can also be used to perform this task. Looking at the temperatures and the residence time it becomes quite obvious that this boiler concept has no problem to fulfill the 850 °C-2 s criteria to guarantee the burnout. Also, the rather narrow temperature window for the SNCR injection is stretched geometrically due to the low cooling rate of the wall super heater. Due to the simulation of an unveven combustion at the grate the temperature distribution at the inlet of the wall superheater shows a difference of 270 °C between average and highest temperature. This is reduced to 19 °C at the outlet of the wall superheater. However some of the temperature homogenization can be attributed to the fact, that strands with higher temperature cool faster due to the higher radiation heat

Table 5.2.: Results for flue gas flow through the wall superheater in the first and second pass

		WSH First pass	WSH Second pass
Average temperature at entrance	°C	984	898
Average temperature at outlet	°C	898	799
Average residence time	s	3	6
Average velocity	m/s	6.6	5.5

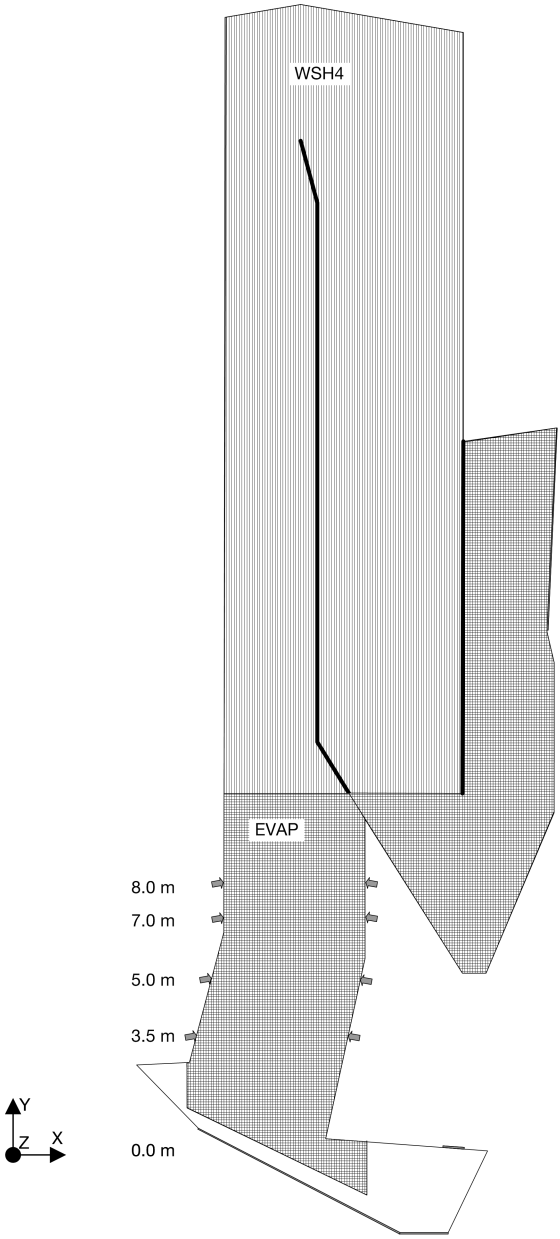

Figure 5.15.: Boiler adapted for wall superheater in the first and second pass

transfer [81]. The more narrow first pass eliminates also a backflow in the empty pass close to the last gas injection level. For this case not so much inert flue gas is transported down to the lower burn out levels diluting the flue gas, and thereby reducing the concentration of NO_x precursors. This eliminated backflow had a positive effect on the NO_x emissions.

This case is marked as BC (Base case) in the following figures.

5.6.2. Improved nozzle arrangement

An additional change in geometry is the improvement of the nozzle arrangement. A visual assessment using contour plots and path lines of the flow through the gas injection cross section in the post combustion zone showed that the gas injected by a stitching arrangement can block the center of the cross section for the flue gas coming from lower levels. This flue gas moves to the part in the cross section where there is less resistance (depending on the pressure drop, over an injection level), which is close to the wall between the nozzles. This is simplified represented in Figure 5.16a. Due to this fact, the unburned flue gas

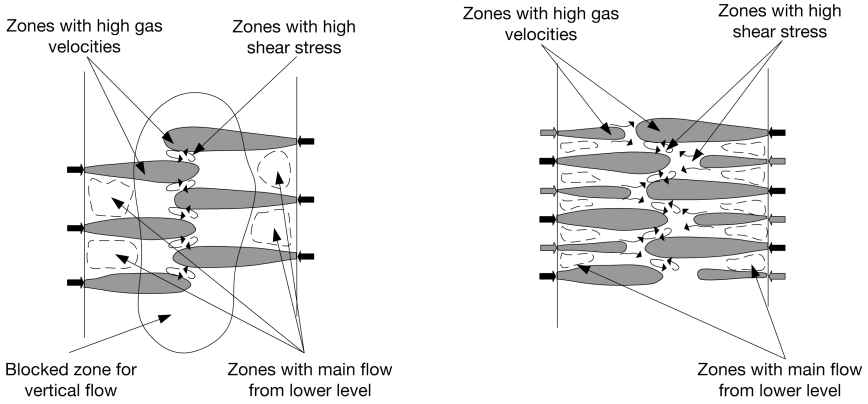

(a) Stitching arrangement

(b) Stitching arrangement with small nozzles to reduce the open cross section

Figure 5.16.: Influence of nozzle arrangement on flow and mixing in the boiler cross section

concentrates at the front wall and therefore even more oxygen is needed there to oxidize it properly. Redistributing the supplied gas by injecting some of it

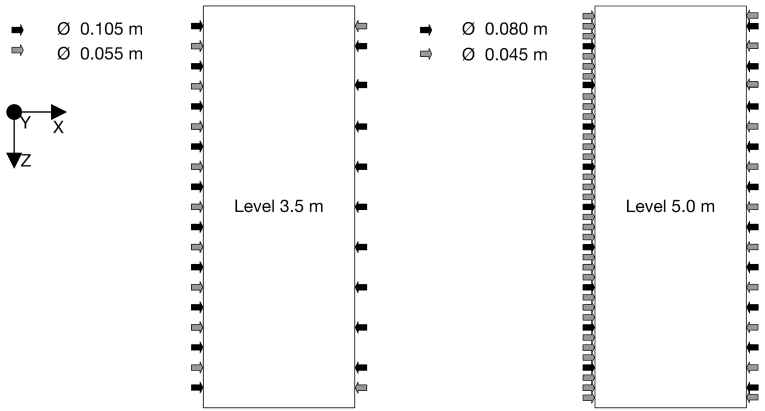

Figure 5.17.: Improved nozzle arrangement for recirculated flue gas and secondary air

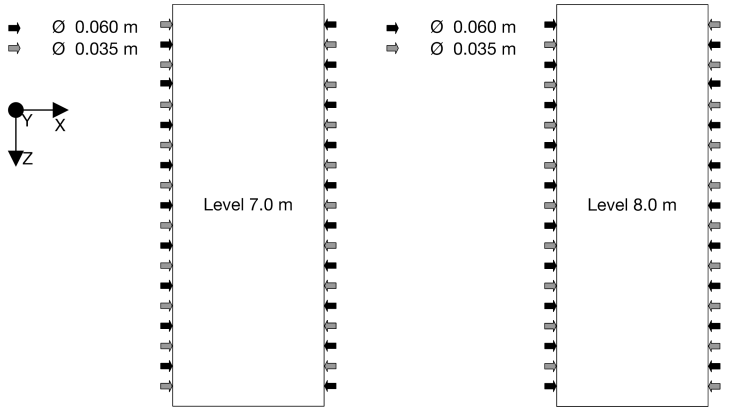

Figure 5.18.: Improved nozzle arrangement for internal recirculated flue gas

with small nozzles in the zones with main flow from lower levels is one option. (See Figure 5.16b) The additional injections increase the shear stress in this zone and combust part of the gas in this zone, reducing the oxygen demand in the same location at the level above. Also, the redistribution of the gas reduces the required volume flow rate injected by the big nozzles, thus less gas is accumulated in the center of the furnace cross section blocking it.

An option to reduce the blocking would be to increase the distance between the nozzles, this approach was not investigated during this work, but could be the topic of further studies. These changes in the nozzle arrangement are performed only for the injection of the secondary air and the internal recirculation. An additional motivation for this task was the big gap of 1.2 m between the nozzles at the injection level of the internally recirculated flue gas, which is reduced to 0.6 m, by using smaller nozzles in-between. For the higher injection levels the injection depth is reduced due to the increased mass flow rate flowing through the boiler cross section. So the mixing is limited to only a smaller part of the cross section. Thus using a small nozzle on the other wall, helps improve mixing and therefore combusting unburned flue gas. The new arrangement for the nozzles is shown in Figure 5.17 and 5.18. In total, 166 nozzles are installed in the furnace, which are about 15 nozzles per meter boiler width. This is much more than for normal boilers, however the reduced excess air needs better mixing to keep the CO emissions at an acceptable level. The lower excess air ratio on the other hand allows the use of smaller flue gas treatment plant, which compensates for the additional cost of the more complex combustion system.

Due to the better mixing and oxygen supply the NO_x emissions drop for the case with the improved nozzle arrangement compared to the old arrangement. Depending on the modeling approach the drop is in the range of 20 mg/Nm^3 to 60 mg/Nm^3.

This case is marked as IN (Improved nozzles) in the following figures.

5.6.3. Variations

Using the improved design of the nozzles additional changes and tests have been performed to unlock the additional potential and justify the more complex combustion system.

5.6.3.1. Bigger nozzles

The shear stress and therefore the mixing depends on diameter of the injecting nozzle [28]. Therefore the nozzle diameter is increased as a test by 30 % for all nozzles to reduce the injection velocity. The lower velocity is still high enough to ensure a proper penetration of the cross section. Bigger nozzles reduce also the distance between two nozzles reducing the area where flue gas can pass from below. For the gas phase approach, an improvement on the NO_x emissions could be achieved, while for the waste bed approach the NO_x emissions increased. A disadvantage of big nozzles on the other hand is the reduction of the achieved impulse during part load operation of the combustion system, when gas flows

have to be reduced. This reduces the mixing and could therefore reduce the flue gas burnout, resulting in higher CO emissions. A solution could be to use separate headers for the small and the big nozzles and reduce the gas flow only from the small or big nozzles and so keep the mixing intensity high. This however increases the cost of the combustion system. Further CFD simulations for part load on this geometry could offer possible solutions to the problem.

This case is marked as BIN (Big improved nozzles) in the following figures.

5.6.3.2. Modified gas supply

As next test the arrangement of the air supply is slightly changed. Looking at the NO_x profiles showed that it is formed mainly close to the front wall at the level of the secondary air injection. The air has too high of an oxygen concentration and oxidizes too much of the precursor species, while NO formed at the flue gas recirculation level is completely reduced to N_2 before it reaches the secondary air level. The idea of this change is to increase the oxidation at the lower level to decrease the TFN before the secondary air level. To achieve this, the recirculated flue gas from the small nozzles of the first level are replaced by a fraction of the secondary air, while the respective recirculated flue gas is injected at the outer two nozzles of the three small nozzles arranged on the front wall between the big nozzles of the secondary air level. This should improve mixing at this location without introducing too much oxygen.

Not enough NO_x can be reduced in the short distance between the two injection levels, therefore no positive effect could be achieved by this change. The NO_x emissions stayed at the same level.

This case is marked as GSM (Gas supply modified) in the following figures.

5.6.3.3. Tilted gas injection

In Section 5.6.2, the blocking of the center of the cross section by injected gas is discussed. One solution could be to increase the distance between the nozzles, which however increases the gap where no mixing occurs. An alternative is to tilt the nozzles upward to allow the flue gas to flow upward in a wider range of the boiler. By increasing the injection angle, the injection depth is slightly reduced since the horizontal impulse is reduced. However the combustion should take place more evenly and the burnable gas should not be concentrated so much on the front wall. The injection angle for all nozzles is set to $+10°$ in respect to the horizontal plane. The NO_x performance for this small modification is impressive. Depending on the NO_x modeling approach an emission reduction of

50 mg/Nm^3 to 160 mg/Nm^3 compared to the improved nozzle design with horizontal injection could be achieved. Also, the gas burnout is slightly improved. The mean temperature in the furnace are reduced by about 30 °C due to the better distribution of the heat release and better mixing of colder injected gas with the hot flue gas.

This case is marked as UP (Upward) in the following figures.

5.6.4. Switched burnout zone

For all previous cases, the burnout occurs rather sharply in one single stage, where the secondary air is added. As discussed in Section 5.5.1, the optimized mixing of the secondary air leads to rather high NO_x values. Spliethoff and Zabetta et al. suggest to add the burnout air in several stages [44], [53]. This approach can be implemented in many different ways; however the good mixing and combustion achieved by the secondary air nozzle arrangement should be kept. Therefore the nozzle arrangement remained unchanged; only the order of the injection levels was changed. The first level of the internal recirculation injection was moved down to 5 m above the grate, while the secondary air level moved up to 7 m. The internally recirculated gas has a composition close to air and therefore supplies some oxygen for the oxidation of the NO_x precursors. However as an average, the flue gas is still under stoichiometric after this stage, thus the NO can be reduced further to N_2 and thereby reducing the TFN. The NO_x values of this case are even lower as for the case with tilted gas injection. It is interesting that all NO_x modeling approaches give values in the same range, while before there was more than a factor of two between the NO_x emission calculated for the different approaches. This implies that this combustion system is definitely an improvement, since it is independent from the modeling approach.

This case is marked as SC (Switched combustion) in the following figures.

Two completely different approaches described above lead to a reduction of the NO_x emission by about 50 % and 75 %. A test combining these two effects is the obvious consequence to reduce the NO_x emissions even further. The levels are arranged like for the SC case and the injections are tilted by +10° as described in Section 5.6.3.3. Unexpectedly no improvement in NO_x emissions could be achieved, the emissions increased even slightly.

This case is marked as SC-UP (Switched combustion upward) in the following figures.

As a last test the secondary air level was switched with the last injection level of the internal recirculation. This case is marked as SH-UP (Switched (combustion) highest upward) in the following figures. All injections are still tilted upward.

There is an improvement in NO_x emission compared to the case SC-UP, but it is minimal and so these two cases are on par with each other. The achieved NO_x concentration with these combustion systems of about 60 mg/Nm^3 are far below the 350 mg/Nm^3. typically known for EFW plants. But they concur with the theory of NO_x formation and reduction discussed in Section 3.2.

5.7. Design criteria analysis

Only the NO_x performance for the different cases has been discussed so far. At the beginning of this chapter two other design criteria for combustion systems are presented. The performance for these criteria is discussed in this Section.

Figure 5.19 shows the NO_x concentration for the above presented cases, the clear trend to lower NO_x concentration independent from the modeling approach can be seen. To confirm these results at least two of these cases should be recalculated using detailed chemical kinetic modeling (DCKM). This was however not possible since the calculation time is in the range of several months per case using the available hardware.

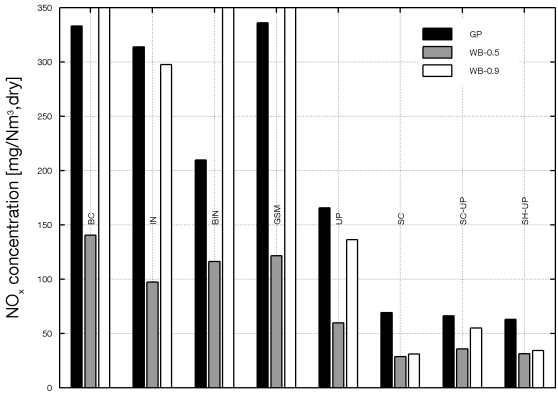

Figure 5.19.: NO_x concentration for the three different approaches for the different cases

Of interest is also how the temperature changes in the furnace when changing the combustion system. This is evaluated by calculating the mass weighted average temperature over the first 9.5 m of the furnace, calculated out of the profiles for the mass weighted average temperature in the cross section and the net mass

flow rate. Also, the maximum temperatures of the mass weighted average temperature profile are compared and presented in Figure 5.20. It can be seen that the cases with the lower NO_x concentration have also about 30 °C lower temperature, this reduces the risk for fouling around the nozzles, which is an important fact for a combustion system relaying on a lot of nozzles. It also decreases the risk for corrosion of the membrane walls in the lower furnace and keeps thereby the availability high. Comparing the maximum mass weighted average temperature in the furnace with the adiabatic flame temperature presented in Table 4.6, shows that by staging the combustion, the maximum temperature can be reduced by about 100 °C compared to the adiabatic flame temperature. Depending on how the different gas streams are added and the heat is released in the post combustion zone. The average gas temperature in the furnace cross section can exceed the calculated adiabatic flame temperature. The adiabatic flame temperature is calculated with the heat distributed on the total mass of the gas participating in the combustion, while in the CFD simulation the temperature in the cross section can be related to a lower gas flow rate, depending on the injection levels. Conventional combustion systems investigated by Dürrschmidt, Jell and Friedrich show maximum average temperatures in the furnace which are up to 100 °C hotter, than for this combustion system [82], [60], [83]. This is an important fact, since it shows that preheating the combustion air causes no additional problems due to higher temperatures in the furnace. Although the evaporation temperature for the HEB concept is more than 100 °C higher compared to state of the art boilers, which also reduces the heat transfer in the lower furnace, the maximum flue gas temperature is lower. Air preheating, air humidification and higher evaporation pressure can therefore be implemented without expecting any additional problems during the combustion process in the high efficiency boiler concept.

The last design criterion for the combustion system is the good burnout of the flue gas. This is hard to evaluate. A method is to check the CO concentration at a defined height. This is critical due to the staged combustion the oxygen supply varies significantly. By choosing a level close to the last air injection the geometries were the secondary air is injected already at 5 m have definitely the best values. Choosing a level with a reasonable distance from the last air injections all CO levels are low. The burnout is influenced by the arrangement of injection levels and the actual flow pattern. A fair method to evaluate the different concepts was developed using the oxygen demand and the net oxygen demand defined by Equations 5.6 and 5.7. If the profile for the net oxygen demand is 0 there is enough oxygen available to oxidize all unburned components of the flue gas. This implies stoichiometric conditions are reached. Starting from this point, the distance to reach a defined oxygen demand in the boiler

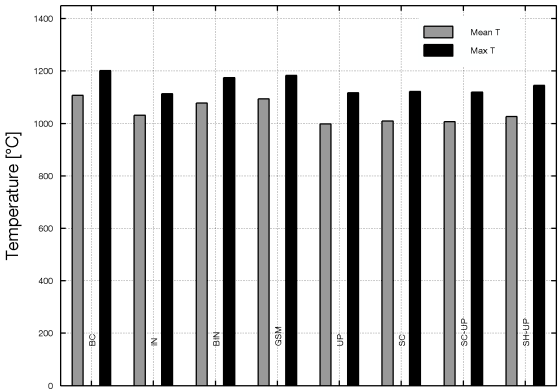

Figure 5.20.: Mean and maximum temperature for the different cases in the lower furnace

cross section is determined. Three oxygen demand levels are compared. These are 1000 ppm, 500 ppm and 100 ppm. 100 ppm of O_2 demand still corresponds to a CO concentration of 250 mg/Nm^3, but to get an accurate value for lower CO concentrations the combustion simulation must be switched to a DCKM simulation and as mentioned above this is not practical for such a big geometry, with the available computing power. The calculated distances for the different cases are compared in Figure 5.21. The lowest distance is achieved by the case with switched combustion and upward injection. Stoichiometry is reached for this case 7 m above the grate. For the cases with not switched combustion it is the case already at 5 m. It is interesting to see that the 100 ppm height (distance + level for stoichiometry) is lowest for the case with switched combustion and upward injection. This can be attributed to the very good secondary air injection. The first injection, of internal recirculated flue gas combusts a major part of the burnable gases, but stoichiometry is not yet achieved. This is responsible for the low NO_x concentration. Flue gas with much lower fraction of burnable gas enters the secondary air level, which was optimized for good mixing and burnout. A surplus of oxygen is added in this level, but combustion is not yet completed. Only one meter above the rest of the internal recirculated flue gas is added, which helps oxidize the rest of the flue gas.

Of the investigated cases, the case switched combustion upward (SC-UP) has the best overall performance. Although the NO_x emissions are not the lowest it has low temperatures in the furnace and has by far the best performance

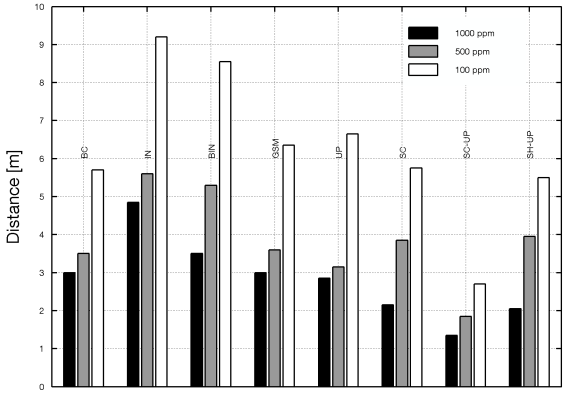

Figure 5.21.: Distance for different O_2 demand levels for the different cases

for the burnout. Therefore this combustion setup is used for some additional tests presented below. Table 5.3 shows an overview on the investigated cases regarding the three design criteria. The excess air ratio at different levels is also listed to show the combustion progress. The excess air ratio is 1.31 after the last gas added. The difference of 0.06 to the design excess air ratio of 1.25 corresponds to the mass of oxygen recirculated with the flue gas, added between 3 m and 3.5 m.

Table 5.3.: Performance assessment of the different cases and excess air ratio λ at different levels

Case	BC	IN	BIN	GSM	UP	SC	SC-UP	SH-UP
NOx	-	-	-	-	+	++	++	++
Temperature	-	+	-	-	+	+	+	+
Bournout	+	-	-	+	+	+	++	+
λ 3.0 m	0.77	0.77	0.77	0.77	0.77	0.77	0.77	0.77
λ 3.5 m	0.83	0.83	0.83	0.83	0.83	0.83	0.83	0.83
λ 5.0 m	1.13	1.13	1.13	1.13	1.13	0.92	0.92	0.92
λ 7.0 m	1.22	1.22	1.22	1.22	1.22	1.22	1.22	1.01
λ 8.0 m	1.31	1.31	1.31	1.31	1.31	1.31	1.31	1.31

In general the design criteria for a combustion system can be summarized as follows: The location air and internally recirculated flue gas is added is rather unimportant. It is important to oxidize the flue gas in several stages while

keeping a reducing atmosphere and mixing it at the same time very intensively is the key to achieve low NO_x concentrations. The step to reach stoichiometry must start from just slightly under stoichiometric and should be followed by at least one additional gas injection to give additional mixing impulse. The external recirculated flue gas should be used as first stage, not only for homogenizing the flue gas coming from the grate but rather add thermal ballast, in the form of N_2, CO_2, and H_2O as early as possible to keep the temperature low.

5.7.1. Sensitivity analysis

As shown in Figure 3.19, depeding on the profiles generated by the fuel conversion model the resulting NO_x concentration can vary by up to 100 mg/Nm^3. To estimate this influence on the performance of the optimized combustion system (SC-UP) a sensitivity analysis was performed with three additional profile sets generated using the same parameters. The NO_x concentration and the distance determined for the O_2 demand vary only slightly for the changed inlet conditions (See Figure 5.22). This implies the combustion model is not tuned only to perform well for one set of inlet conditions.

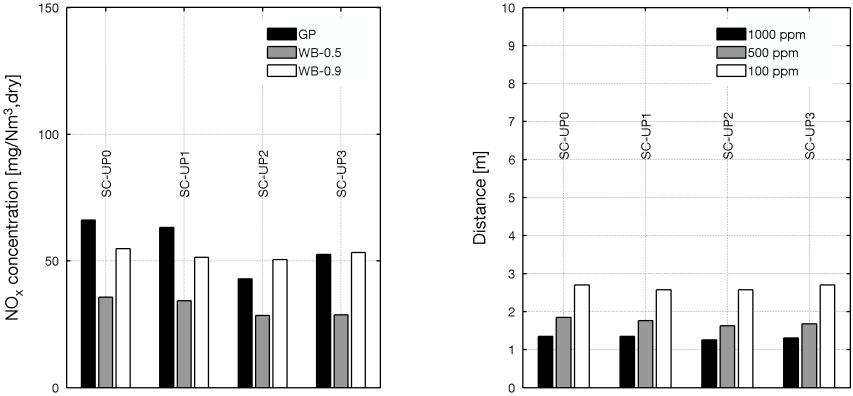

(a) NO_x concentration (b) O_2 demand distances

Figure 5.22.: NO_x concentration and O_2 demand distances for the sensitivity study

5.7.2. Overload investigation

An additional test for the optimized geometry is an overload test, for the system with overfeeding of the grate. This should confirm the improved mixing achievable with this arrangement. All gas streams are kept constant while the throughput of waste incinerated is increased by 10 %. This reduces the overall excess air ratio from 1.25 to 1.14, which is in the level of modern pulverized coal power plants. At the same time, the air randomization in the fuel conversion model was set to increase the channeling effects of the waste bed, to make the combustion even more inhomogeneous. The profiles have been calculated for the improved nozzle (IN) and switched combustion upward (SC-UP) cases. Comparing the profiles for CO and O_2 showed that the combustion progress is similar to the case with design waste throughput and good burnout levels are achieved. The NO_x emissions are higher than for the design load, which is explained by the changed stoichiometry and the higher mass flow rate of fuel nitrogen added to the combustion. As a general conclusion it implies the combustion system can handle even more extreme conditions than what it was designed for without problems, making such a combustion design a good option for the HEB boiler concept.

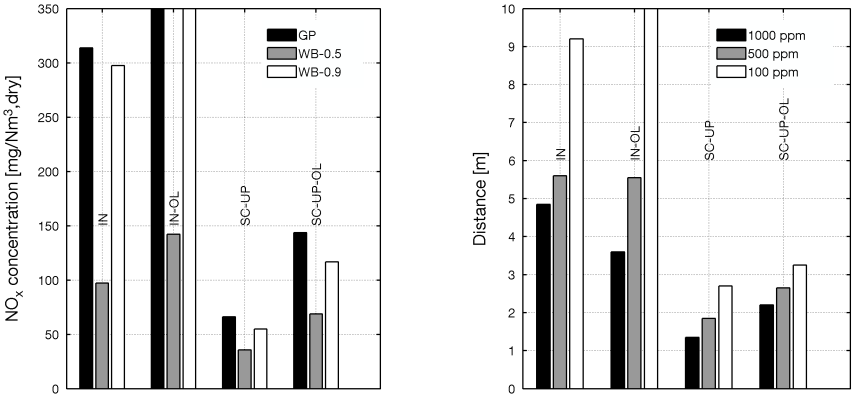

(a) NO_x concentration (b) O_2 demand distances

Figure 5.23.: NO_x concentration and O_2 demand distances for normal load and overload (OL) cases

6. Recommendations

In this work a concept for a new EFW plant was presented. It was designed and optimized using different numerical methods. Some additional thoughts and summarizing discussion points are presented in this chapter to show why and how such a plant concept should be implemented.

6.1. Control strategy

The plant performance depends strongly on its design. During operation however the control system ensures that the plant is operated as intended and all implemented features serve their purpose. For such a sophisticated combustion system, the control system is of special importance. As stated by Maurer the combustion control system is no longer only installed to keep the combustion stable but also to control the combustion in such a way that the emissions stay low. Therefore, it should be called combustion and emission control system [115].

6.1.1. Combustion control

Operating a boiler at low excess air ratios makes a fast control of the air supply necessary. Normally the oxygen concentration of the flue gas is measured at the boiler outlet. Due to special design of the wall superheater, the flue gas has an extra-long residence time which results in a long dead time of about 20 s before fluctuations in the combustion reach the end of the boiler. So the oxygen sensor has to be moved closer to the combustion to be able to react faster. Some sensors do not work at higher temperatures, while others cover only a short range and therefore get average concentration of only a part of the flue gas. Several local oxygen measurements could be combined to control the oxygen concentration and thereby the combustion.

6.1.2. Emission control

Controlling the NO_x emissions by influencing the combustion is more difficult. As discussed in Section 5.7 it is important to keep a reducing flue gas atmosphere

as long as possible and oxidize the flue gas stepwise while it is mixed well. To control the oxygen content in the furnace the internal recirculation is used since it is used to extract excess oxygen gas from the lower furnace. As shown in Figure 5.11b the oxygen concentration in the internal recirculated gas is in the range of 17 vol.% to 19 vol.%. To ensure a low oxygen concentration in the furnace, some unburned gas must be present in the internal recirculated gas. The CO concentration of the extracted gas is already measured for safety reasons. This signal should be used as well to control the volume flow rate of the extracted gas. The CO concentration depends rather strongly on the current combustion situation and therefore fluctuates faster than other signals. So the signal should be damped and combined with other inputs like a general set point and maximum gradients for the extracted gas flow to keep the combustion stable. The CO concentration in the extracted gas should be in the range of 1000 ppm to 3000 ppm to ensure low oxygen values in the furnace. This is still far below the flammability limits for CO in air [34] and the gas temperature is also too low for CO combustion. Therefore there is no risk in operating the system in such a way, as long as the duct after the fan is not leaking and no CO enters the boiler house. This implies that the fan should be positioned as close to the reinjection point of the gas as possible, to reduce the risk. Additional CO monitors outside the duct on the pressure side of the fan should be included in the control system.

6.1.3. Load control

The HEB concept is designed for maximum power production. Due to the high fluctuations of renewable energies it may be economical or even necessary to take part in the load control to stabilize the electrical grid. This defines new requirements to the control system since it is optimized for stable operation and not to follow a load profile. Also, the part load capabilities of EFW plants are not ideal since unlike in coal power plants the heat is released in one single location. With the staged combustion the part load capabilities might be better. This requires however more extensive simulation and a plant to validate the results.

6.2. Further optimization potential

During this investigation, the focus was on optimizing the energy efficiency and combustion with special focus on NO_x emissions. There is however a lot of additional potential for the use of numerical methods to improve the operation of EFW plants.

After combustion the flue gas enters the empty radiation passes. The flow in this part of the boiler can be optimized. Especially the transition points between passes hold a lot of potential to optimize the flow. For the convective pass it is important that the flue gas arrives as homogenous as possible to reduce corrosion and erosion. However the mixing possibilities in the empty passes are rather limited.

First tests of particle simulation in EFW boilers have been performed by Römer [64]. With the particle trajectories it is possible to predict favorite places for fly ash deposits. The gas injection and the transition points between the passes can be optimized in such a way that fouling occurs mainly in locations where it can be removed easily during operation and therefore reduce the time for cleaning during maintenance. An additional interesting option is to optimize the transition points between second and third passes in such a way to remove more of the bigger particles there. This could reduce the fouling in the convective part but depending on the design could result in higher ID fan power. A detailed investigation is necessary to estimate the potential of this idea.

For a coal power plant an optimization of flue gas ducts was performed using CFD simulation. The aim of the investigation was to reduce the power of the ID fan. A reduction of 8.3 % was achieved for a fan with 11.3 MW power requirements [144]. For the HEB concept especially the duct for the external and internal recirculated flue gas are of interest for such an investigation, as well as the flue gas flow through the flue gas treatment plant.

6.3. Availability consideration

The high efficient boiler concept was designed as the name suggests for high efficiency. Kamuk however states that the efficiency is only the second important plant characteristic behind the availability [16]. This is obvious since the most efficient plant cannot be operated economically if it is not running. During the design of the plant, possible risks reducing the availability have been considered. The technologies used and implemented designs are discussed here again to determine the risk for such a plant.

6.3.1. Grate, furnace and combustion system

The grate has to withstand the combustion with hot air. Compared to typical plants, the temperature is 100 °C to 200 °C higher. While some plants use oxygen enrichment to increase the combustion temperature, this plant concept tries to avoid an increase of flue gas temperatures. Air humidification and a low

excess air ratio are used to keep the temperature of the waste bed in a typical range for reverse acting grates. This is confirmed by comparing the simulated gas temperature at the exit of the waste bed for a conventional boiler [83] and the boiler simulated during this work. The grate bars themselves however will have a temperature in the range of 350 °C which is slightly higher than the combustion air temperature. This reduces the life time of the grate bars, which is normally in the range of several years; however the plant availability should not be influenced if the grate bars are checked and replaced regularly. This implies the grate can have the same availability as the already installed reverse acting grates.

The staged combustion concept allows controlling the heat release in the furnace. It is optimized in such a way that the maximum average temperature in the furnace cross section is about 100 °C lower compared to conventional furnaces. This reduces the risk of ash melting. At the same time, it has to be considered that the wall temperature is about 100 °C hotter. The strip between the pipes of the membrane wall should therefore be kept as small as possible to keep its temperature low and reduce its risk of corrosion, as suggested by Wilpshaar [143]. Also, a thin layer of refractory or ceramic coating should be used to protect the wall cladded with Inconel.

The startup of the boiler is a critical phase since some components are still cold and the flue gas might condensate which increases the risk for corrosion. This is especially important for the external flue gas recirculation duct and fan. The duct should be preheated with hot air before the flue gas recirculation is started. Also, at shutdown, hot air should be used to flush the duct and thereby reduce the risk of corrosion.

For the lower furnace the availability could even increase due to the lower flue gas temperatures, which decrease fouling and ash melting. The lower furnace is one of the most critical parts of the plant influencing the overall availability.

6.3.2. Superheater and convective pass

The options for increasing the availability of the superheater are discussed in detail in Section 3.1.1. Therefore here only the implemented options are listed once more.

The final superheater is implemented as wall superheater, although no reference plant for this type superheater exists yet. Tests with smaller test panels look rather promising. After some experience with wall superheaters, the HEB concept can be implemented as designed. The long residence time and the homogenization of the temperature before the convective pass reduce the risk of

corrosion in this part of the boiler. The pipes and the membrane wall not covered with refractory should be covered with nano ceramic coating to have an additional protective layer. The pipes of the convective part of the boiler are designed with an increased wall thickness. The additional lifetime increases the availability compared to state of the art plants.

6.3.3. High temperature flue gas treatment

The flue gas dedusting for the HEB concept is designed for 325 °C. For EFW plants electrostatic precipitators are used only for temperatures up to 250 °C. In the cement industry ESP's and baghouse filters are installed at temperature's exceeding the 325 °C, experience from there operation can be transferred to reduce the risk for the operation of the dedusting at this temperature.

6.3.4. Other components

The rest of the plant concept consists of components used in EFW plants or coal power plants for many years. Therefore no additional potential for reduced availability is introduced by using these components. With carefully detail engineering and additional detailed simulation for some parts of the plant it should be possible to operate this plant concept with a higher availability than normal plants.

6.4. Implementation of innovations

As discussed in Section 6.3 some of the technologies used for the design of the HEB concept are not state of the art. Constructing a green field project exactly as described in this thesis would be possible. If however some aspect does not work as intended the whole concept could be buried forever.

Therefore the concept should be implemented step by step and each new project should profit from the gained experience.

- The steam cycle concept is in successful operation with slightly lower live steam parameters in Amsterdam for several years and is therefore considered a proven technology.
- As a first step the air humidification can be implemented. This is a rather simple technology and can also be retrofitted if a wet flue gas treatment is present. The benefit for efficiency and the plant operation itself make this a very good option.

- An option for new boilers is the change in boiler design for the first and second pass. Reducing the cross section in the first pass increases the speed and eliminates backflows. This option holds no additional risk.
- The change in the combustion system is rather serious, but it can be implemented without preheated air, and thereby reducing the risk for the lower furnace. This can be implemented for plants, where strict NO_x emission limits have to be met. The combustion system maybe also implemented as a retrofit in a plant which already has flue gas recirculation.
- The increased wall thickness for the superheater pipes, is also a risk free option and can be implemented right away.
- Air preheating to this high temperature should definitely not be implemented in one step and without air humidification. Some plants with more moderate air temperatures should be implemented first to see the different effects. Air preheating goes hand in hand with feed water preheating to higher temperatures, since the air should be preheated with heat normally used in the economizer.

7. Summary

In the research project "Efficient power generation from municipal solid waste" potentials in waste incineration with regard to energy efficiency and combustion optimization were investigated. Numerical methods have been adapted to be used for energy from waste boilers and the water steam cycle. These methods have further been used to plan and optimize a 400000 t/a plant with two combustion lines.

First the water steam cycle has been optimized. The use of a wall superheater allows to increase the live steam temperature with reduced risk for corrosion to 500 °C. The higher temperature along with the external reheater concept, in operation in Amsterdam since 2007, makes it possible to set the live steam pressure to as high as 177 bar. This is mainly limited by the natural circulation in the boiler and the available steam turbines for this plant size. The higher pressure makes it possible to expand the steam longer, before extracting steam at higher pressures for feed water preheating. This allows an increase in feed water temperature up to 300 °C. The feed water is preheated in the optimized plant by 5 feed water preheaters and waste heat from the flue gas condenser as well as air preheater. At the pressure level for the third feed water preheater the steam is piped to a external reheater heated by saturated steam from the drum. This results in reheat parameters of 23 bar and 340 °C;

As a second step the heat profile generated during the combustion process is investigated. Parameter studies for different settings of excess air ratio, air preheating, flue gas recirculation and air humidification have been performed. Tendencies of these studies have been combined to optimize the available heat in the boiler. The excess air ratio is reduced from 1.65 to 1.25; however the adiabatic flame temperature increases only from 1225 °C to 1240 °C. This is achieved by a combination of flue gas recirculation, air preheating and air humidification. The available high value heat (above 325 °C) is thereby increased from 75 % to 91.5 % of the gross heat input.

The plant with optimized steam cycle and combustion settings has a net electric efficiency of 37.1 %, when operated in condensing mode with a hybrid cooling tower. Such a high efficiency ensures waste incineration an important position in modern and sustainable waste management systems. A study was performed

to investigate the power loss of the plant during combined heat and power operation. Surplus heat from the flue gas condenser is used in a first stage directly and in a second stage with a steam driven absorption heat pump. At maximum heat output the plant's overall efficiency results in 103.2 %, based on the lower heating value. The net electric efficiency is still very high at 28.8 % while the possible heat supply to a district heating network with 95 °C feed and 40 °C return temperature is 74.4 % of the gross heat input.

As a third step computational fluid dynamic (CFD) was used to optimize the combustion process itself choosing the gas temperature in the furnace, burn out of combustible gases and NO_x emissions as optimization criteria. An extensive investigation of the available NO_x model was performed to identify the influence of the individual parameters. Two different approaches and two different settings for the second approach have been used for further investigation to cover a broader range of possible results.

The combustion concept of the modeled boiler is based on air staging, with external and internal flue gas recirculation. Sets of profiles are generated for the different combustion settings with the developed waste conversion model. Different settings for internal recirculation rates were investigated for 5 different excess air ratios on the grate, ranging from 0.85 to 1.05, with an overall excess air ratio of 1.35. For all excess air ratios the waste is partially gasified on the grate and gas with excess oxygen is available at the end of the grate for the internal recirculation. For an excess air ratio with the lowest NO_x emissions, combustion with humidified combustion air was investigated. The lower oxygen partial pressure in the over fire air has a positive effect on the NO_x formation. Additional calculations have been made for the minimal and maximal excess air ratio on the grate without external flue gas recirculation.

The NO_x emissions tend to drop with increasing internal as well as external recirculation rate. The NO_x reduction effect for the internal recirculation is caused by the reduced oxygen availability in the main combustion zone of the furnace. For the case with increased external flue gas recirculation the NO_x formation is influenced by better mixing in the lower furnace and additional partial oxidation of the NO_x precursors in this stage.

Generally the lower excess air ratio on the grate leads to lower emissions. However the built in randomization in the fuel conversion model does not allow individuating a clear trend. Additional calculations with several profiles generated from the same settings are necessary for this investigation.

After the better understanding of the NO_x formation during the post combustion process, a boiler with staged combustion was designed. Changes in the nozzle arrangement and air supply have been investigated. Five different geometries

have been tested with different parameters, resulting in eight different geometry variations. A very positive effect could be seen by tilting all gas injections from horizontal to +10°. The effects causing the improvement are a better flow pattern with more effective mixing.

The changes in geometry aimed on changing the oxygen availability in the lower furnace. The biggest improvement was achieved when the internal recirculation is injected below the over fire air. This configuration corresponds to a gas burnout in several stages. Oxygen is added gradually under continuous mixing of the flue gas.

To check the independence of the results from the inlet profiles a sensitivity study with four different profiles was performed for one of the best cases. The fluctuations of NO_x emissions decreased compared to sensitivity tests performed during the NO_x model validation for an unstaged case.

The burn out quality of the combustion concept is evaluated by comparing the distance of different concentrations of unburned gas to the point where theoretical enough oxygen is available for complete combustion. All concepts have similar good values, which is caused by the four stages of intense mixing of the flue gas in the furnace.

The best geometry shows that with staged combustion it is possible to reduce NO_x emission from 250 mg/Nm^3 down to below 60 mg/Nm^3 on dry basis. Along with the NO_x emission the temperature profile is improved since the heat is released in several steps, which allows the flue gas to cool in between. The average flue gas temperature in the boiler is reduced by 100 °C. The same is also valid for the highest average temperature in the boiler cross section. This improves the fouling behavior in the lower furnace and therefore improves the availability of the boiler.

Investigations for staged combustion showed an optimum stoichiometric ratio of 0.83 in the post combustion zone to achieve the lowest NO_x emission. This optimum is not a global optimum for the combustion of the specific fuel, but is rather determined by the combustion system itself. A change in geometry, especially in the oxygen supply has much more potential in improving the emissions than tuning parameters on a given geometry. For the staged combustion it can be said that the NO_x emission are lowest if the burnout is performed stepwise with very good mixing in each step.

Additional measures for increased availability have been implemented in this plant design. The biggest is the use of the wall superheater. It does not only allow to generate live steam at 500 °C without the risk for corrosion, but decreases the cooling rate of the flue gas in the temperature window of 1000 °C to 800 °C. A residence time of 9 s is achieved for this temperature window, which

is more time for the slow sulfatation reaction to reach nearly equilibrium. This reduces the corrosion in convective superheaters in the following pass. The first and second passes are designed in such a way that there are high flow velocities (6.5 m/s) in the first pass and lower velocities in the second pass. This reduces the possibilities for backflow and other unwanted flow instabilities. The superheater pipes are designed with 2 mm additional wall thickness. The change in wall temperature is with 0.2 °C negligible. The additional lifetime of the superheater due to thicker walls should be significant.

The plant designed, using the here presented numerical methods, implies a huge change compared to state of the art energy from waste plants. All these changes do not have to be implemented in one step, but rather stepwise, to be able to reduce the total risk. Among the first steps could be the air humidification and the change in design of first and second pass, followed by the change in over fire gas arrangement.

Finally a quote or rather a credo of a good friend who contributed much to this work, inspirational wise as well as with his programming skills: "There is always room for improvement!" This credo applies not only to the processes in energy from waste plants themselves, but also to the numerical models and methods used for their optimization.

Bibliography

[1] VGB PowerTech, *Konzeptstudie Referenzkraftwerk Nordrhein-Westfalen: (RKW NRW)*. 2004.

[2] European Parliament, Council, "DIRECTIVE 2008/98/EC OF THE EUROPEAN PARLIAMENT AND OF THE COUNCIL of 19 November 2008 on waste and repealing certain Directives: Waste framework directive."

[3] M. J. Murer, H. Spliethoff, M. A. van Berlo, C. M. W. d. Waal, and O. Gohlke, "Comparison of energy efficiency indicators for energy-from-waste plants," in *Sardinia 2009 Symposium* (R. Cossu, ed.), 2009.

[4] N. J. Themelis, "Changes in public perception of role of waste-to-energy for sustainable waste management of MSW," in *19th Annual North American Waste-to-Energy Conference (NAWTEC19)* (M. J. Castaldi, M. White, and J. Austin, eds.), 2011.

[5] M. Münster, *Energy System Analysis of Waste-to-Energy technologies*. PhD thesis, Aalborg University, Aalborg, 2009.

[6] M. Gleis, "Pyrolyse und Vergasung," in *Energie aus Abfall* (K. J. Thomé-Kozmiensky and M. Beckmann, eds.), pp. 438–465, Neuruppin: TK Verlag, 2010.

[7] S. Consonni, "Waste gasification and energy efficiency," in *Sardinia 2011 Symposium* (R. Cossu, ed.), 2011.

[8] O. Gohlke and M. J. Murer, "Anwednung von Energiekennzahlen für die Abfallverbrennung," in *Energie aus Abfall* (K. J. Thomé-Kozmiensky and M. Beckmann, eds.), pp. 3–30, Neuruppin: TK-Verl., 2011.

[9] European Parliament, Council, "DIRECTIVE 2000/76/EC OF THE EUROPEAN PARLIAMENT AND OF THE COUNCIL of 4 December 2000 on the incineration of waste," in *Official Journal of the European Union* (European Parliament, Council, ed.).

[10] Bundesgesetzblatt, "Siebzehnte Verordnung zur Durchführung des Bundes-Immissionsschutzgesetzes (Verordnung über die Verbrennung und die Mitverbrennung von Abfällen - 17. BImSchV): 17. BImSchV."

[11] H. Fehrenbacher, J. Giegrich, and S. Mahmood, "Beispielhafte Darstellung einer vollständigen, hochwertigen Verwertung in einer MVA unter besonderer Berücksichtigung der Klimarelevanz: Im Auftrag des Umweltbundesamtes: Forschungsbericht 205 33 311 UBA-FB 001092."

[12] M. A. van Berlo and J. Wandschneider, *Value from waste: Waste fired powerplant the new standard for recovery of sustainable energy, metals and building materials from urban waste.* Amsterdam and The Netherlands: Afvalenergiebedrijf, the city of Amsterdam, 2006.

[13] Bundesgesetzblatt, "Siebenunddreißigste Verordnung zur Durchführung des Bundesimmissionsschutzgesetzes (Verordnung zur Absicherung von Luftqualitätsanforderungen – 37. BImSchV)."

[14] VDI, "Stellungnahme des VDI zum Vorschlag der Europäischen Kommission für eine Richtlinie über die Förderung der Kraft-Wärme-Kopplung auf der Grundlage des Nutzwärmebedarfs im Energiebinnenmarkt: KOM (2002) 415."

[15] C. Wünsch, *Vermeidung von Treibgasemissionen durch Steigerung der Energieeffizienz deutscher Müllverbrennungsanlagen.* Pirna: Eigenverl. des Forums für Abfallwirtschaft und Altlasten, 1 ed., 2011.

[16] I. Multi-Media Productions (USA), "21st Century Bussines on Waste to Energy: Interview with Head of department Bettina Kamuk," 15.05.2012.

[17] S. Andersson, J. Froitzheim, E. Larsson, and J. Pettersson, "Sulphur recirculation for increased electricity production in MSWI," in *Venice 2010 Symosium* (R. Cossu, ed.), 2010.

[18] H. Hunsinger, "Verfahren und Vorrichtung zur Flugstrom-Sulfatierung von Rauchgasinhaltsstoffen," 2009.

[19] C. Kastner, *Analyse des thermischen Verhaltens der Aschekomponenten mittels TGA - Versuch und thermodynamischen Berechnungen: Master Thesis.* Munich: Lehrstuhl für Energiesysteme, Technische Universität München, 2012.

[20] M. A. van Berlo and P. Simoes, "High-efficiency waste-to-energy: Amsterdam's experiences after four years of operation," in *Sardinia 2011 Symposium* (R. Cossu, ed.), 2011.

[21] W. Spiegel, G. Magel, T. Herzog, W. Müller, and W. Schmidl, "Empirische Befunde am Kessel - Wärmestromdichte korreliert mit Korrosionsdynamik," in *Energie aus Abfall* (K. J. Thomé-Kozmiensky and M. Beckmann, eds.), pp. 271–288, Neuruppin: TK Verlag, 2010.

[22] A. Schütz, M. Günthner, G. Motz, O. Greißl, and U. Glatzel, "Characterisation of novel precursor-derived ceramic coatings with glass filler particles on steel substrates," *Surface and Coatings Technology*, 2012.

[23] O. H. Madsen and T. W. Sødring, "A new concept to improve the electrical efficiency based on the combustion process," in *ISWA World Congress* (ISWA, ed.), 2011.

[24] H. Rüegg and G. Ziegler, "Dampferzeuger für überhitzten Dampf für Verbrennungsanlagen mit korrosiven Rauchgasen," 01.07.1999.

[25] H. Effenberger, *Dampferzeugung*. Berlin: Springer, 2000.

[26] Eurpean Comission, *Reference document on the best available techniques for waste incineration: Integrated Pollution Prevention and Control*. Eurpean Comission, 2006.

[27] T. Klasen, *Erstellung und Validierung eines mathematischen Modells für die heterogene Verbrennung auf dem Müllrost und dessen Anwendung bei CFD-Simulationen hinsichtlich einer optimierten Feuerungstechnik*. PhD thesis, Universität Gesamthochschule Essen, Essen, 2003.

[28] R. Doležal, *Dampferzeugung: Verbrennung, Feuerung, Dampferzeuger*. Berlin [u.a.]: Springer, berichtigter nachdr. ed., 1990.

[29] H. Eberius, T. Just, and S. Kelm, "NOx-Schadstoffbildung aus gebundenem Stickstoff in Propan-Luft-Flammen," *VDI-Bericht*, vol. Nr. 498, 1983.

[30] K. M. Hafner, *Untersuchung zur Bildung brennstoffabhängiger Stickoxide bei der Abfallverbrennung mittels on-line analytischer Messmethoden*. PhD thesis, Technische Universität München, Munich, 2004.

[31] J. A. Miller and C. T. Bowman, "Mechanism and modeling of nitrogen chemistry in combustion," *Progress in Energy and Combustion Science*, vol. 15, no. 4, pp. 287–338, 1989.

[32] T. Kolb, *Experimentelle und theoretische Untersuchungen zur Minderung der NOx-Emission technischer Feuerungen durch gestufte Verbrennungsführung*. PhD thesis, Universität Karlsruhe, Karlsruhe, 1990.

[33] T. Just and S. Kelm, "Mechanismen der NOx-Entstehung und -Minderung bei technischen Verbrennung," *Industriefeuerung*, vol. 38, 1986.

[34] S. R. Turns, *An introduction to combustion: Concepts and applications*. Boston and Mass. [u.a.]: McGraw-Hill, 2 ed., 2000.

[35] C. Fenimore, "Reaction of fuel-nitrogen in rich flame gases," *Combustion and Flame*, vol. 26, pp. 249–256, 1976.

[36] H. Spliethoff, *Power generation from solid fuels*. Heidelberg [Germany] and and New York: Springer, 2010.

[37] L. Sørum, Ø. Skreiberg, P. Glarborg, A. Jensen, and K. Dam-Johansen, "Formation of NO from combustion of volatiles from municipal solid wastes," *Combustion and Flame*, vol. 124, no. 1-2, pp. 195–212, 2001.

[38] P. Glarborg, K. Dam-Johansen, and J. A. Miller, "The reaction of ammonia with nitrogen dioxide in a flow reactor: Implications for the NH2 + NO2 reaction," *International Journal of Chemical Kinetics*, vol. 27, no. 12, pp. 1207–1220, 1995.

[39] T. Reynolds, P. Reynolds, and R. Pachaly, "Ein Vergleich der Möglichkeiten von SCR und SNCR," in *Energie aus Abfall* (K. J. Thomé-Kozmiensky and M. Beckmann, eds.), pp. 667–682, Neuruppin: TK-Verl., 2011.

[40] B. v. d. Heide, "Das SNCR-Verfahren - Entwicklungsstand und Perspektiven," in *Energie aus Abfall* (K. J. Thomé-Kozmiensky and M. Beckmann, eds.), pp. 683–708, Neuruppin: TK-Verl., 2011.

[41] M. Baur, A. Sigg, and R. Halter, "NOx–Abscheidung mit dem DyNOR SNCR-Verfahren," in *Energie aus Abfall* (K. J. Thomé-Kozmiensky and M. Beckmann, eds.), pp. 755–769, Neuruppin: TK Verlag, 2010.

[42] R. Karpf and T. Krüger, "Energetische Optimierung von Abgasreinigungsverfahren hinter Abfallverbrennungsanlagen," in *Energie aus Abfall* (K. J. Thomé-Kozmiensky and M. Beckmann, eds.), pp. 499–528, Neuruppin: TK-Verl., 2011.

[43] P. Chomec, "SCR DeNOx systems in Hitachi Zosen Inova's European EFW-facilities," in *19th Annual North American Waste-to-Energy Conference (NAWTEC19)* (M. J. Castaldi, M. White, and J. Austin, eds.), 2011.

[44] H. Spliethoff, *Großtechnische Untersuchung der Stickstoffoxidminderung mit dem Schwerpunkt Brennstoffstufung an einer Schmelzkammerfeuerung.* Düsseldorf: VDI-Verlag, 1992.

[45] R. Salzmann and T. Nussbaumer, "Fuel staging for NOx-reduction in biomass combustion: experiments and modeling," *Energy & Fuels*, vol. 15, no. 3, pp. 575–582, 2001.

[46] H. Maier, R. Spiegelhalder, A. Kicherer, H. Spliethoff, and I. Hägele, "Luftstufungstechniken am Brenner und im Feuerraum zur Minderung von NOx-Emissionen in Kohlenstaubflammen," in *VDI Berichte Nr. 992* (VDI, ed.), 1991.

[47] U. Zuberbühler and G. Baumbach, *Entwicklung eines Feuerungskonzeptes zur Verbesserung des Ausbrandes bei gleichzeitiger NOx-Minderung bei der Holzverbrennung im gewerblichen Bereich: BWPLUS Projektträgerschaft Programm Lebensgrundlage Umwelt und ihre Sicherung.* PhD thesis, Forschungszentrum Karlsruhe, Universität Stuttgart, BWPLUS, 2000.

[48] H. Hunsinger and H. Seifert, "Primärmaßnahmen zur NOx-Minderung in Abfallverbrennungsanlagen," in *Energie aus Abfall* (K. J. Thomé-Kozmiensky and M. Beckmann, eds.), vol. 9, pp. 573–590, Neuruppin: TK, 2012.

[49] J. J. E. Martin, J. Horn, and O. Gohlke, "Verfahren zur Verbrennungsgaszuführung," 2008.

[50] O. Gohlke and R. Koralewska, "Feuerungstechnische Maßnahme zur NOx-Reduzierung in Abfallverbrennungsanlagen - Very Low Nox-Verfahren," in *Energie aus Abfall* (K. J. Thomé-Kozmiensky and M. Beckmann, eds.), vol. 559-572, Neuruppin: TK, 2012.

[51] U. Martin, *Investigation of a new process for thermal treatment of waste based on gasification and post combustion: Diplomarbeit.* Munich: Lehrstuhl für Energiesysteme, Technische Universität München, 2011.

[52] J. Wolfrum, *Chemische Elementarprozesse bei der Bildung und Beseitigung von Schadstoffen in Verbrennungsvorgängen.* Heidelberg and: Tecflamseminar, 1985.

[53] E. C. Zabetta, M. Hupa, and K. Saviharju, "Reducing NOx-emissions using fuel staging, air staging, and selective noncatalytic reduction in synergy," *Industrial & Engineering Chemistry Research*, vol. 44, no. 13, pp. 4552–4561, 2005.

[54] U. Greul, *Experimentelle Untersuchung feuerungstechnischer NOx-Minderungsverfahren bei der Kohlenstaubverbrennung.* Dusseldorf: VDI Verlag, 1998.

[55] G. E. Moore, "Cramming more components onto integrated circuits," *Electronics*, vol. 38, no. 8, 1965.

[56] W. Dong, *Design of Advanced Industrial Furnaces Using Numerical Modeling Method.* PhD thesis, KTH Kungliga Tekniska Högskol, Stockholm, 2000.

[57] B. Epple, ed., *Simulation von Kraftwerken und wärmetechnischen Anlagen.* Wien and and New York and NY: Springer, 2009.

[58] M. Angerer, *Implementierung und Reduktion eines detaillierten Chemiemodells zur Verbrennungsbeschreibung in CFD: Bachelor thesis.* Munich: Lehrstuhl für Energiesysteme, Technische Universität München, 2011.

[59] A. A. Frank, M. J. Castaldi, and M. R. Nakamura, "Numerical Modeling of Pollution Formation in Waste-to-Energy Systems Using Computational Fluid Dynamics," in *19th Annual North American Waste-to-Energy Conference (NAWTEC19)* (M. J. Castaldi, M. White, and J. Austin, eds.), 2011.

[60] S. Jell, *Simulation der Wärmeübertragung in einer Müllverbrennungsanlage: Semesterarbeit.* Munich: Lehrstuhl für Energiesysteme, Technische Universität München, 2012.

[61] H. Hunsinger, J. Vehlow, B. Peters, and H. Frey, "Performance of a pilot waste incinerator under different air/fuel ratios," in *IT3*, 2000.

[62] Bonnenberg und Drescher, "Optische Eigenschaften der Asche und deren Bedeutung für die Feuerraumtemperaturmessung: Teil 2: - Kesseldiagnosesystem - Akustische Gastemperaturmessung," 2009.

[63] S. Grahl and M. Beckmann, "Wärmeübertragung bei hinterlüfteten und hintergossenen Feuerfest-Plattensystemen," in *Energie aus Abfall* (K. J. Thomé-Kozmiensky and M. Beckmann, eds.), Neuruppin: TK-Verl., 2011.

[64] T. Römer, *Simulation von Flugaschepartikelbahnen in Müllverbrennungsanlagen: Master Thesis.* Munich: Lehrstuhl für Energiesysteme, Technische Universität München, 2012.

[65] C. Wolf, *Erstellung eines Modells der Verbrennung von Abfall auf Rostsystemen unter besonderer Berücksichtigung der Vermischung: Ein Beitrag zur Simulation von Abfallverbrennungsanlagen.* Stuttgart: Fraunhofer-IRB-Verl, 2005.

[66] S. Dürrschmidt, *Parameterstudie mit Brennstoffumsetzungsmodell und CFD-Simulation für die Müllverbrennung: Semesterarbeit.* Munich: Lehrstuhl für Energiesysteme, Technische Universität München, 2010.

[67] L. B. M. v. Kessel, *Stochastic disturbances and dynamic of thermal processes with application to municipal solid waste combustion.* 2003.

[68] B. Peters, "Modellierung der Festbettverbrennung mit der Diskreten Partikel Methode (DPM)," in *25. Deutscher Flammentag* (K. Görner, ed.), 2011.

[69] B. Brosch, E. Simsek, S. Wirtz, V. Scherer, and M. H. Waldner, "Gekoppelte DEM/CFD Simulation einer Hausmüllverbrennungsanlage," in *25. Deutscher Flammentag* (K. Görner, ed.), 2011.

[70] M. R. Nakamura and M. J. Castaldi, "Mixing and residence time analysis of municipal solid waste particles by different numbers of moving b bars and reciprocation speed of a grate system," in *19th Annual North American Waste-to-Energy Conference (NAWTEC19)* (M. J. Castaldi, M. White, and J. Austin, eds.), 2011.

[71] R. Warnecke, T. Marzi, M. Weghaus, and S. Wirtz, "Brennstoff- und Rostmodell zur Beschreibung der Vorgänge im Feuerraum: GKS-Feuerungsmodell," 2007.

[72] J. Behling, P. Danz, T. Marzi, M. Weghaus, R. Warnecke, A. Al-Zuhairi, and K. Görner, "Verbesserte Feuerraummodellierung durch empirische Untersuchung zur Flüchtigenfreisetzung aus Abfallbrennstoffen und Biomassen," in *25. Deutscher Flammentag* (K. Görner, ed.), 2011.

[73] Y. Yang, Y. Goh, R. Zakaria, V. Nasserzadeh, and J. Swithenbank, "Mathematical modelling of MSW incineration on a travelling bed," *Waste Management*, vol. 22, no. 4, pp. 369–380, 2002.

[74] D. Kurz, U. Schnell, and G. Scheffknecht, "CFD-Simulation einer Holzhackschnitzel-Rostfeuerung nach der Euler-Euler Methode," in *25. Deutscher Flammentag* (K. Görner, ed.), 2011.

[75] R. Koralewska and C. Wolf, "Großtechnische Validierung eines CFD-Modells in Verbindung mit einem Brennbettmodell für die thermische Abfallbehandlung in Rostfeuerungsanlagen," in *22. Deutscher Flammentag*, 21.-22.09.2005.

[76] U. Martin, *Beschreibung der Brennstoffumsetzung im Brennbett von Rostfeuerungen: Semesterarbeit.* Munich: Lehrstuhl für Energiesysteme, Technische Universität München, 2010.

[77] H. Hunsinger and H. Seifert, "Einfluss der Verbrennungsluftführung auf den Feststoffabbrand und auf das Schadstoffverhalten bei der Hausmüllverbrennung auf dem Rost," in *Optimierungspotential der Abfallverbrennung* (K. J. Thomé-Kozmiensky, ed.), pp. 135–160, Neuruppin: TK, 2003.

[78] N. Böcker, *Untersuchung der Abhängigkeit der Schlackequalität und Temperaturverteilung im Brennbett von der Feuerraumgeometrie eines Müllkessels: Diplomarbeit.* Munich: Lehrstuhl für Energiesysteme, Technische Universität München, 2011.

[79] N. Böcker, *Entwicklung eines Modells zur Eindüsung von gasförmigen Medien in grobes CFD-Gitter: Semesterarbeit.* Munich: Lehrstuhl für Energiesysteme, Technische Universität München, 2010.

[80] M. J. Murer, H. Spliethoff, C. M. W. d. Waal, S. Wilpshaar, B. Berkhout, M. A. J. v. Berlo, O. Gohlke, and J. J. E. Martin, "High efficient waste-to-energy in Amsterdam: getting ready for the next steps," *Waste Management & Research*, vol. 29, no. 10 Suppl, pp. S20–S29, 2011.

[81] M. J. Murer, S. Dürrschmidt, U. Martin, H. Spliethoff, S. Wilpshaar, C. M. W. d. Waal, and O. Gohlke, "Optimierung von Müllfeuerungen mit Hilfe von CFD Modellierung: Validierung an der HR-AVI Amsterdam," in *25. Deutscher Flammentag* (K. Görner, ed.), 2011.

[82] S. Dürrschmidt, *Untersuchung von gestuften Verbrennungen in Bezug auf Schadstoffminimierung und Temperaturprofile: Diplomarbeit.* Munich: Lehrstuhl für Energiesysteme, Technische Universität München, 2011.

[83] U. Friedrich, *Untersuchung der Abhängigkeit der Schlackequalität und der Temperaturverteilung über dem Brennbett von der Feuerraumgeometrie eines Müllkessels: Diplomarbeit.* Munich: Lehrstuhl für Energiesysteme, Technische Universität München, 2012.

[84] I. SAS IP, *ANSYS 14.0 Help: Theory Guide.* 2011.

[85] G. d. Soete, "Overall reaction rates of NO and N2 formation from fuel nitrogen," *Symposium (International) on Combustion*, vol. 15, no. 1, pp. 1093–1102, 1975.

[86] F. Schimpf, *Implementierung eines erweiterten SNCR Mechanismus in CFD: Semesterarbeit.* Munich: Lehrstuhl für Energiesysteme, Technische Universität München, 2011.

[87] H. Seifert and D. Merz, *Primärseitige Stickoxidminderung als Beispiel für die Optimierung des Verbrennungsvorgangs in Abfallverbrennungsanlagen.* 2003.

[88] J. Brouwer, M. Heap, D. Pershing, and P. Smith, "A model for prediction of selective noncatalytic reduction of nitrogen oxides by ammonia, urea, and cyanuric acid with mixing limitations in the presence of co," *Symposium (International) on Combustion*, vol. 26, no. 2, pp. 2117–2124, 1996.

[89] N. A. Vogl, *Modellierung der Entstehung und Reduzierung von NOx mit Computational Fluid Dynamics: Master Thesis.* Munich: Lehrstuhl für Energiesysteme, Technische Universität München, 2010.

[90] M. Javurek, "Fluent Scheme Dokumentation." 2001.

[91] H. Herden, G. Lohe, J. Kühnel, and C. Moser, "Zusammensetzung und Eigenschaften von Rostaschen aus verschiedenen Müllheizkraftwerken," *Müll und Abfall*, vol. 2, pp. 75–79, 2007.

[92] A. A. Frank and M. J. Castaldi, "CFD analysis of NOx-formation in waste-to-energy systems using detailed chemical kinetic modeling," in *20th Annual North American Waste-to-Energy Conference (NAWTEC20)* (M. J. Castaldi, M. White, and J. Austin, eds.), 2012.

[93] J. J. E. Martin, "Maximale Baugröße von Abfallverbrennungsanlagen," in *Energie aus Abfall* (K. J. Thomé-Kozmiensky and M. Beckmann, eds.), pp. 3–20, Neuruppin: TK Verlag, 2007.

[94] O. Poulsen, "Technicl innovations in new 500.000 t/year WTE-facility in the city center of Copenhagen (Amager), Denmark," in *51. Tutzing-Symposion* (O. Gohlke, ed.), 2012.

[95] U. Seiler, "Energetisches Optimierungspotential bei Abfallverbrennungsanlagen," in *Optimierung der Abfallverbrennung 2* (K. J. Thomé-Kozmiensky and M. Beckmann, eds.), pp. 241–254, Neuruppin: TK, 2005.

[96] M. Otten and G. Bergsma, "Beter één AVI met een hoog rendement dan één dichtbij Hoeveel transport van afval is nuttig voor een hoger energierendement? Better one WtE-installation with high energy efficiency than one nearby; How much transport is allowed for increasing energy efficiency?," 2010.

[97] F. Weber and U. Maschke, "Optimierungspotential bei der Abdampfkondensation von Kühlwassersystemen - unter den Anforderungen von Stromerzeugung und Wärmeauskoppelung," in *Energie aus Abfall* (K. J. Thomé-Kozmiensky and M. Beckmann, eds.), pp. 257–270, Neuruppin: TK Verlag, 2010.

[98] B. Leidinger, *Rauchgasableitung über Kühltürme: Rechenmodelle für d. Immissionsprognose*. Berlin: Schmidt, 1986.

[99] L. Musil and K. Knizia, *Die Thermodynamik des Dampfkraftprozesses: Erster Band*. Springer-Verlag, third ed., 1966.

[100] B. Kamuk, "Technical, economical, operating consequences by operating at extreme steam parameters," in *WtERT Annual Meeting Europe 2010* (M. Jakuttis, ed.), 2010.

[101] R. Dräger, A. Seitz, O. Gohlke, and M. Busch, "Energieeffizienz und Kesselkonzepte," in *Energie aus Abfall* (K. J. Thomé-Kozmiensky and M. Beckmann, eds.), pp. 235–256, Neuruppin: TK Verlag, 2010.

[102] F. Kailbauer, S. Krämer, and U. Priesmeier, "Schritte zur Wirkungsgradsteigerung bei MVA-Neuanlagen," in *Optimierung der Abfallverbrennung 1* (K. J. Thomé-Kozmiensky, ed.), pp. 247–256, Neuruppin: TK, 2004.

[103] R. Schu and R. Leithner, "Mehrstufige Dampfüberhitzung - Effizienzsteigerung von Ersatzbrennstoff-, Biomasse- und Sloarthermiekraftwerken," in *Energie aus Abfall* (K. J. Thomé-Kozmiensky and M. Beckmann, eds.), Neuruppin: TK, 2008.

[104] A. Bandilla, "Ersatzbrennstoffeinsatz in einem Industriekraftwerk mit hohem elektrischem Wirkungsgrad," in *Energie aus Abfall* (K. J. Thomé-Kozmiensky and M. Beckmann, eds.), pp. 501–512, Neuruppin: TK Verlag, 2006.

[105] J. Wandschneider, "Netto-Wirkungsgrad elektrisch größer dreißig Prozent - Grundsätzliche Potentiale in Abfallverbrennungsanlagen," in *Energie aus Abfall* (K. J. Thomé-Kozmiensky and M. Beckmann, eds.), pp. 65–82, Neuruppin: TK Verlag, 2010.

[106] H.-P. Aleßio and M. Mück, "Möglichkeiten und Grenzen der Effizinzsteigerung in Abfallverbrennungsanlagen," in *Energie aus Abfall* (K. J. Thomé-Kozmiensky and M. Beckmann, eds.), pp. 117–148, Neuruppin: TK Verlag, 2010.

[107] K. Villani and J. d. Greef, "Exploiting the low-temperature end of WTE-boilers," in *Venice 2010 Symosium* (R. Cossu, ed.), 2010.

[108] M. J. Murer, H. Spliethoff, R. Dräger, A. Seitz, and O. Gohlke, "Exergetic analysis of heat transfer and efficiency in EFW plants," in *Venice 2010 Symosium* (R. Cossu, ed.), 2010.

[109] Siemens AG Energy Sector, "Case study: steam turbines for waste-to-energy."

[110] Siemens AG Energy Sector, "SST-700 industrial steam turbines."

[111] Siemens AG Energy Sector, "Siemens steam turbine SST-3000 series: for combined cycle applications."

[112] I. Dinçer and M. A. Rosen, *Exergy*. Amsterdam and and Boston and and Heidelberg: Elsevier, op. 2007.

[113] H. Schwetlick and H. Kretzschmar, *Numerische Verfahren für Naturwissenschaftler und Ingenieure: Eine computerorientierte Einführung ; mit 34 Tabellen*. Leipzig: Fachbuchverl., 1 ed., 1991.

[114] R. Schu and M. Born, "Erhöhung der Energieeffizienz bei Abfallverbrennungsanlagen durch Prozessführung und Anlagenschaltung," in *Optimierung der Abfallverbrennung 3* (K. J. Thomé-Kozmiensky and M. Beckmann, eds.), pp. 283–328, Neuruppin: TK, 2006.

[115] M. Maurer, *Feuerführung in Müllverbrennungsanlagen mit wassergekühlten Vorschubrosten*. PhD thesis, RWTH Aachen, Aachen, 2000.

[116] M. J. Murer, H. Spliethoff, C. M. W. d. Waal, T. Schäfer, and O. Gohlke, "Relative dependency of measurement uncertainty for boiler and plant efficiency," in *Venice 2010 Symosium* (R. Cossu, ed.), 2010.

[117] E. Fleck and J. J. E. Martin, "Martin Rückschub-Rost Vario," in *Energie aus Abfall* (K. J. Thomé-Kozmiensky and M. Beckmann, eds.), pp. 229–237, Neuruppin: TK-Verl., 2011.

[118] M. Beckmann and W. Spiegel, "Optimierung von Abfallverbennungsanlagen," in *Optimierung der Abfallverbrennung 3* (K. J. Thomé-Kozmiensky and M. Beckmann, eds.), Neuruppin: TK, 2006.

[119] M. Markovic, E. Bramer, and G. Brem, "Reversed combustion of waste on a grate," in *Venice 2010 Symosium* (R. Cossu, ed.), 2010.

[120] B. Kamuk, "Skiing hill - The new 2.000 tpd WTE facility in the city of copenhagen," in *19th Annual North American Waste-to-Energy Conference (NAWTEC19)* (M. J. Castaldi, M. White, and J. Austin, eds.), 2011.

[121] J. J. E. Martin, E.-C. Langhein, D. Brebric, and M. Busch, "Die Martin Trockenentschlackung mit integrierter Klassierung," in *Energie aus Abfall* (K. J. Thomé-Kozmiensky and M. Beckmann, eds.), pp. 65–79, Neuruppin: TK, 2009.

[122] T. Åbyhammar, "Treatment of moist fuel," 2000.

[123] M. Gaderer, *Abgaskondensationsanlagen: Stand der Technik, Schaltungsvarianten und Entwicklungen.* München, 2008.

[124] M. O. Westermark, "Method and arrangement for condensing flue gases," 1989.

[125] M. Becker, *Untersuchung der Luftbefeuchtung und -vorwärmung in Müllverbrennungsanlagen mit Warmwasser aus der Abgaskondensation: Semesterarbeit.* Munich: Lehrstuhl für Energiesysteme, Technische Universität München, 2012.

[126] R. Karpf, "Flue gas cleaning systems status and trends," in *WtERT Annual Meeting Europe 2010* (M. Jakuttis, ed.), 2010.

[127] C. Müller, "Abfallverbrennung und Wärmeverwertung - Optimierung der Energieeffizienz," in *Energie aus Abfall* (K. J. Thomé-Kozmiensky and M. Beckmann, eds.), Neuruppin: TK, 2009.

[128] D. Hoffmann, "Wärmerückgewinnung ungenutzter thermischer Energie aus Rauchgasen in Biomassekraftwerken mittels innovativem CEECON-Konzept," in *Kraftwerkstechnik* (M. Beckmann and A. Hurtado, eds.), Neuruppin: TK-Verl., 2011.

[129] M. Holmgren, "X STEAM FOR MATLAB: X Steam for Matlab is a implementation of the IAPWS IF97 standard formulation.," 2007.

[130] D. Hammarström Stoltz, J. Holmér, J. Leng, D. Melin, M. J. Murer, and G. Wennberg, *Design of a generation IV nuclear power plant: Group porject.* Stockholm: Royal Institute of Technology, 2007.

[131] "Matlab," 2011.

[132] BALCKE-DÜRR, "Electrostatic precipitators," 2012.

[133] I. AirTek, "Dry electrostatic precipitators," 2012.

[134] 3M Ceramic Textiles and Composites, "Advanced textile for high temperature filter bags," 2012.

[135] D. Francisco Bermudez, *Investigation of concepts for use of high temperature electrostatic precipitators in energy from waster plants: Thesis.* Munich: Lehrstuhl für Energiesysteme, Technische Universität München, 2011.

[136] K. Strauß, *Kraftwerkstechnik: zur Nutzung fossiler, nuklearer und regenerativer Energiequellen.* Heidelberg [Germany] and and New York: Springer-Verlag, 6. aktualisierte auflage ed., 2009.

[137] European Parliament, Council, "Directive 2010/31/EU of the European Parliament and of the Council of 19 May 2010 on the energy performance of buildings: energy performance of buildings."

[138] Rambøll and Aalborg University, *Varmeplan Danmark*. 2008.

[139] I. Obernberger, "Decentralized biomass combustion: state of the art and future development11Paper to the keynote lecture of the session "Processes for decentralized heat and power production based on cumbustion" at the 9th European Bioenergy Conference, June 1996, Copenhagen, Denmark," *Biomass and Bioenergy*, vol. 14, no. 1, pp. 33–56, 1998.

[140] U.S. Department of Energy, "Considerations when selecting a condensing economizer," 2002.

[141] C. Cord'Homme and E. Gartner, "Energy from waste plants: technology developments on the combustion systems: CDR treatment, enriched air combustion,...," in *Sardinia 2009 Symposium* (R. Cossu, ed.), 2009.

[142] R. Scholz and M. Beckmann, "Verfahrenstechnische Möglichkeiten der Optimierung bei Rostfeuerungen zur Abfallbehandlung," in *Optimierungspotential der Abfallverbrennung* (K. J. Thomé-Kozmiensky, ed.), pp. 87–135, Neuruppin: TK, 2003.

[143] S. Wilpshaar, "Membrane Wall Inconel Corrosion in Amsterdam's High Efficient WFPP," in *PREWIN General Assembly Meeting*, 2012.

[144] D. Depta and N. Oldhafer, "Wirkungsgradsteigerung von Kohlekraftwerken mit Hilfe von CFD-Simulationen der Luft- und Rauchgaskanäle in bestehenden Anlagen," in *Kraftwerkstechnik* (M. Beckmann and A. Hurtado, eds.), Neuruppin: TK-Verl., 2010.

A. Appendix

Optimization steps for the heat source system.

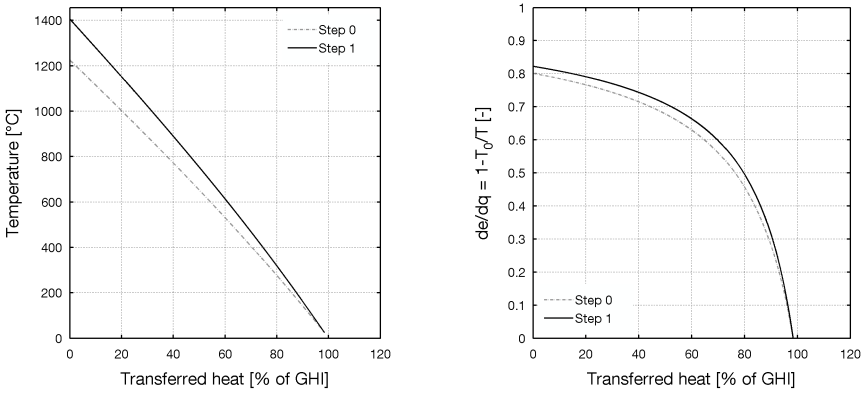

(a) Temperature-heat diagram

(b) Quality-heat diagram

Figure A.1.: Step 1: reducing excess air ratio to 1.35

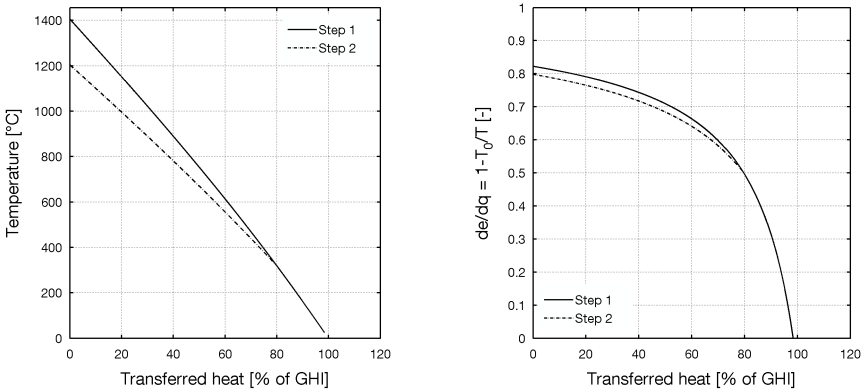

(a) Temperature-heat diagram (b) Quality-heat diagram

Figure A.2.: Step 2: implementing 25 % flue gas recirculation

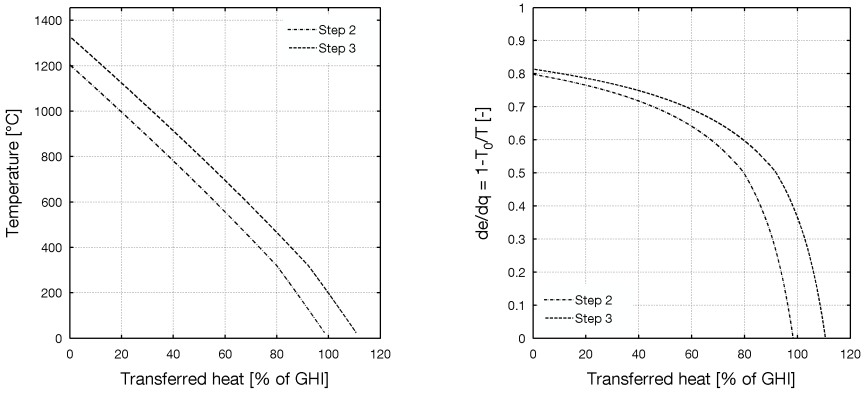

(a) Temperature-heat diagram (b) Quality-heat diagram

Figure A.3.: Step 3: preheating the combustion air to 275 °C

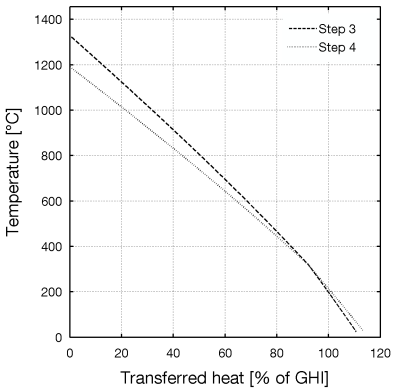

(a) Temperature-heat diagram

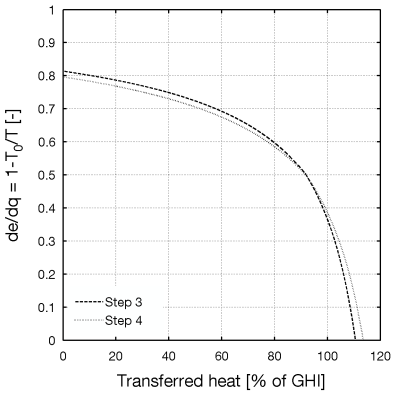

(b) Quality-heat diagram

Figure A.4.: Step 4: humidification of combustion air to 15.8 vol.%

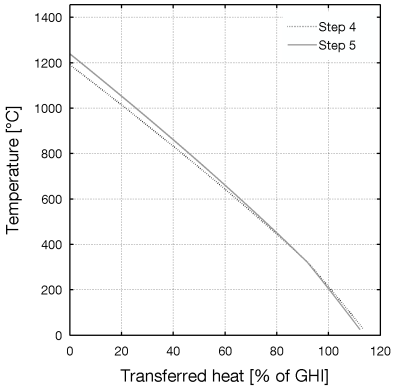

(a) Temperature-heat diagram

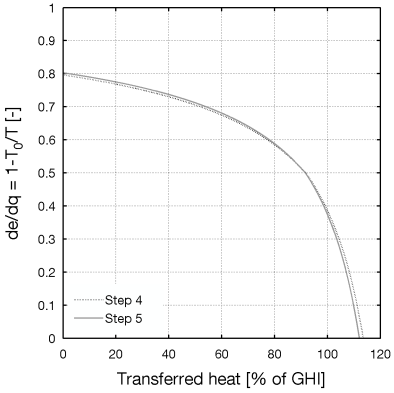

(b) Quality-heat diagram

Figure A.5.: Step 5: reduction of excess air to 1.25

B. Appendix

Table B.1.: Overview on 83 simulated parameter variations with main information (λ_{PA} / external recirculated flue gas [kNm^3/h] / internal recirculated flue gas [kNm^3/h]). The missing simulations in the column λ_{PA} 0.85 RECI are simulation 8 in column λ_{PA} 0.85 no RECI and in column λ_{PA} 0.85.

Simulation	λ_{PA} 0.85	λ_{PA} 0.90	λ_{PA} 0.95	λ_{PA} 1.00	λ_{PA} 1.05
1	0.85 / 27.5 / 0	0.9 / 27.5 / 0	0.95 / 27.5 / 0	1.0 / 27.5 / 0	1.05 / 27.5 / 0
2	0.85 / 27.5 / 3	0.9 / 27.5 / 3	0.95 / 27.5 / 3	1.0 / 27.5 / 3	1.05 / 27.5 / 3
3	0.85 / 27.5 / 6	0.9 / 27.5 / 6	0.95 / 27.5 / 6	1.0 / 27.5 / 6	1.05 / 27.5 / 6
4	0.85 / 27.5 / 9	0.9 / 27.5 / 9	0.95 / 27.5 / 9	1.0 / 27.5 / 9	1.05 / 27.5 / 9
5	0.85 / 27.5 / 12	0.9 / 27.5 / 12	0.95 / 27.5 / 12	1.0 / 27.5 / 12	1.05 / 27.5 / 12
6	0.85 / 27.5 / 15	0.9 / 27.5 / 15	0.95 / 27.5 / 15	1.0 / 27.5 / 15	1.05 / 27.5 / 15
7	0.85 / 27.5 / 18	0.9 / 27.5 / 18	0.95 / 27.5 / 18	1.0 / 27.5 / 18	1.05 / 27.5 / 18
8	0.85 / 27.5 / 21	0.9 / 27.5 / 21	0.95 / 27.5 / 21	1.0 / 27.5 / 21	1.05 / 27.5 / 21
9	0.85 / 27.5 / 24	0.9 / 27.5 / 24	0.95 / 27.5 / 24	1.0 / 27.5 / 24	1.05 / 27.5 / 24
10	0.85 / 27.5 / 27	0.9 / 27.5 / 27	0.95 / 27.5 / 27	1.0 / 27.5 / 27	1.05 / 27.5 / 27

Simulation	λ_{PA} 0.85 no RECI	λ_{PA} 1.05 no RECI	λ_{PA} 0.85 RECI	λ_{PA} 0.85 HUM
1	0.85 / 0 / 0	1.05 / 0 / 0		0.85 / 28.9 / 0
2	0.85 / 0 / 3	1.05 / 0 / 3	0.85 / 9.4 / 21	0.85 / 28.9 / 3
3	0.85 / 0 / 6	1.05 / 0 / 6	0.85 / 18.3 / 21	0.85 / 28.9 / 6
4	0.85 / 0 / 9	1.05 / 0 / 9		0.85 / 28.9 / 9
5	0.85 / 0 / 12	1.05 / 0 / 12	0.85 / 36.7 / 21	0.85 / 28.9 / 12
6	0.85 / 0 / 15	1.05 / 0 / 15		0.85 / 28.9 / 15
7	0.85 / 0 / 18	1.05 / 0 / 18		0.85 / 28.9 / 18
8	0.85 / 0 / 21	1.05 / 0 / 21		0.85 / 28.9 / 21
9	0.85 / 0 / 24	1.05 / 0 / 24		0.85 / 28.9 / 24
10	0.85 / 0 / 27	1.05 / 0 / 27		0.85 / 28.9 / 27

C. Appendix

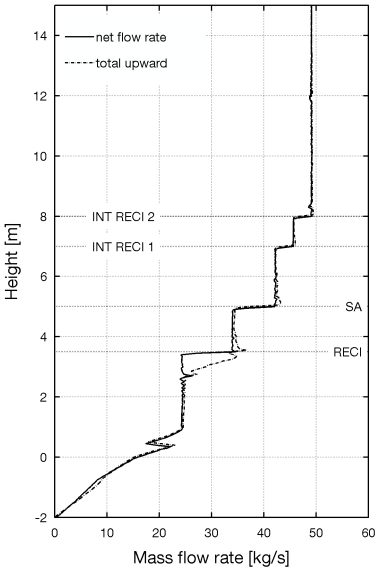

Figure C.1.: Vertical profiles for mass flow rates for the boiler with narrow first pass and wall superheater